NASA Contractor Report 177608

Image-Based Ranging and Guidance for Rotorcraft

P. K. A. Menon

CONTRACT NCC2-575
December 1991

National Aeronautics and
Space Administration

NASA Contractor Report 177608

Image-Based Ranging and Guidance for Rotorcraft

P. K. A. Menon

Georgia Institute of Technology
School of Aerospace Engineering
Atlanta, GA 30332-0150

Prepared for
Ames Research Center
CONTRACT NCC2-575
December 1991

National Aeronautics and
Space Administration

Ames Research Center
Moffett Field, California 94035-1000

Table of Contents

1. Introduction

Vision-based ranging has emerged as the central problem in automating the helicopter nap-of-the-earth flight regime. Current status of the research in vision-based ranging at NASA Ames is summarized in Reference 1. The present work is a component of this research effort.

The recovery of three dimensional geometry from two dimensional scenes is based on the fact that if one has at least two views of a scene obtained from different vantage points, the difference between the location of corresponding objects in the images is a measure of the range. The process of finding the corresponding objects within the field of view is the *correspondence problem* in machine vision literature. Correspondence problem can be solved if all the images unambiguously contained every object in the scene. Since real imaging devices have limited field of view and resolution, concept of correspondence is in reality a *correspondence hypothesis*. The relative object displacement obtained by satisfying the correspondence hypothesis in these images are called *disparities*. The farther the objects are with respect to the imaging device, the less the observed disparity would be. For instance, objects that are very far away would appear at nearly the same location in the images, while closer objects will exhibit a large disparity. If the disparity of the corresponding objects in an image sequence could be measured, the perspective projection equations could be used to compute the scene depth. This fact forms the basis for a large majority of vision-based ranging methods discussed in the literature. Sometimes, establishing correspondence between several views of the scene may improve the range estimation accuracy.

Two distinct families of techniques can be identified for satisfying the correspondence hypothesis. Methods which establish correspondence between relativly few chosen features of interest in the images are termed *feature based* methods. On the other hand, techniques which attempt to establish the correspondence between every point in the images are called *field-based* methods. The focus of present research effort is on field-based ranging technique. The present research has its basis in the robot vision literature [2].

In the present work, a family of field-based ranging algorithms are cast in an analytical format. An advantage of the analytical approach is that it reveals the means for systematic performance improvement. If desired, additional heuristics may be included in the formulation to enhance the algorithm performance.

These ranging algorithms have their basis in a mathematical approximation of the correspondence hypothesis together with the perspective projection geometry. The central ideas in the present work are:

- Mathematical approximation of the correspondence hypothesis
- The use of incremental perspective projection in the correspondence hypothesis approximation to yield vision-based ranging equations
- Methods for estimating ranging equation parameters

Ensuing chapters in this report are based on a few papers written over the past three years. The motivation and summary of the research is given at the beginning of each chapter, followed by the paper. The contributions of the present research are given in a condensed form in the Conclusions section.

A part of the research effort was expended in synthesizing a guidance law for performing obstacle avoidance using the image-based sensor data. The range data generated by image-based sensors are generally discrete and are available only at about 10 % of the points on the image. An optimal guidance law that explicitly uses the discrete range data together with a nonlinear point-mass vehicle

model was formulated using the calculus of variations. Details of this guidance law development and implementation are given in Chapter 6.

2. Development of a Field-Based Ranging Equation

Initial phases of the present research focussed on ranging using motion image sequences generated by a single camera fixed to a moving vehicle. A ranging scheme using temporal image sequences is developed based on the *Optical Flow Constraint Equation* of Horn and Schunck [3]. The optical flow constraint equation relates the temporal partial derivatives with the spatial partial derivatives of the image irradiance E as:

$$\frac{\partial E}{\partial t} + \frac{\partial E}{\partial x_p} u + \frac{\partial E}{\partial z_p} v = 0 \tag{2.1}$$

where $(x_p,\ z_p)$ are the major and minor axes of the image plane while u and v are called the optical flow components. Generally, the ranging problem is treated in a two-step fashion. First, the optical flow components u and v are computed. Since just one expression is available for the calculation of two quantities, an additional condition has to be imposed to obtain a unique solution. Horn and Schunk [3] propose the use of a *smoothness constraint* for the optical flow components to alleviate this difficulty. The optical flow components are then used for computing the range.

Instead of this two step process, incremental perspective projection can be combined directly with the optical flow constraint to yield a ranging equation. Since such a concatenation is direct for the case of purely translational motion of the camera, this case was investigated first.

The perspective projection relationships for a camera located at a position $(x_0,\ y_0)$ are given by

$$x_p = \frac{f(x - x_0)}{(y - y_0)}, \quad z_p = \frac{f(z - z_0)}{(y - y_0)} \tag{2.2}$$

These equations can be differentiated to yield the optical flow components as

$$u = \frac{[x_p \dot{y}_0 - f\dot{x}_0]}{(y - y_0)}, \qquad v = \frac{[z_p \dot{y}_0 - f\dot{z}_0]}{(y - y_0)} \tag{2.3}$$

Substituting these in the optical flow constraint equation yields an *Optical Navigation Equation* as :

$$\frac{\partial E}{\partial t} = -\left[\frac{\partial E}{\partial x_p}(x_p \dot{y}_0 - f\dot{x}_0) + \frac{\partial E}{\partial z_p}(z_p \dot{y}_0 - f\dot{z}_0)\right] \frac{1}{(y - y_0)} \tag{2.4}$$

This equation can be used to compute the range $(y - y_0)$ from the image irradiance partial derivatives and camera position components. A simulated scene was used to test the algorithm performance. A paper based on this research was presented at the *1989 AIAA Guidance, Navigation, and Control Conference* discussing the details of this investigation. This paper is included in this chapter.

Passive Navigation Using Image Irradiance Tracking

P. K. A. Menon* and B. Sridhar†
NASA Ames Research Center
Moffett Field, CA 94035

Abstract

Rotorcraft operating at low altitudes require navigational schemes for locating the terrain and obstacles. Due to the covert nature of missions to be accomplished, a passive navigation scheme is desirable. This paper describes the development of a passive navigation scheme combining image sequences from a vehicle mounted camera with vehicle motion variables. Geometric properties of perspective projection together with an image irradiance tracking scheme at each pixel are used to determine the range to various objects within the field-of-view. Derivation of the numerical algorithm and simulation results are given. Other applications of the proposed approach include navigation for autonomous planetary rovers and telerobots.

1 Introduction

The problem of determining the scene geometry from on-board sensors is emerging as a central issue in nap-of-the-earth helicopter flight guidance[1,2]. The objective of passive navigation is to use image-based sensors such as FLIR and low-light level TV to determine the range to various objects within the field-of-view. Several approaches to the passive navigation problem have been suggested in recent literature[1,3–6]. Approaches for passive navigation using stereo image pairs have also been reported[7]. However, with the exception of Reference 1, none of these techniques appear to have been developed to a point where they can be used for vehicle navigation. Moreover, there exists an ambiguity regarding the interpretation of the visual navigation task. With the exception of Reference 1, previous researchers have tended to interpret image based passive navigation as the process of simultaneously determining the vehicle motion and object position parameters from an image sequence. This can be shown to produce an under-determined system and the solution can be obtained only by imposing an additional super-criterion. The present approach, however, assumes that the vehicle motion parameters are known from the on-board inertial navigation system. As a result, the navigation task is to use the available image sequence together with the inertial navigational information to determine the relative location of various objects within the field of view.

The data available in a monochromatic image is a distribution of image irradiance specified as a function of imaging device aperture coordinates. Various points in an image obtained from a moving vehicle will exhibit an irradiance distribution change as a function of time. This change depends on the relative location of various objects, vehicle motion parameters and the surface reflectance. If the surface reflectance is assumed to remain constant, then the observed image irradiance distribution change is entirely due to the relative location of various objects within the field-of-view and vehicle motion parameters. In this case, if the vehicle motion parameters and the imaging device constants are known, it is possible to determine the realtive location of various points within the field of view. At this early stage in research, the investigation will be restricted to objects that are

*Member AIAA, Georgia Institute of technology, Atlanta. Mailing Address : FSN Branch, MS 210-9

†Research Scientist, Member AIAA, FSN Branch, MS 210-9

stationary with respect to the earth fixed frame. Additionally, only pure translational motion of the vehicle will considered.

The approach presented in this paper has its roots in the *optical flow constraint equation* derived by Horn and Schunck[3,4,8]. With the assumption that the objects within the field-of-view are fixed, this equation is combined with perspective projection geometry and the inertial navigation system data to derive a direct navigational equation. This navigational equation relates the spatial and temporal partial derivatives of the image irradiance with the distance to various objects within the field-of-view and the vehicle motion parameters. An expression for determining the spatial and temporal sampling intervals required for satisfactory performance of the proposed scheme is next derived. Details of this analysis are given in Section 2. In Section 3, an optimal approach for estimating various partial derivatives is synthesized using the Calculus of Variations[9,10]. This approach requires the solution of a linear, second-order partial differential equation. Using the existing theory of such partial differential equations[11], the solution is obtained by assuming a product decomposition. Spatial discretization of this solution then produces feedback scheme for tracking the image irradiance as well as a systematic approach for estimating the spatial and temporal partial derivatives.

The performance of the proposed navigation scheme is demonstrated using a simulated image sequence in Section 4. Conclusions and future research directions are indicated in Section 5.

2 The Navigation Scheme

Assuming that the image is rectangular with the major axis parallel to the horizontal, one may define the major axis as the X_p axis and the minor axis as the Z_p axis. The Y_p axis is normal to the image plane. The origin of this *image plane* coordinate system may be at the center of the aperture or at one of the corners. In the present research, the origin is chosen to be at the bottom left hand corner of the camera aperture. An image is defined as an irradiance distribution $E(x_p, z_p)$ in the $X_p - Z_p$ plane, with E being the irradiance specified on a gray scale at a point (x_p, z_p) on the image. To avoid the complications that can arise while considering an inverted image as is encountered in real cameras, the *front image plane*[12] will be used for image description. It is assumed in the ensuing analysis that the image irradiance distribution is continuous except at finite number of regions. Thus, for the purposes of the present analysis, effects such as spatial image discretization and gray scale quantization are ignored. The image plane is assumed to be located at a distance l_1, l_2, l_3 from the origin of the vehicle body axis system, and oriented with respect to the body axis by three rotations $\epsilon_1, \epsilon_2, \epsilon_3$. The vehicle body axis system may be related to an earth fixed frame through three Euler angles ψ, θ, ϕ and three translations x_0, y_0, z_0. The vehicle inertial navigation system is assumed to produce estimates of $x_0, y_0, z_0, \psi, \theta, \phi$ and their time derivatives. Let the location of the various objects within the field-of-view with respect to the earth fixed frame be x, y, z. Various coordinate systems outlined in the foregoing are illustrated in Figure 1.

Any point x_p, z_p corresponding to an object in the image plane is related to its location with respect to the earth-fixed frame through various translations and rotations, together with the perspective projection. Considering pure translations, if one assumes that the camera is located at the origin of the vehicle body coordinate system and aligned with it, the relation between an image point and its position with respect to the earth fixed frame is given by

$$x_p = \frac{f(x - x_0)}{(y - y_0)} \tag{1}$$

$$z_p = \frac{f(z - z_0)}{(y - y_0)} \tag{2}$$

Here, f is the imaging device focal length. As in the research of Horn and Schunck[3,4,8], the following assumptions are next invoked :

1. The underlying image irradiance distribution is smooth in the sense that first spatial partial derivatives exist everywhere on the image, except at finite number of regions.

2. The perceived change in image irradiance at each point in the image plane is entirely due to the motion of the imaging device, and not due to changes in the scene reflectance.

These assumptions lead to the expression

$$\frac{dE}{dt} = 0 \tag{3}$$

It is to be emphasized that higher order derivatives of the irradiance may also be equated to zero. This fact may be exploited to resolve navigational anomalies in certain situations. However, the resulting navigational scheme will be more complex. This issue will not be pursued any further in this paper. Next, expanding equation (3) yields

$$\frac{\partial E}{\partial t} + \frac{\partial E}{\partial x_p}\dot{x}_p + \frac{\partial E}{\partial z_p}\dot{z}_p = 0 \tag{4}$$

Expression (4) is the Horn-Schunk optical flow constraint equation. The apparent velocity of the image $\dot{x}_p, \dot{z}_p$ in this expression are called optical flow components.

Next, differentiating the perspective projection equations (1), (2) with respect to time and noting that the objects are fixed relative to the earth fixed frame leads to the equations :

$$\dot{x}_p = \frac{[x_p\dot{y}_0 - f\dot{x}_0]}{(y - y_0)} \tag{5}$$

$$\dot{z}_p = \frac{[z_p\dot{y}_0 - f\dot{z}_0]}{(y - y_0)} \tag{6}$$

Substituting these relations in the optical flow constraint equation results in

$$\frac{\partial E}{\partial t} = -\left[\frac{\partial E}{\partial x_p}(x_p\dot{y}_0 - f\dot{x}_0) + \frac{\partial E}{\partial z_p}(z_p\dot{y}_0 - f\dot{z}_0)\right]\frac{1}{(y - y_0)} \tag{7}$$

Expression (7) is the *optical navigation equation.* If the spatial and temporal partial derivatives of the image irradiance at any instant are known, equation (7) may be used to solve for the depth $(y - y_0)$ since the vehicle velocity components $\dot{x}_0, \dot{y}_0, \dot{z}_0$ and a particular pixel location in the image plane x_p, z_p are known. It is important to note that anomalies of various kinds can arise while applying this equation to real image sequences. For instance, points in the image at which the spatial irradiance gradients are discontinuous, the expression (7) may not have a solution. It is assumed here that such points can be edited-out of the image sequence using additional criteria.

Before proceeding to use equation (7), the discrete nature of the imaging process needs to be examined to determine the acceptable spatial and temporal data rates required for obtaining a realistic estimate of the scene depth. Clearly, the trade-off between spatial and temporal sampling intervals must be examined before synthesizing a numerical algorithm. The simplest way to carry-out this analysis is to replace the partial derivatives in expression (7) by finite differences. This yields

$$\frac{\Delta E_1}{\Delta t} = -\left[\frac{\Delta E_2}{\Delta x_p}(x_p\dot{y}_0 - f\dot{x}_0) + \frac{\Delta E_3}{\Delta z_p}(z_p\dot{y}_0 - f\dot{z}_0)\right]\frac{1}{(y - y_0)} \tag{8}$$

Here ΔE_1 is the difference in the irradiance at a point x_p, z_p at the begining and end of temporal sampling, ΔE_2 is the irradiance difference varying x_p while holding the time t and z_p fixed, and ΔE_3 is the irradiance difference varying z_p while holding t and x_p fixed. Δt, Δx_p, Δz_p are the spatial and temporal sampling intervals. To ensure a numerically well-conditioned system, the spatial and temporal irradiance differences should be more or less equal. Imposing this requirement in (8) leads to :

$$\Delta t = \Delta x_p \Delta z_p (y - y_0)/N_r \tag{9}$$

where

$$N_r = -\left[\Delta z_p(x_p\dot{y}_0 - f\dot{x}_0) + \Delta x_p(z_p\dot{y}_0 - f\dot{z}_0)\right] \tag{10}$$

Thus, if the required depth sensitivity, vehicle velocity components, camera focal length, pixel location and the spacing between pixels along the $X_p - Z_p$ directions are known, desirable temporal

sampling interval can be computed using this expression. Since the sampling interval given by (9) depends on the pixel location, different sampling intervals will be specified at various parts of the image. For instance, if the vehicle were travelling along the Y direction in the earth fixed frame, the sampling interval at the center of the image can be very large, while the sampling interval at the image periphery should be small. In this situation, the smallest sampling interval may be used for the entire image to simplify calculations. It is important to remember that the expression (9) provides only an upper bound on the sampling interval. Normally, a sampling interval between one fifth to one tenth this value should be employed.

Once the spatial and temporal sampling intervals are selected, the only remaining issue is the method for computing partial derivatives. There are several techniques available for computing partial derivatives in the literature[13]. Most of these techniques suggest data smoothing prior to derivative computations. This is an essential step because derivative computation is an inherently noise amplifying process. In the following, a technique based on optimal control theory will be advanced for the computation of spatial and temporal partial derivatives.

3 Estimation of Partial Derivatives

The success of the proposed navigation depends on estimating a consistent set of image irradiance partial derivatives. The finite difference technique has been the main approach employed by previous investigators while using the optical flow constraint equation. While the simplicity of this approach is attractive, it has no noise attenuating properties. This is a serious limitation while dealing with real image sequences. An alternate approach for partial derivative estimation based on the integral least square error criterion will be developed in the following.

Let the model of the image under consideration be $E_M(x_p, z_p, t)$ and the actual image is given by $E(x_p, z_p, t)$. The objective of the estimation scheme is to produce a relatively noise free estimate of spatial and temporal partial derivatives. To meet this objective, define the instantaneous error between the model and the actual image as

$$r(x_p, z_p, t) = E(x_p, z_p, t) - E_M(x_p, z_p, t) \quad (11)$$

It is desired to compute the partial derivatives of the image model $\partial E_M/\partial t, \partial E_M/\partial x_p, \partial E_M/\partial z_p$ using the measured irradiance and the error between the image model and the actual image. The image model will be continuously updated to closely *track* the actual image. Then the partial derivatives can be computed as

$$\frac{\partial E_M}{\partial t} = \frac{\partial E}{\partial t} - \frac{\partial r}{\partial t} \quad (12)$$

$$\frac{\partial E_M}{\partial x_p} = \frac{\partial E}{\partial x_p} - \frac{\partial r}{\partial x_p} \quad (13)$$

$$\frac{\partial E_M}{\partial z_p} = \frac{\partial E}{\partial z_p} - \frac{\partial r}{\partial z_p} \quad (14)$$

In order to develop estimates of the error partial derivatives, consider the following optimization problem

$$\min_{r(x_p,z_p,t)} \int_{t_0}^{t_f} \int_{x_{p0}}^{x_{pf}} \int_{z_{p0}}^{z_{pf}} \left\{ r^2 + \alpha \left[\frac{\partial r}{\partial x_p}\right]^2 + \beta \left[\frac{\partial r}{\partial z_p}\right]^2 + \gamma \left[\frac{\partial r}{\partial t}\right]^2 \right\} dz_p dx_p dt, \quad (15)$$

with given constants α, β, γ. These constants can be chosen to regulate the relative magnitudes of the error partial derivatives. A large value would tend to decrease the partial derivatives implying a nearly uniform error distribution, while a smaller weight would permit larger error variations in the image plane. Additionally, these weights can be used to correct for errors in the camera optics by constraining the partial derivative magnitudes in certain directions. In the integral (15), t_0 is the initial time, x_{p0} and x_{pf} define the left and right edges of the image, and z_{p0} and z_{pf} are the bottom and top edges of the image.

The problem defined in (15) is a least square error estimation problem involving three independent variables. The necessary condition for optimality is given by[9]

$$r - \alpha\frac{\partial^2 r}{\partial x_p^2} - \beta\frac{\partial^2 r}{\partial z_p^2} - \gamma\frac{\partial^2 r}{\partial t^2} = 0 \qquad (16)$$

Equation (16) is a second order linear partial differential equation and can be solved for certain set of boundary conditions[11]. In the present situation, the image is rectangular and the error is assumed to decrease from the left edge to the right edge and from bottom edge to the top edge. It is desirable that the tracking error decreases monotonically over time. Additionally, the error is required to approach zero for sufficiently large t, x_p, z_p.

An approach for obtaining the solution to (16) is to assume that the image error has a decomposition of the form

$$r = r_1(t)r_2(x_p)r_3(z_p) \qquad (17)$$

The only justification that can be advanced for using such a decomposition is that the resulting system of equations can be solved in closed form. Substituting this decomposition in the necessary condition for optimality (16) permits one to convert the second order partial differential equation into three second order linear ordinary differential equations of the form

$$\frac{d^2 r_1}{dt^2} = \frac{C_1}{\gamma} r_1 \qquad (18)$$

$$\frac{d^2 r_2}{dx_p{}^2} = \frac{C_2}{\alpha} r_2 \qquad (19)$$

$$\frac{d^2 r_3}{dz_p{}^2} = \frac{C_3}{\beta} r_3 \qquad (20)$$

Here, C_1, C_2, C_3 are three constants which satisfy the algebraic equation

$$1 - C_1 - C_2 - C_3 = 0 \qquad (20)$$

Monotonically decreasing error in both spatial and temporal directions requires

$$C_1 > 0,\ C_2 > 0,\ C_3 > 0 \qquad (21)$$

In this case, a closed form solution for equation(16) can be shown to be

$$r = Ke^{-[a(t-t_0)+b(x_p-x_{p0})+c(z_p-z_{p0})]} \qquad (22)$$

where

$$a = \sqrt{C_1/\gamma},\ b = \sqrt{C_2/\alpha},\ c = \sqrt{C_3/\beta} \qquad (23)$$

and K is an arbitrary constant. In expression (23), any two of the three constants C_1, C_2, C_3 can be arbitrarily chosen, the third one being determined by the constraint equation (20).

Differentiating expression (22), the spatial and temporal partial derivatives of the error can be computed as

$$\frac{\partial r}{\partial x_p} = -br \qquad (24)$$

$$\frac{\partial r}{\partial z_p} = -cr \qquad (25)$$

$$\frac{\partial r}{\partial t} = -ar \qquad (26)$$

Thus, at any pixel in the image plane, the spatial and temporal partial derivatives of the error can be computed if the spatial and temporal error between the image model and the actual image are known. Next, recognizing the fact that the image is spatially discretized, the image model may be updated at each pixel by integrating its temporal partial derivative with appropriate initial conditions. For instance, if an Euler integration scheme were employed for the temporal partial derivative,

$$E_M(t_{i+1}) = E_M(t_i) + h\left[\frac{\partial E}{\partial t} + a(E - E_M)\right]_{t=t_i} \qquad (27)$$

In this expression, h is the integration step size, normally chosen to be the image frame rate. Expression (27) is the image irradiance tracking equation which ensures that the image model is close to the actual image. The actual image partial derivatives $\partial E/\partial t, \partial E/\partial x_p, \partial E/\partial z_p$ are computed using finite difference approximations. In image

sequences with relatively unchanging spatial irradiance gradients, these may be assumed zero, letting the tracking process to compensate for this value.

The foregoing analysis may next be used to synthesize a navigation scheme. At a particular pixel in the image, the spatial and temporal partial derivatives of the image can be computed using expressions (24)-(26). The temporal error is then integrated with the initial condition on the image model irradiance to obtain the image model for the next time step. The temporal sampling interval for this image irradiance tracking scheme is chosen based on equation (9) and the values of C_1, γ. Various constants involved in the computations can be selected based on the quality of the tracked image. A schematic block diagram of proposed the navigation scheme is given in Figure 2.

4 Results and Discussions

The navigation algorithm was implemented in a simulation employing a piece-wise planar scene. The piece-wise planar scene is made up of joined rectangular planes of equal height with a continuous irradiance distribution across the surface. A horizontal section through this simulated scene is given in Figure 3. Corresponding irradiance distribution is given in Figure 4.

Figures 5 shows the imaging device trajectory, and both the actual and estimated scene depths at a pixel using the present navigation scheme. The anomalies that arise at image irradiance gradient discontinuities may be observed in this figure. These anomalies arise due to the fact that the image model lags behind the actual image. As a result, at points where the irradiance gradients are discontinuous, the spatial and temporal derivatives do not change simultaneously. While this lag is not too serious in regions of small irradiance change, it becomes increasingly inaccurate whenever the irradiance gradients undergo jumps.

To a degree, these anomalies can be corrected by decreasing the temporal sampling interval. Alternately, one may either use a higher-order irradiance tracking scheme or process the computed range estimates through a low-pass filter. The latter approach was employed in the present study. Figures 6 and 7 show the depth estimates obtained using range filters with two different time constants. This investigation reveals that the proposed navigation scheme can be made to work satisfactorily in simulated image sequences. Detailed computations using real image sequences are currently under way.

5 Conclusions

An image-based passive navigation scheme for rotorcraft was described. This scheme estimates the scene depth by tracking the image irradiance using a proportional feedback law. Feasibility of this approach was explored using a simulated image sequence.

The contributions of the present research are the following:

- Derivation of the image based navigational equation combining the motion parameters with the spatial and temporal irradiance gradients.
- Formulation of the range estimation problem as a distributed parameter observer problem with spatio-temporal irradiance distribution as an input.
- Feedback solution of this problem using the Calculus of Variations.

This scheme is currently being evaluated using real image sequences. Work on a navigation scheme using higher-order tracking schemes and multiple image sequences is also underway.

Acknowledgement

The research support for the first author under NASA Grant NAG 2 - 463 from Ames Research Center is gratefully acknowledged.

References

[1] Sridhar, B., and Phatak, A. V., "Simulation and Analysis of Image-Based Navigation System for Rotorcraft Low-Altitude Flight",

AHS National Specialist's Meeting on Automation Applications of Rotorcraft, Atlanta, GA., April 4-6, 1988.

[2] Cheng, V. H. L., "Obstacle Avoidance Automatic Guidance", *AIAA Guidance, Navigation, and Control Conference*, Minneapolis, Minnesota, August 15-17, 1988.

[3] Horn, B. K. P., *Robot Vision*, McGraw Hill, New York, 1986.

[4] Horn, B. K. P., and Schunck, B. G., "Determining Optical Flow", *Artificial Intelligence*, Vol. 17, 1981, pp. 185-203.

[5] Hildreth, E. C., "Computations Underlying the Measurement of Visual Motion", *Artificial Intelligence*, Vol. 23, 1984, pp. 309-354.

[6] Negahdaripour, S., and Horn, B. K. P., "Direct Passive Navigation", *IEEE Transactions on Pattern Analysis and Machine Intelligence*, Vol. PAMI-9, Jan. 1987, pp. 168-176.

[7] Balasubramanyam, P., and Snyder, M. A., "Computation of Motion in Depth Parameters : A First Step in Stereoscopic Motion interpretation", *Proceedings of the Image Understanding Workshop*, Vol II, Cambridge, MA, April 6-8, 1988.

[8] Schunk, B. G.,"The Image Flow Constraint Equation", *Computer Vision, Graphics, and Image Processing*, Vol. 35, 1986, pp. 20-46.

[9] Weinstock, R., *Calculus of Variations with Applications*, Dover, New York, 1983.

[10] Bryson, A.E., and Ho, Y.C., *Applied Optimal Control*, Hemisphere, Washington, 1975.

[11] Pipes, L. A., *Applied Mathematics for Engineers and Physicists*, McGraw-Hill, New York, 1958.

[12] Duda, R. O., and Hart, P. E., *Pattern Classification and Scene Analysis*, John Wiley, New York, 1973.

[13] Carnahan, B., Luther, H. A., and Wilkes, J. O.,*Applied Numerical Methods*, John Wiley, NY, 1969.

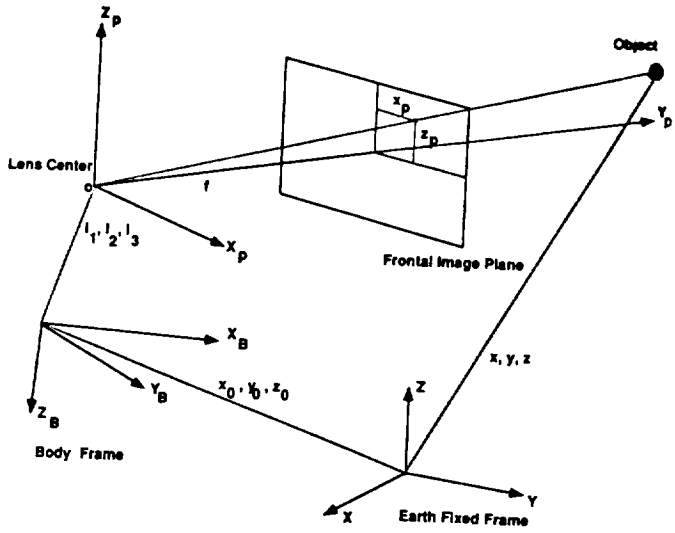

Fig. 1. Coordinate Systems.

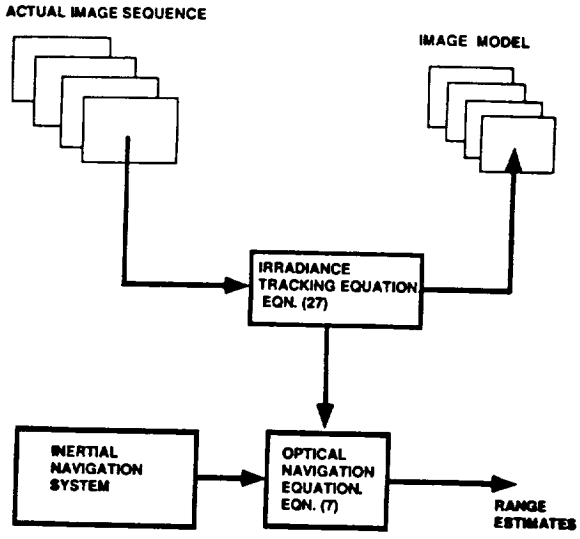

Fig. 2. Image-Based Passive Navigation Scheme

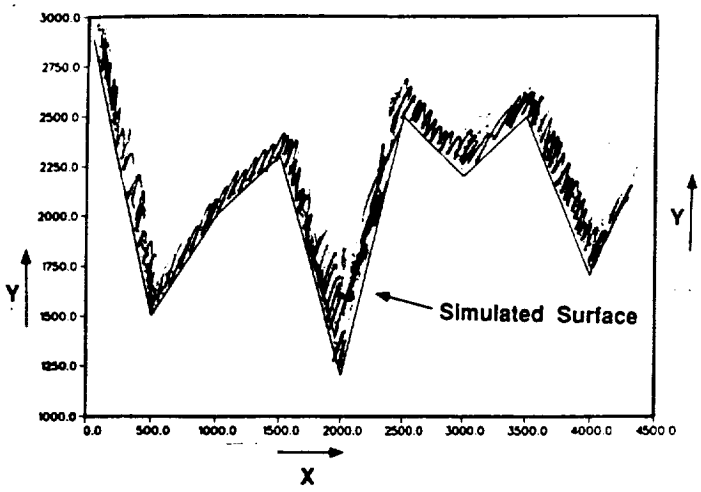

Fig. 3. Horizontal Cross Section through the Simulated Scene

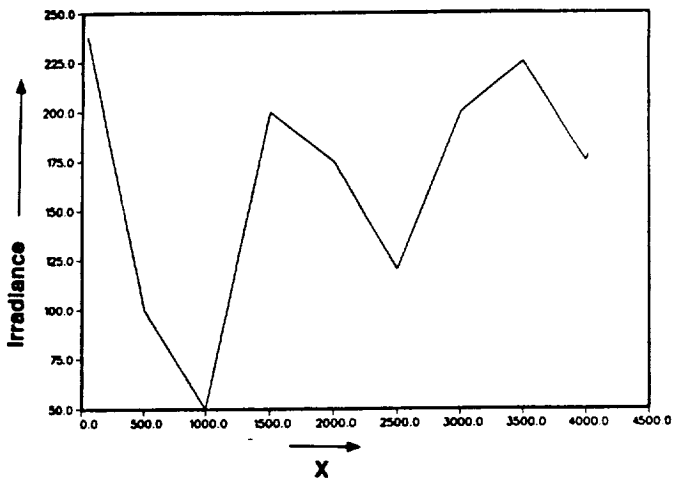

Fig. 4. Irradiance Distribution on the Simulated Scene

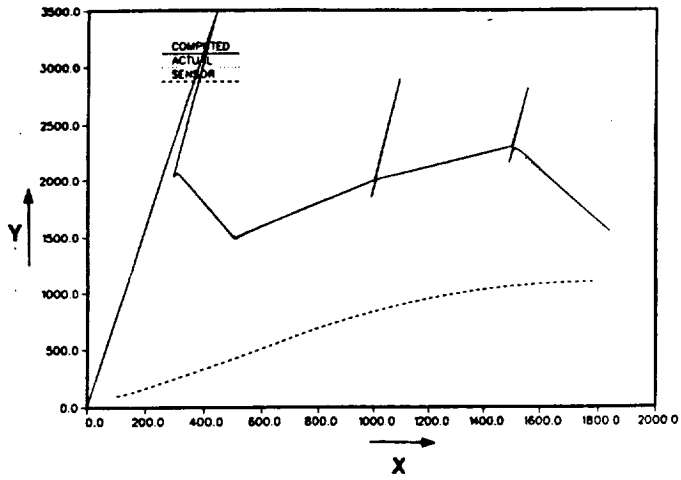

Fig. 5. Range Estimate Obtained using the Navigation Scheme

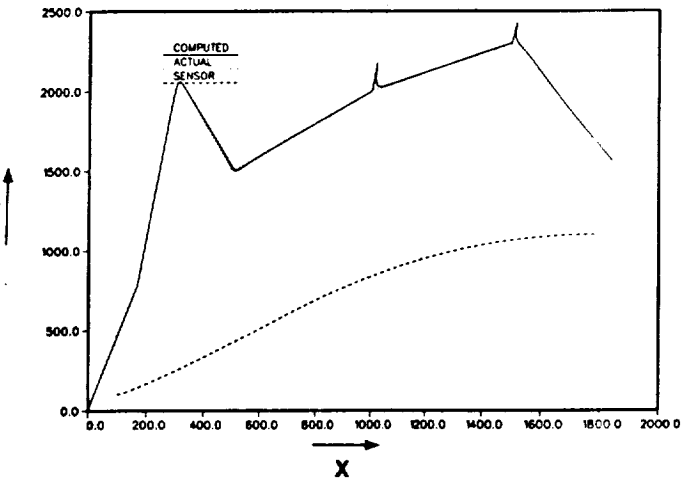

Fig. 6. Range Estimate with a Low-Pass Filter

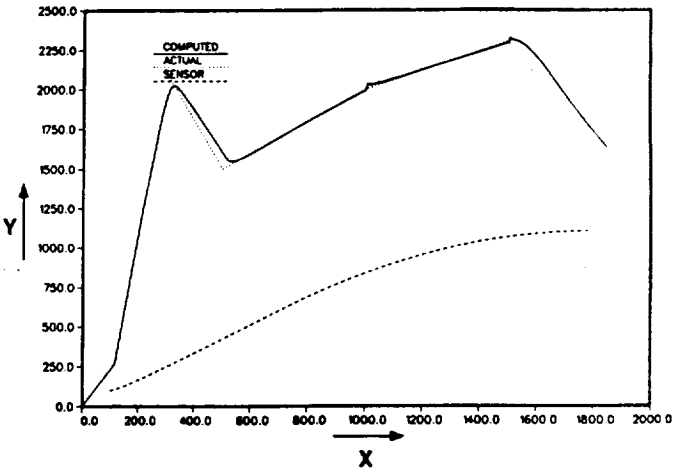

Fig. 7. Range Estimate using a Slower Low-Pass Filter

3. Ranging Based on Taylor Series Expansion

The ranging scheme described in the previous chapter suffers from a major disadvantage, viz., since the optical flow constraint equation relates temporal irradiance partial derivative with the spatial irradiance partial derivatives and optical flow, it is not clear how it can be modified for stereo image sequences. Furthermore, since the images are discrete, the concept of a temporal partial derivative is artificial.

To alleviate these conceptual difficulties, multi-dimensional Taylor series approximation of the correspondence hypothesis is next introduced. Given an image $E(x_p,\ y_p)$, define the gradient vector $\mathbf{g}$ and the Hessian matrix $\mathbf{H}$ as:

$$\mathbf{g} = \begin{bmatrix} \partial E/\partial x_p \\ \partial E/\partial y_p \end{bmatrix}, \quad \mathbf{H} = \begin{bmatrix} \partial^2 E/\partial {x_p}^2 & \partial^2 E/\partial x_p \partial y_p \\ \partial^2 E/\partial y_p \partial x_p & \partial^2 E/\partial {y_p}^2 \end{bmatrix} \tag{3.1}$$

For a pair of images $E_1,\ E_2$, the correspondence hypothesis may be stated as:

$$E_1(x_p,\ y_p) = E_2(x_p + \Delta x_{p2},\ y_p + \Delta y_{p2}) \tag{3.2}$$

$$E_2(x_p,\ y_p) = E_1(x_p + \Delta x_{p1},\ y_p + \Delta y_{p1}) \tag{3.3}$$

Defining the disparity vector $\mathbf{r}$,

$$\mathbf{r} = \begin{bmatrix} \Delta x_p \\ \Delta y_p \end{bmatrix} \tag{3.4}$$

the correspondence hypothesis can be expanded in a Taylor series as :

$$E_1 - E_2 = {\mathbf{g}^T}_2 \mathbf{r}_2 + \frac{1}{2} {\mathbf{r}^T}_2 \mathbf{H}_2 \mathbf{r}_2 + \ldots\ldots \tag{3.5}$$

$$E_2 - E_1 = {\mathbf{g}^T}_1 \mathbf{r}_1 + \frac{1}{2} {\mathbf{r}^T}_1 \mathbf{H}_1 \mathbf{r}_1 + \ldots\ldots \tag{3.6}$$

Such an expansion does not require any explicit reference to time, enabling the development of an algorithm that is useful for both stereo and motion image sequences. Additionally, the algorithm performance can be improved by including higher-order terms in the Taylor series approximation. A benefit of this formulation is that it no longer needs the concept of optical flow, a concept that is often stated to be artificial in real imaging devices [4].

Next, the incremental perspective projection relationships at a pixel $(x_p,\ y_p)$ can be found to be :

$$\Delta x_p = \frac{(x_p \Delta z_0 - f \Delta x_0)}{z - z_0 - \Delta z_0}, \quad \Delta y_p = \frac{(y_p \Delta z_0 - f \Delta y_0)}{z - z_0 - \Delta z_0} \tag{3.7}$$

These incremental perspective projection relationships can be combined with either (3.5) or (3.6) to yield depth. An alternate procedure is to assume that an object at (x_p, y_p) in the first image is the same as that observed at (x_p, y_p) in the second image. This assumption leads to $\mathbf{r}_1 = -\mathbf{r}_2$. In this case, adding and subtracting the two expansions and substituting for the incremental perspective projection relationships yield the ranging and range error equations as

$$E_1 - E_2 = \frac{1}{2}\left[\{\frac{\partial E_1}{\partial x_p} + \frac{\partial E_2}{\partial x_p}\}[x_p \Delta z_0 - f\Delta x_0] + \{\frac{\partial E_1}{\partial y_p} + \frac{\partial E_2}{\partial y_p}\}[y_p \Delta z_0 - f\Delta y_0]\right] \frac{1}{z - z_0 - \Delta z_0} + \ldots\ldots \quad (3.8)$$

$$0 = \left[\{\frac{\partial E_1}{\partial x_p} - \frac{\partial E_2}{\partial x_p}\}[x_p \Delta z_0 - f\Delta x_0] + \{\frac{\partial E_1}{\partial y_p} - \frac{\partial E_2}{\partial y_p}\}[y_p \Delta z_0 - f\Delta y_0]\right] \frac{1}{z - z_0 - \Delta z_0} + \ldots\ldots \quad (3.9)$$

The first equation can be used for computing the range $(z - z_0)$ while the second equation is useful for determining the error involved in the range calculation. If the computational resources permit, it may be beneficial to use higher-order terms in this series. Note that these expressions have not been previously obtained in the literature.

The spatial partial derivatives necessary for the computation of range can be obtained using finite difference approximations. Further details on algorithm derivation and implementation is given in the following paper, which was presented at *1990 AIAA Guidance, Navigation, and Control Conference.*

Image Based Range Determination

P. K. A. Menon*and B. Sridhar†
NASA Ames Research Center
Moffett Field, CA 94035

Abstract

Flight vehicles operating at low altitudes such as rotorcraft require range determination schemes for locating the terrain and obstacles. The development of a ranging scheme combining image sequences from vehicle mounted passive imaging sensors and the vehicle motion variables obtained from an on-board inertial navigation system is described. This approach can handle sequences from more than one imaging device. Derivation of the numerical algorithm and the performance results using a laboratory image sequence are given. Other applications of the proposed approach include ranging schemes for autonomous planetary rovers and telerobots.

Introduction

The development of position determination schemes such as inertial navigation systems (INS) and global positioning systems (GPS) has now reached a point where flight vehicles could be located within a few meters with respect to predefined coordinate frames at any point on earth. While the accuracy of these systems are impressive, they cannot provide acceptable solutions to the problem of relative position determination in a changing or uncertain environment. This is due to the fact that it is neither possible nor is it desirable to construct apriori data bases incorporating every detail of the operational environment. Use of conventional imaging Radar or the more recent scanning Laser range finders are obvious solutions to this problem. However, these devices require the radiation of electromagnetic energy which may not be desirable if the on-board power availability is low or if covert missions are contemplated. These factors have motivated the recent research on ranging schemes using passive imaging devices such as conventional or low light level television and infrared imaging sensors. Indeed, passive ranging has emerged as a central issue in nap-of-the-earth helicopter flight guidance[1,2] and autonomous planetary rover mission[3,4,5]. The research reported in this paper is primarily motivated by the current interest in automating the nap-of-the-earth helicopter flight.

In the past, the research activity in the passive ranging problem was largely driven by the robotics discipline[6]. Several approaches to the image based range determination problem have been suggested in recent literature[6-10]. Specifically, Reference 7 outlines the development of an image-based recursive range determination scheme for nap-of-the-earth helicopter flight. In that approach, various features of interest in an image sequence such as the edges or regions of high contrast were used to determine the range to various objects within the field-of-view. Techniques such as this may be termed as *feature-based* ranging to distinguish them from techniques that do not explicitly use any features for range determination. Image-based ranging algorithms that do not explicitly employ features are termed *field-based approaches.*

The number of simultaneous imaging devices employed defines another category of ranging schemes. For example, the task of range estimation using a temporal sequence of images from a

*Member AIAA, School of Aerospace Engineering, Georgia Institute of technology, Atlanta. Mailing Address : FSN Branch, M.S. 210-9, NASA Ames Research Center

†Research Scientist, Member AIAA, FSN Branch, MS 210-9

single imaging device is called the motion ranging problem or the *Cyclopian* ranging problem after the one eyed monster from Greek mythology. On the other hand, schemes employing images from two or more cameras simultaneously are called *Stereo* ranging schemes.

In the robotics literature, ranging tasks appear to include the simultaneous determination of vehicle motion parameters also[6,9-12]. In the case of a single imaging device, this process can be shown to produce an under-determined system and the solution can be obtained only by imposing an additional constraint. In the approach developed in the present work, the vehicle motion parameters and the relative location of the imaging devices are assumed to be known, perhaps from the on-board inertial navigation system. The ranging algorithm uses this data together with the given image sequence to construct the distance to various points within the field-of-view.

Images obtained from sensors mounted on a moving vehicle will exhibit irradiance changes at each pixel. These changes depend on the relative location of various objects, vehicle motion parameters, relative location of the imaging devices, the scene surface reflectance and the location of illumination. If the surface reflectance and the illumination are assumed to remain constant during the imaging process, then the observed image irradiance changes at each pixel are entirely due to the relative location of various objects within the field-of-view and vehicle motion parameters. Additionally, if all the objects within the field of view are assumed fixed with respect to an inertial frame, then the irradiance change at each pixel location is indicative of the range to these objects. In this case, if the vehicle motion parameters and the imaging device constants are known, it is possible to determine the relative location of various points within the field of view. The ensuing analysis will deal with monochromatic images. The data available in such an image is a distribution of irradiance specified as a function of imaging device aperture coordinates. Cartesian image coordinate system will be used here since most imaging devices used currently are rectangular.

All the ranging algorithms reported in the literature have their basis in the so called *correspondence hypothesis*. According to this hypothesis, if it were possible to establish the correspondence between various objects in a pair of images and to measure the displacement of these objects on the image plane, then the perspective projection geometry can be employed for computing the range to these objects. The object displacement in the image plane is sometimes termed as *disparity* in the machine vision literature. In feature-based ranging techniques, the disparity is computed only between a few objects of interest in the image plane. On the other hand, in field based techniques, the disparity is determined at every point in the image plane.

In the field-based scheme discussed in this paper, the correspondence hypothesis is approximated using multi-dimensional Taylor series. In the special case where a temporal image sequence is considered, the lowest degree correspondence equation turns out to be the *optical flow constraint equation*[6,13,14]. In Reference 8, with the assumption that the objects within the field-of-view were fixed, this equation was combined with perspective projection geometry and the inertial navigation system data to derive a direct ranging equation. This ranging equation related the image irradiance spatial partial derivatives with the distance to various objects within the field-of-view. An expression for determining the spatial sampling intervals required for satisfactory performance of the proposed scheme was also derived. The central requirement in using this approach is the availability of spatial and temporal partial derivatives of the image irradiance. An optimal approach for estimating various partial derivatives was synthesized using the Calculus of Variations[15]. The performance of the ranging scheme was then demonstrated using a simulated image sequence.

A field-based range determination technique was outlined in Reference 8. The chief accomplishment there was the derivation of an *Optical Ranging Equation*. This paper presents an improved version of the ranging equation together with a *Range Error Equation*. These expressions are useful for cyclopian image sequences as well as stereo image sequences, and require only the spatial par-

tial derivatives of the image irradiance. The performance of this ranging scheme is demonstrated using a laboratory generated image sequence. Although the algorithm is capable handling the vehicle rotation and translation, the discussions in this paper will be limited to the translational motion case.

The Ranging Scheme

To avoid the complications that can arise while considering an inverted image as is encountered in real imaging devices, the frontal image plane[16] representation will be used for image description. Consider an image coordinate system as shown in Figure 1. In this figure, the major axis of the image plane is designated as the X_p axis and the minor axis is labelled the Y_p axis. The Z_p axis is normal to the image plane, aligned with the axis of the lens. The origin of this image plane coordinate system is located at the center of the aperture. In this coordinate system, an image may be defined as an irradiance distribution $E(x_p, y_p)$ in the X_p, Y_p plane, with E being the irradiance specified on a gray scale at a point x_p, y_p on the image plane. It is assumed in the ensuing analysis that the image irradiance distribution is continuous everywhere in the image plane except at finite number of regions. Thus, for the purposes of the present analysis, effects such as spatial image discretization and gray scale quantization are ignored.

The lens center is assumed to be located at the origin of the vehicle body axis system and the lens axis is aligned along this coordinate system. The vehicle body axis system may be related to an inertial frame through yaw, pitch, roll rotations ψ, θ, ϕ and three translations x_0, y_0, z_0. For the present research, the vehicle attitudes are assumed to be zero and the on-board inertial navigation system is assumed to produce estimates of x_0, y_0, z_0. Let x, y, z be the location of an object within the field-of-view, specified with respect to the inertial frame. The coordinates corresponding to this object on the image plane is x_p, y_p.

The point x_p, y_p corresponding to the object in the image plane is related to its location with respect to the inertial frame x, y, z through various translations and rotations of the vehicle body frame, together with the perspective projection. Effectively, the perspective projection collapses a three dimensional scene into a two dimensional plane. The objective of any ranging scheme is to invert this projection. The development that enables such an inverse transformation is the *correspondence hypothesis.*

The correspondence Hypothesis

The fact which allows the recovery of three dimensional geometry from a two dimensional scene is that if one has at least two views of a scene obtained from different vantage points, then the difference between the location of the corresponding objects in the two image planes is a measure of the range. The apparent object displacement in these two images is called *disparity.* The farther the objects are with respect to the imaging device, the lesser would be the observed disparity. For instance, objects that are very far away would appear at nearly the same location in the two images, while close objects will exhibit a large disparity. If the disparity of the corresponding objects in an image sequence could be measured, then equations for perspective projection could be used to compute the scene depth.

Let $E_1(x_p, y_p)$ be the image of a scene and $E_2(x_p, y_p)$ be another view of the same scene from a different vantage point. Assuming that the two images contain all the objects of interest and that to a large degree, the irradiance of the scene is independent of the vantage points from which the images were obtained, one may write the relations

$$E_1(x_p, y_p) = E_2(x_p + \Delta x_{p2}, y_p + \Delta y_{p2}) \qquad (1)$$

$$E_2(x_p, y_p) = E_1(x_p + \Delta x_{p1}, y_p + \Delta y_{p1}) \qquad (2)$$

The equations (1), (2) state that an object at the point x_p, y_p in the first image will appear at the point $x_p + \Delta x_{p1}, y_p + \Delta y_{p1}$ in the second image. Similarly, an object located at the x_p, y_p point in the second image will appear at the point $xp + \Delta x_{p2}, y_p + \Delta y_{p2}$ in the first image. Here,

$\Delta x_{p1}, \Delta y_{p1}, \Delta x_{p2}, \Delta y_{p2}$ are the disparities between the corresponding objects in the two images. The depth information is encoded in these disparities. It will be demonstrated subsequently that if these quantities can be determined, then the location of the objects with respect to the inertial frame can be computed using perspective projection geometry.

Note that the correspondence hypothesis is not valid at every point on the two images. Depending upon the relative locations of the various objects within the field of view and the relative locations of the imaging devices, the correspondence hypothesis will hold good only in certain regions of the image. This is due to the various occlusions that can arise from the angle of viewing and the camera aperture dimensions. Note that if more than two images of the same scene were available, then it is possible to write correspondence equations such as (1) and (2) between every pair of them.

The correpondence hypothesis may be satisfied in various ways. In general, the task of satisfying the correspondence leads to an $n \times m$ search for $2 \times n \times m$ quantities, with n being the number of pixels per column of the image and m being the number of pixels per row of the image. That is, at each pixel on the image, one searches for the disparities along the two directions between two images. Although additional information is available to limit the search domain, this process is impractical and computationally ill conditioned.

A family of techniques called the feature based methods[7] attempt to decrease the complexity involved in satisfying the correspondence hypothesis by first extracting the features of interest in the image such as edges or regions of high contrast and then establishing correspondence between them. This step reduces the correspondence task by a significant amount. Pixel by pixel correlation has also been employed for satisfying the correspondence hypothesis[17].

In the present paper, an alternate approximation for satisfying the correspondence hypothesis will be advanced. In this technique, the correspondence equations (1) and (2) are first expanded using a Taylors series, to yield

$$E_1(x_p, y_p) - E_2(x_p, y_p) = \frac{\partial E_2(x_p, y_p)}{\partial x_p} \Delta x_{p2} + \frac{\partial E_2(x_p, y_p)}{\partial y_p} \Delta y_{p2} + \ldots\ldots \quad (3)$$

$$E_2(x_p, y_p) - E_1(x_p, y_p) = \frac{\partial E_1(x_p, y_p)}{\partial x_p} \Delta x_{p1} + \frac{\partial E_1(x_p, y_p)}{\partial y_p} \Delta y_{p1} + \ldots\ldots \quad (4)$$

Expressions (3) and (4) relate the irradiance spatial partial derivatives to the irradiance change and the image disparities. The second order terms in these expansions will typically involve the Hessian matrix, while the third term can only be expressed as a tensor. Truncating this series produces various orders of approximation. Clearly, the linear approximation is preferable since it leads to a simple algorithm. Hence, in all that follows, the nonlinear terms in the Taylor series expansion will be dropped.

In the special case where the disparities $\Delta x_p, \Delta y_p$ arise from vehicle motion yielding apparent image velocities u, v at a pixel in the image, i.e. $\Delta x_p = u\Delta t, \Delta y_p = v\Delta t$, the equations (3) and (4) with higher order terms dropped is the *optical flow constraint equation* given by Horn and Schunk[13]. In this case, the velocity components u, v are called the optical flow components. In the present paper, this characterization is avoided because the disparities $\Delta x_{p1}, \Delta y_{p1}, \Delta x_{p2}, \Delta y_{p2}$ may arise from sources other than vehicle motion. Moreover, even in such temporal image sequences, it has been suggested that the optical flow concept is artificial[18]. By adopting the point of view proposed in the foregoing, equations (3) and (4) may be used not only for temporal image sequences such as those encountered in cyclopian vision problems but also for stereo image sequences or images obtained from multiple cameras.

In the next section, it will be demonstrated that these expressions can be used together with the geometry of perspective projection to obtain a ranging equation. That analysis will also lead to the derivation of an equation for computing the range error.

The Optical Ranging Equation

Assuming that the lens center is located at the origin of the vehicle body coordinate system and aligned with it, the relation between an image point x_p, y_p and the position of the corresponding object with respect to the inertial frame x, y, z is given by the perspective projection equations

$$x_p = f(x - x_0)/(z - z_0) \tag{5}$$

$$y_p = f(y - y_0)/(z - z_0) \tag{6}$$

Here, f is the imaging device focal length, and x_0, y_0, z_0 are the location of the vehicle with respect to the inertial frame. Note that if the cameras are offset from the origin of the vehicle body axis system and not aligned with it, additional coordinate transformations will have to be incorporated in the analysis.

Next consider a translation of the imaging device by a small distance $\Delta x_0, \Delta y_0, \Delta z_0$ in the positive direction. These variables could also be interpreted as the displacement of the second imaging device relative to the first as in stereo ranging schemes. It is assumed that the location of the object point x, y, z remains unchanged during this motion. In this case, the object located at the point x, y, z in the scene, and observed at the point x_p, y_p in the previous image plane would now appear at the point $x_p + \Delta x_p, y_p + \Delta y_p$ on the image plane, i. e

$$x_p + \Delta x_p = f(x - x_0 - \Delta x_0)/(z - z_0 - \Delta z_0) \tag{7}$$

$$y_p + \Delta y_p = f(y - y_0 - \Delta y_0)/(z - z_0 - \Delta z_0) \tag{8}$$

Subtracting (5), (6) from the expressions (7), (8), results in

$$\Delta x_p = \frac{(x_p \Delta z_0 - f \Delta x_0)}{z - z_0 - \Delta z_0} \tag{9}$$

$$\Delta y_p = \frac{(y_p \Delta z_0 - f \Delta y_0)}{z - z_0 - \Delta z_0} \tag{10}$$

Note that if the direction of motion is changed, the resulting displacement in the image plane can be computed by changing the signs of the variables $\Delta x_0, \Delta y_0, \Delta z_0$.

Expressions (9) and (10) may next be used to eliminate the variables $\Delta x_{p1}, \Delta y_{p1}, \Delta x_{p2}, \Delta y_{p2}$ in the correspondence equation pair (3), (4). At each pixel location x_p, y_p this yields :

$$E_1 - E_2 = \left\{ \frac{\partial E_2}{\partial x_p}[x_p \Delta z_0 - f \Delta x_0] + \frac{\partial E_2}{\partial y_p}[y_p \Delta z_0 - f \Delta y_0] \right\} \frac{1}{z - z_0 - \Delta z_0} \tag{11}$$

$$E_2 - E_1 = -\left\{ \frac{\partial E_1}{\partial x_p}[x_p \Delta z_0 - f \Delta x_0] + \frac{\partial E_1}{\partial y_p}[y_p \Delta z_0 - f \Delta y_0] \right\} \frac{1}{z - z_0 - \Delta z_0} \tag{12}$$

Adding and subtracting the expressions (11) and (12), one may rewrite these two equations as

$$E_1 - E_2 = \frac{1}{2}\left[\{ \frac{\partial E_1}{\partial x_p} + \frac{\partial E_2}{\partial x_p} \}[x_p \Delta z_0 - f \Delta x_0] + \{ \frac{\partial E_1}{\partial y_p} + \frac{\partial E_2}{\partial y_p} \}[y_p \Delta z_0 - f \Delta y_0] \right] \frac{1}{z - z_0 - \Delta z_0} \tag{13}$$

$$0 = \frac{1}{2}\left[\{ \frac{\partial E_1}{\partial x_p} - \frac{\partial E_2}{\partial x_p} \}[x_p \Delta z_0 - f \Delta x_0] + \{ \frac{\partial E_1}{\partial y_p} - \frac{\partial E_2}{\partial y_p} \}[y_p \Delta z_0 - f \Delta y_0] \right] \frac{1}{z - z_0 - \Delta z_0} \tag{14}$$

The expression (13) is the *Optical Ranging equation* relating the irradiance difference at the same pixel locations in the two images with the spatial partial derivatives in the image planes and the scene depth. This expression has not been previously reported.

The expression (14), on the other hand, predicts the degree of error in approximating the correspondence equations using the first two terms of the Taylor series expansion. This is a consequence of the fact that if the image irradiance distribution was indeed linear, the spatial partial derivatives

will remain the same in both images E_1 and E_2. Interestingly, the expression (14) also reveals that for the same contrast level, image-based range estimation is more accurate for objects that are near. Assuming that the irradiance differences $(E_1 - E_2)$ are nonzero, the expression (13) can be manipulated to the form

$$z = z_0 + \Delta z_0 + \left[\{\frac{\partial E_1}{\partial x_p} + \frac{\partial E_2}{\partial x_p}\}[x_p \Delta z_0 - f\Delta x_0] + \{\frac{\partial E_1}{\partial y_p} + \frac{\partial E_2}{\partial y_p}\}[y_p \Delta z_0 - f\Delta y_0]\right] \frac{1}{2(E_1 - E_2)} \quad (15)$$

Expression (15) can be used to compute the scene depth z if the image irradiances E_1, E_2, camera parameters $f, x_p, y_p, \Delta x_0, \Delta y_0, \Delta z_0$ and the spatial partial derivatives $\partial E_1/\partial x_p$, $\partial E_1/\partial y_p$, $\partial E_2/\partial x_p$, $\partial E_2/\partial y_p$ were available.

Next, the x, y coordinates can be determined using the inverse of the perspective projection equations together with the optical ranging equation as follows.

$$x = x_0 + \frac{x_p \Delta z_0}{f} + \left[\{\frac{\partial E_1}{\partial x_p} + \frac{\partial E_2}{\partial x_p}\}[x_p \Delta z_0 - f\Delta x_0] + \{\frac{\partial E_1}{\partial y_p} + \frac{\partial E_2}{\partial y_p}\}[y_p \Delta z_0 - f\Delta y_0]\right] \frac{x_p}{2f(E_1 - E_2)} \quad (16)$$

$$y = y_0 + \frac{y_p \Delta z_0}{f} + \left[\{\frac{\partial E_1}{\partial x_p} + \frac{\partial E_2}{\partial x_p}\}[x_p \Delta z_0 - f\Delta x_0] + \{\frac{\partial E_1}{\partial y_p} + \frac{\partial E_2}{\partial y_p}\}[y_p \Delta z_0 - f\Delta y_0]\right] \frac{y_p}{2f(E_1 - E_2)} \quad (17)$$

In the preceding development, it is important to note that anomalies of various kinds can arise while applying the ranging equation to real image sequences. This is because of the fact that this development assumes that the first partial derivatives exist and that at least locally, a linear approximation is valid for the image irradiance. Additionally, in regions of near uniform irradiance, or in regions where the spatial irradiance gradients are discontinuous, the expressions (15)-(17) may not have a solution. It is assumed here that such points can be edited-out of the image sequence by the use of an appropriate threshold.

The Computational Algorithm

The first step in the implementation of the ranging algorithm is the computation of image spatial partial derivatives. Several techniques are available for computing partial derivatives in the literature[6]. A prominent one amongst them is the Fourier transform technique. Although fast algorithms are available for their computation, the calculations are far from routine. In Reference 8, a partial derivative estimation scheme based on optimal control theory was advanced. Since this technique has not been completely evaluated, a simple central differencing scheme will be used to compute the spatial partial derivatives in the present research.

According to the central difference scheme, if i is the pixel location along the x_p direction and j the pixel location along the y_p direction, with the distance between pixels being $\delta x, \delta y$, the spatial partial derivatives are can be approximated by the relations

$$\frac{\partial E}{\partial x_p} \approx \frac{E(i+1) - E(i-1)}{2\delta x} \quad (18)$$

$$\frac{\partial E}{\partial y_p} \approx \frac{E(j+1) - E(j-1)}{2\delta y} \quad (19)$$

The partial derivative estimates given by the expressions (18) and (19) are rather crude, and do not exhibit any noise attenuating characteristics at all. Research on more advanced partial derivative computation schemes are currently underway. Once the spatial partial derivatives are computed, equations (15), (16), (17) can be used to determine the location of various objects within the field-of-view.

A block diagram of the ranging algorithm is shown in Figure 2. Two views of the candidate scene are first used to compute the spatial derivatives of the images. Next, the second image is subtracted from the first to obtain irradiance changes at each pixel. In the regions where the irradance

change is close to zero, the scene depth is not computed, since the ranging equation is not valid in these regions. Instead, these points are assigned the maximum scene depth. The spatial gradients and the irradiance changes are then combined with imaging device coordinates in the given inertial frame $x_0, y_0, z_0, \Delta x_0, \Delta y_0, \Delta z_0$ to obtain the x, y, z coordinates.

When a new image becomes available, the first image in the sequence is dropped and these calculations are repeated. In some image sequences, the estimated range can be inaccurate due to noise, digitization errors or computational errors. In this situation, one may collect several images of the scene from the same vantage point. These images may then be averaged to yield relatively noise-free range estimates. An alternate approach would be to apply a defocusing operator[6] to the image sequence before carrying out the range calculations.

Results and Discussions

Several laboratory image sequences were used for demonstrating the performance of the ranging algorithm. A pair of images from this laboratory image sequence is shown in Figures 3 and 4. The scene consisted of a dark wall with a table in the foreground. Two computer monitors, an H shaped object and three pencils were then placed on this table. This image sequence was obtained using a CCD (Charge Coupled Device) camera with a field-of-view of about 45 degrees and a focal length of about 6 mm. The gray scale consisted of 256 levels corresponding to 8 bit digitization of the CCD image. The CCD output was digitized and processed on a workstation.

Gray scale coded spatial partial derivatives corresponding to the images in Figure 3 and 4 are shown in Figures 5 and 6. Note that these are the average of the irradiance partial derivatives in the two images. In order to produce this representation, the gradients are first normalized such that they are in the range ± 128. The result is then biased by 128 such that the level black represents the maximum negative gradient, while the white level represents the maximum positive gradient. Figure 7 gives the irradiance difference between two images shown in Figure 3 and 4. Once again, the differences are normalized and scaled such that the largest negative value would correspond to the black level and the largest positive value would correspond to the white level. Based on the image digitizer characteristics, in regions where the irradiance differences were smaller than 15 levels of gray, range computations were not carried out.

Range calculations were next carried out using this image irradiance data. Although a 3-D representation of the result was desirable, no satisfactory computer packages were available. Instead, the range data was once again coded in terms of a gray scale. Figure 8 shows the result of applying the ranging equation to the present image sequence. In this figure, objects that are at zero range are represented by the black color, while the points that are far, or the points at which range data is not available are indicated in white. It may observed from this figure that the relative location of various objects in the image sequence are clearly recovered. The range computations appear sparse because of the threshold employed at the input. Lowering this threshold will result in a denser range field, but will also contribute to several inaccurate range values.

To a degree, these anomalies can be corrected by decreasing the image sampling interval. Alternately, one may either use an improved partial derivative estimation scheme or implement a ranging algorithm based on higher-order correspondence equation. The present investigation reveals that the proposed ranging scheme works satisfactorily in laboratory image sequences. Work is currently underway to apply this technique to image sequences obtained from a helicopter flight.

Conclusions

An image-based passive navigation scheme for rotorcraft was described. This scheme estimates the scene depth using irradiance differences and spatial partial derivatives of an image sequence together with imaging device parameters. Performance of the ranging algorithm was demonstrated using a laboratory image sequence.

The contributions of the present research are the following:

- Development of an image correspondence equation valid for both cyclopian and stereo ranging schemes.
- Derivation of the *Optical Ranging Equation* combining the vehicle and imaging device parameters with irradiance differences and the spatial irradiance gradients.
- Derivation of a *Range Error Equation* to aid in evaluating the results generated by the ranging equation.
- Demonstration of the performance of this algorithm using a laboratory image sequence.

Improvements on this ranging algorithm is an on-going research activity.

Acknowledgements

The research support for the first author under NASA Cooperative Agreement NCC2-575 from Ames Research Center is gratefully acknowledged.

The ranging algorithm was implemented on a SUN workstation by Mr. Chima Njaka. The image sequences and the range data display software used in this paper were generated by Mr. R. Soursa of NASA Ames Research Center.

We thank the FSN Branch Chief Dr. Dallas Denery for his interest in this work.

References

[1] Cheng, V. H. L., and Sridhar, B., "Considerations for Automated Nap-of-The-earth Rotorcraft Flight", *Proceedings of the 1988 American Control Conference*, Atlanta, GA, June 15-17, 1988.

[2] Cheng, V. H. L., "Concept Development of Automatic Guidance for Rotorcraft Obstacle Avoidance", *IEEE Transactions on Robotics and Automation*, Vol. 6, No. 2, April 1990, pp. 252-257.

[3] Baker, K., "MRSR- Managing the Landing Hazards", *Mars Rover Sample Return Scale Workshop* Final Report, Pasadena, CA, June 8-9, 1988.

[4] de Vries, J. P., and Norton, H. N., "A Mars Sample Return Mission Using a Rover for Sample Aquisition", *The Case for Mars II*, C. P. McKay (Ed.), *American Astronautical Society*, 1985.

[5] Hall, E. L., "Vision Sensing Techniques in Aeronautics and Astronautics", in *Machine Intelligence and Autonomy for Aerospace Systems*, E. Heer and H. Lum (eds.) , Vol 115 *Progress in Astronautics and Aeronautics*, American Institute of Aeronautics and Astronautics, 1989.

[6] Horn, B. K. P., *Robot Vision*, McGraw Hill, New York, 1986.

[7] Sridhar, B., and Phatak, A. V., "Simulation and Analysis of Image-Based Navigation System for Rotorcraft Low-Altitude Flight", *AHS National Specialist's Meeting on Automation Applications of Rotorcraft*, Atlanta, GA., April 4-6, 1988.

[8] Menon, P. K. A., and Sridhar, B.,"Passive Navigation Using Image Irradiance Tracking", *AIAA Guidance, Navigation, and Control Conference* , August 14-16, 1989, Boston, MA.

[9] Negahdaripour, S., and Horn, B. K. P., "Direct Passive Navigation", *IEEE Transactions on Pattern Analysis and Machine Intelligence*, Vol. PAMI-9, Jan. 1987, pp. 168-176.

[10] Skifstad, K. and Jain, R.,"Range Estimation from Intensity Gradient Analysis", *Machine Vision and Applications*, Vol. 2, 1989, pp. 81-102.

[11] Hildreth, E. C., "Computations Underlying the Measurement of Visual Motion", *Artificial Intelligence*, Vol. 23, 1984, pp. 309-354.

[12] Aggarwal, J. K., and Nandhakumar, N.,"On the Computation of Motion from Sequences

of Images - A Review", *Proceedings of the IEEE*, Vol. 76, No. 8, August 1988, pp. 917-935.

[13] Horn, B. K. P., and Schunck, B. G., "Determining Optical Flow", *Artificial Intelligence*, Vol. 17, 1981, pp. 185-203.

[14] Schunk, B. G.,"The Image Flow Constraint Equation", *Computer Vision, Graphics, and Image Processing*, Vol. 35, 1986, pp. 20-46.

[15] Weinstock, R., *Calculus of Variations with Applications*, Dover, New York, 1983.

[16] Duda, R. O., and Hart, P. E., *Pattern Classification and Scene Analysis*, John Wiley, New York, 1973.

[17] Barniv, Y.,"Application of Velocity Filtering to Optical Flow Calculations", NASA TM 102802, August 1990.

[18] Bertero, M., Poggio, T. A., and Torre, V.,"Ill-Posed Problems in Early Vision", *Proceedings of the IEEE*, Vol. 76, No. 8, August 1988 pp. 869-889.

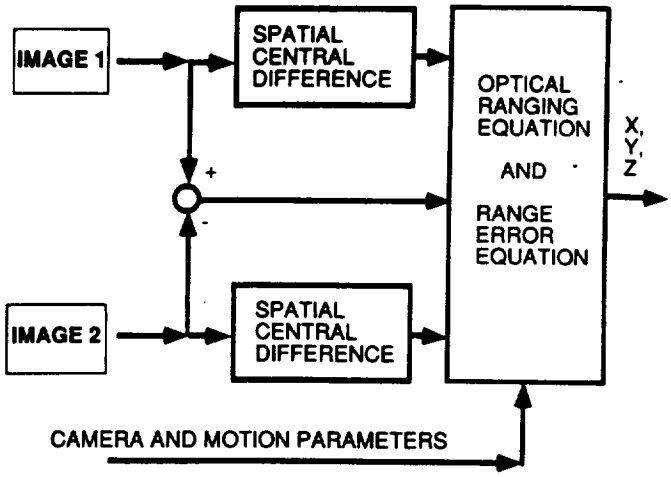

Fig. 2. Image-Based Passive Ranging Scheme

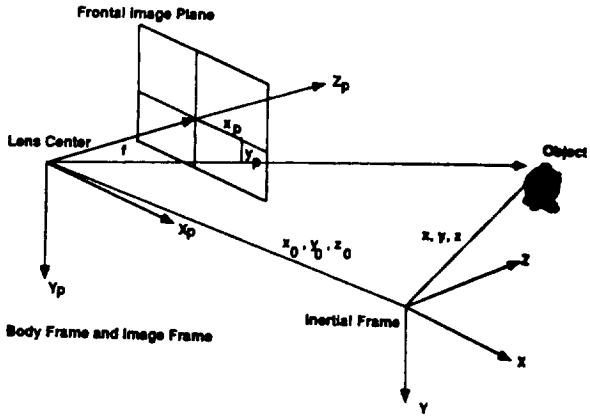

Fig. 1. The Coordinate Systems

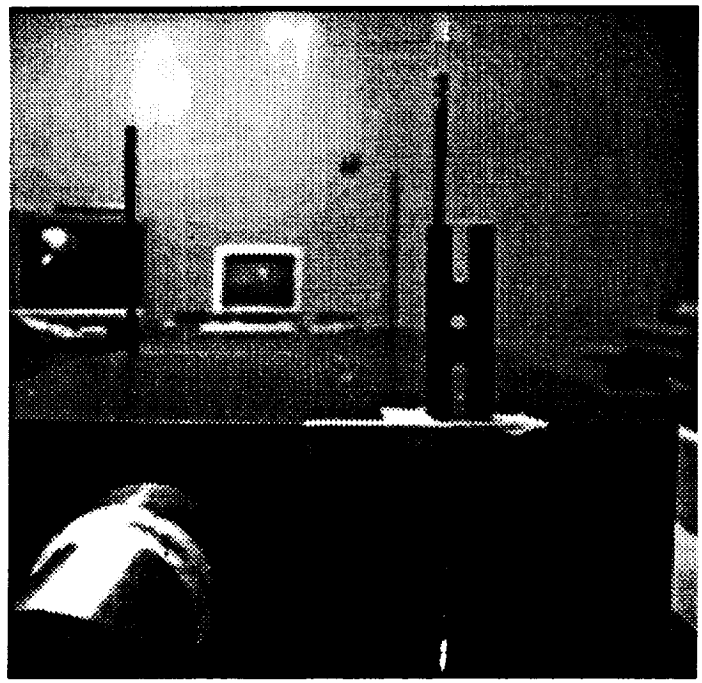

Fig. 3. First Image of a Laboratory Scene

Fig. 4. Second Image of the Laboratory Scene

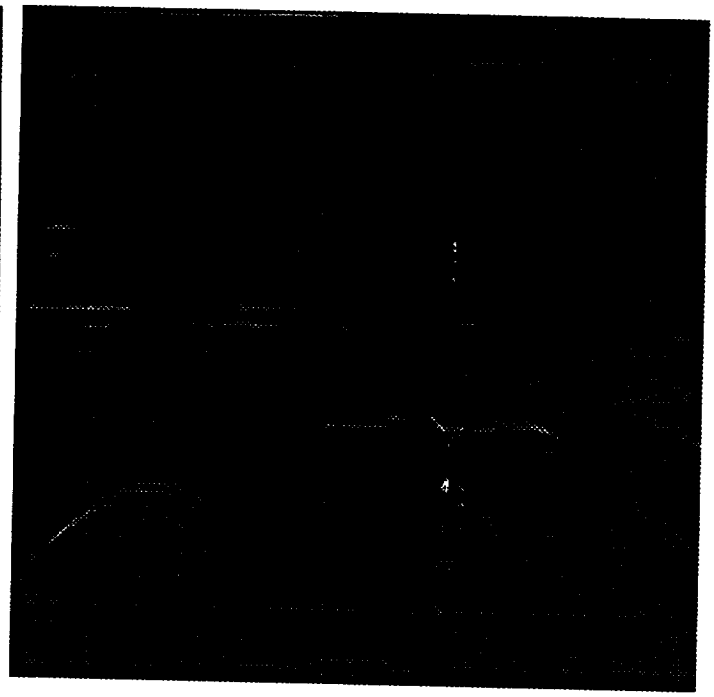

Fig. 6. Gray Scale Coded Spatial Partial Derivative of the Laboratory Scene in the Vertical Direction

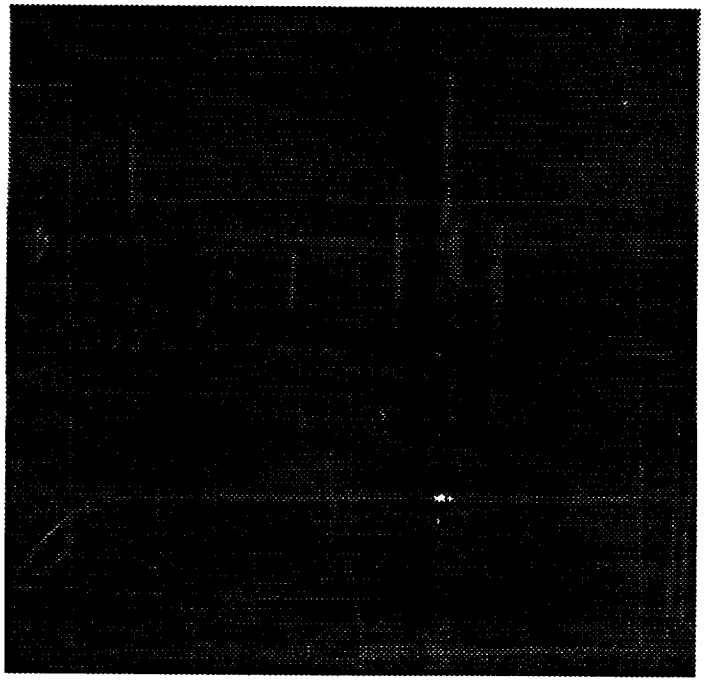

Fig. 5. Gray Scale Coded Spatial Partial Derivative of the Laboratory Scene in the Horizontal Direction

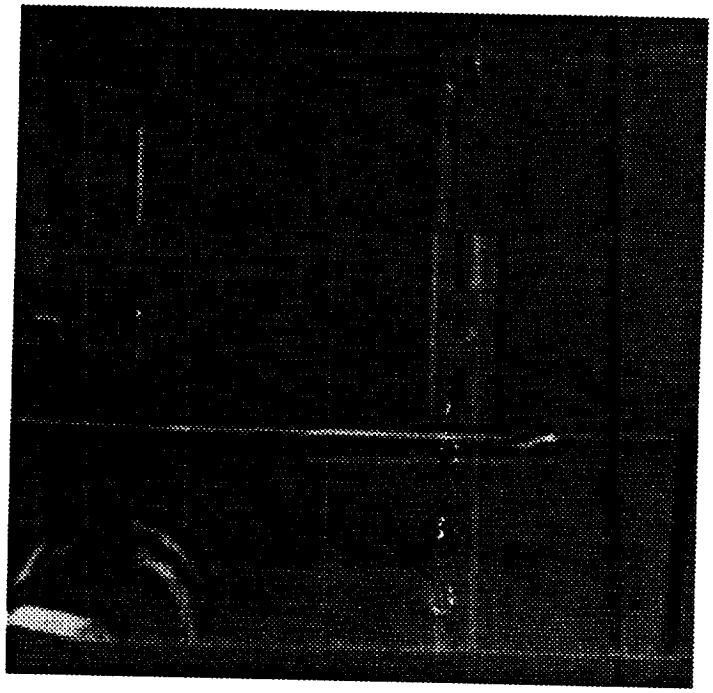

Fig. 7. Gray Scale Coded Irradiance Difference Between the Two Images at Each Pixel

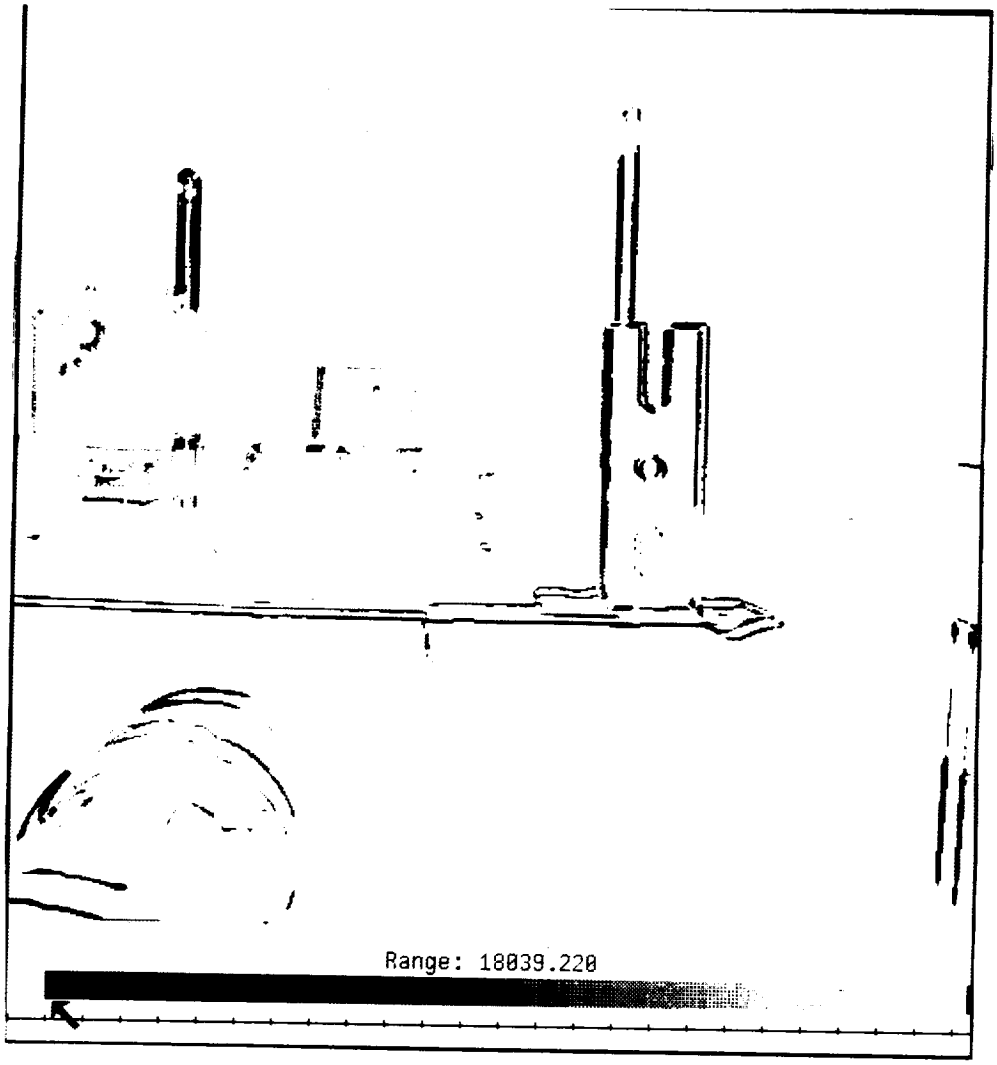

Fig. 8. Gray Scale Coded Range Estimate to Various Objects in the Field-of-View

4. A Partial Derivative Estimation Method and its use in Vision-Based Ranging

In the previous chapter it was demonstrated that vision-based ranging can be accomplished if the image irradiance spatial partial derivatives were known together with camera parameters. Due to the noise encountered in real image sequences, it is desirable to carry out noise attenuation together with partial derivative estimation. Techniques discussed in the literature for noise attenuated partial derivative estimation are all frequency domain based [2]. Such an approach is inconvenient because the complete image must be available before the partial derivatives can be determined.

An alternative approach permitting derivative computation as a part of image collection was next pursued. The approach employs an approximation popular in the study of linear partial differential equations arising in mechanical vibrations. The approximation involves the factoring of a function of two variables as a product of two functions that vary as a function of one independent variable each. This factorization reduces a partial differential equation into a set of ordinary differential equation. Thus, the partial derivative estimation problem can be expressed as a set of total derivative estimation problems for which solutions already exist. Additionally, by employing causal estimators, the partial derivative computation can be carried out as the image data is being collected. Combining this partial derivative estimation scheme with the ranging equation developed in Chapter 3 then results in a fast method for vision-based ranging. A paper describing this research was presented at the *1991 SPIE Symposium on Optical Engineering and Photonics in Aerospace Sensing*, and is given in this chapter.

Up to this point, the vision-based ranging formulations assumed that the camera orientation in the pair of images were the same. In practical situations, it is important to include both the translational and rotational displacements of the imaging devices. Such an extension is nontrivial since additional reference frames that may be translating and rotating with respect to the camera frame need to be included in the analysis. A paper discussing these extensions was presented at the *1991 AIAA Guidance, Navigation, and Control Conference* and is also included in this chapter.

A Fast Algorithm for Image-Based Ranging

P. K. A. Menon*, G. B. Chatterji† and B. Sridhar‡

Mail Stop 210-9, NASA Ames Research Center

Moffett Field, CA 94035

ABSTRACT

Image-based ranging has emerged as a critical issue in the low altitude operation of flight vehicles such as rotorcraft and planetary landers. These flight regimes require ranging systems for recovering the geometry of the terrain and obstacles for use with guidance algorithms. The development of a ranging equation combining image irradiance together with various order spatial partial derivatives and the vehicle motion parameters is discussed. The ranging equation is in the form of a polynomial in scene depth. Two-dimensional linear filters are then used to compute the coefficients of this polynomial to result in a fast image-based ranging algorithm. Performance of the algorithm is demonstrated using laboratory images.

1 INTRODUCTION

The problem of determining the position of various obstacles in a changing or uncertain environment is central to the development of guidance policies for autonomous vehicles. Imaging Radar and scanning

*School of Aerospace Engineering, Georgia Institute of technology, Atlanta. Mailing Address : MS 210-9, NASA Ames Research Center

†Member of the Professional Staff, Sterling Software

‡Research Scientist, FSN Branch

Laser range finders are two direct solutions to this problem. However, these devices require the radiation of electromagnetic energy which may not be desirable if the on-board power availability is low or if covert missions are contemplated. Recent research on ranging schemes using passive imaging devices such as conventional or low light level television and infra-red imaging sensors is motivated by these factors. Specifically, the passive ranging problem is considered a critical issue in nap-of-the-earth helicopter flight guidance[1,2] and autonomous planetary rover mission[3,4,5].

Most of the research activity in the image-based ranging problem is driven by the Robotics discipline[6]. Recently, several ranging approaches have been suggested in the literature[6-11]. These techniques are based on the intuitive notion that the images obtained from sensors mounted on a moving vehicle will exhibit changes in irradiance at each pixel location as a function of time. These changes depend on the relative location of various objects in the field-of-view, vehicle motion parameters, location of the imaging devices with respect to the vehicle, the scene surface reflectance and the location of illumination. If the surface reflectance and the illumination are assumed to remain constant during the imaging process, then the observed image irradiance changes at each pixel can be related to the location of various objects within the field-of-view and the camera-vehicle parameters. Additionally, if all the objects within the field of view are assumed fixed with respect to an inertial frame, the irradiance change at each pixel location can be related to the range to these objects. In this case, if the vehicle motion parameters and the imaging device constants are known, the relative location of various points within the field of view can be determined. The ensuing analysis will deal with monochromatic images. A Cartesian image coordinate system will be used here since most imaging devices used currently are rectangular.

In the Robotics literature, ranging tasks appear to include the simultaneous determination of vehicle motion parameters also[6,9,12]. If a single imaging device is used, this process produces an under-determined

system of equations and the solution can be obtained only by imposing an additional constraint. In the present work, the vehicle motion parameters and the relative location of the imaging devices are assumed to be known from an inertial navigation system on-board the vehicle. The ranging scheme uses this data together with the given image sequence to construct the distance to various points within the field-of-view.

Image-based ranging schemes use the correspondence between various objects in an image sequence to determine the *disparities*. These disparities can be used together with perspective projection equations to obtain the range. In this paper, the correspondence problem is first satisfied using a multi-dimensional Taylor series involving disparities between the two images. Next, the disparities are eliminated in favor of the vehicle-camera motion parameters and scene depth using the perspective projection relationships. This process yields a polynomial for the scene depth at every pixel location. This equation is referred to as the *Optical Ranging Polynomial* in the present work. This equation may be thought of as the generalization of the optical ranging equation discussed in Reference 11. The coefficients of the optical ranging polynomial depend on the irradiance difference between the two images and various order irradiance spatial partial derivatives. A system of two-dimensional linear filters are next synthesized to compute the required partial derivatives. Due to the simplicity in implementing these filters, the partial derivatives can be computed at a high data rate, often faster than the video frame rates. The result is a fast image-based ranging algorithm. The performance of the ranging scheme is demonstrated using laboratory images.

2 THE RANGING SCHEME

To maintain consistency with the existing literature, the frontal image plane[13] representation will be used for image description. The various coordinate systems employed in this paper are illustrated in Figure 1. This figure shows the image coordinate system together with the vehicle body coordinate system and the inertial coordinate system. The origin of the image plane coordinate system is located at the center of

the aperture. An image is defined as an irradiance distribution $E(x_p, y_p)$ in this coordinate system, with E being the irradiance specified in a gray scale at a point x_p, y_p on the image plane. The ensuing analysis assumes that the image irradiance distribution is continuous everywhere in the image plane except at finite number of regions. This is a reasonable assumption because the underlying imaging process involves integration, a process that smoothens out the discontinuities. For the purposes of the present analysis, errors arising out of spatial image discretization and gray scale quantization will be ignored.

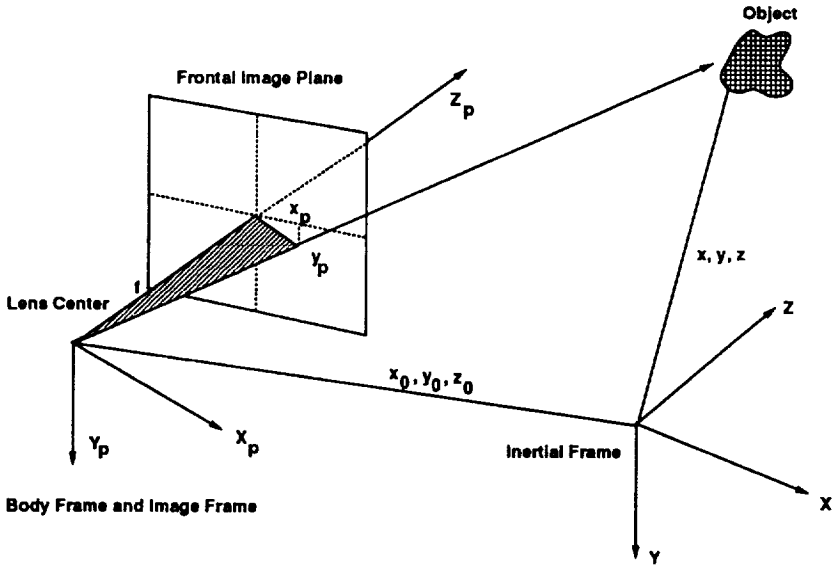

Figure 1: The Coordinate System

To simplify the development, the lens center is assumed to be located at the origin of the vehicle body axis system and the lens axis is aligned along this coordinate system. Moreover, the analysis will assume only pure translational motions for the camera. Although the procedure to include the rotational motion is rather direct, it will be developed in a more complete detail elsewhere. The on-board inertial navigation system is assumed to produce accurate estimates of camera-vehicle displacement x_0, y_0, z_0. In the case of stereo camera arrangement, it is assumed that the relative displacement between the two cameras is also accurately known. Let x, y, z be the location of an object within the field-of-view, specified with respect

to the inertial frame. The coordinates corresponding to this object on the image plane is x_p, y_p. If the camera moves to a new position $x_0 + \Delta x_0, y_0 + \Delta y_0, z_0 + \Delta z_0$ the object point will move to a new position $x_p + \Delta x_p, y_p + \Delta y_p$ in the image plane. The apparent displacement in the image plane caused by the camera motion $\Delta x_p, \Delta y_p$ are called the *disparity*. The disparity depends on the range to the object and the camera parameters. The objective of the ranging scheme is to use this information to determine the object location x, y, z. If the disparity of a corresponding object in an image pair is known, then the equations for perspective projection can be used to compute the scene depth. While several distinct approaches are available for disparity determination[6,7], the present work will employ a multi-dimensional Taylor series expansion as the basis for establishing correspondence.

Let $E_1(x_p, y_p)$ and $E_2(x_p, y_p)$ be a pair of images of a scene obtained from two different different vantage points. Assuming that these two images contain all the objects of interest and that to a large degree, the perceived irradiance of the scene is independent of the camera location, the correspondence hypothesis can be expressed as

$$E_1(x_p, y_p) = E_2(x_p + \Delta x_p, y_p + \Delta y_p) \tag{1}$$

$$E_2(x_p, y_p) = E_1(x_p - \Delta x_p, y_p - \Delta y_p) \tag{2}$$

Here, $\Delta x_p, \Delta y_p$ are the disparities between the corresponding objects in the two images. The depth information is encoded in these disparities.

Note that the correspondence hypothesis expressed in (1) and (2) are valid only in a limited sense, and not for all points in the two images. This is due to the various occlusions that can arise from the angle of viewing and the camera aperture dimensions. Note that equations such as (1), (2) can be written for

any number of images, provided the occluding objects are edited out.

In the present research, the expressions (1) and (2) will be expanded in a Taylor series to enable the computation of the disparities. Such an expansion treats disparities as perturbations about specified pixel locations. The error involved in such an approximation depends on the number of terms included. Define the disparity vector $\mathbf{r}$, the irradiance gradient vector $\mathbf{g}$, and the irradiance Hessian matrix $\mathbf{H}$ as

$$\mathbf{r} = \begin{bmatrix} \Delta x_p \\ \Delta y_p \end{bmatrix}, \quad \mathbf{g} = \begin{bmatrix} \partial E/\partial x_p \\ \partial E/\partial y_p \end{bmatrix}, \quad \mathbf{H} = \begin{bmatrix} \partial^2 E/\partial {x_p}^2 & \partial^2 E/\partial x_p \partial y_p \\ \partial^2 E/\partial y_p \partial x_p & \partial^2 E/\partial {y_p}^2 \end{bmatrix} \tag{3}$$

Equations (1) and (2) can now be expanded using a multi-dimensional Taylor's series to yield

$$E_1 - E_2 = \mathbf{g}_2\mathbf{r} + \frac{1}{2}\mathbf{r}^T\mathbf{H}_2\mathbf{r} + ... \tag{4}$$

Similarly,

$$E_2 - E_1 = -\mathbf{g}_1\mathbf{r} + \frac{1}{2}\mathbf{r}^T\mathbf{H}_1\mathbf{r} - ..... \tag{5}$$

Expressions (3) and (4) relate the irradiance spatial partial derivatives to the irradiance change and the image disparities. It is awkward to write the third term in this series using the vector-matrix notation because it contains a Tensor. In all that follows, a lower case bold face letter will denote a vector, while an upper case bold face letter will be used to denote a matrix.

In the special case where the disparities $\Delta x_p, \Delta y_p$ arise from vehicle motion yielding apparent image velocities u, v at a pixel in the image, i.e. $\Delta x_p = u\Delta t, \Delta y_p = v\Delta t$, the equations (4) and (5) with just the first term on the right hand side is the *optical flow constraint equation*[14]. In this case, the apparent image velocity components u, v are called the optical flow velocities. This characterization is avoided here

because the disparities $\Delta x_p, \Delta y_p$ may arise from other sources also, stereo camera arrangement being an example. By adopting the point of view proposed in the foregoing, equations (3) and (4) may be used not only for temporal image sequences such as those encountered in Cyclopean vision problems, but also for stereo image sequences or images obtained from multiple cameras.

Adding and subtracting the expressions (4) and (5) results in

$$E_1 - E_2 = \frac{1}{2}\Big[\mathbf{g}_1 + \mathbf{g}_2\Big]\mathbf{r} + \frac{1}{4}\mathbf{r}^T\Big[\mathbf{H}_2 - \mathbf{H}_1\Big]\mathbf{r} + ... \tag{6}$$

$$0 = \Big[\mathbf{g}_2 - \mathbf{g}_1\Big]\mathbf{r} + \frac{1}{2}\mathbf{r}^T\Big[\mathbf{H}_1 + \mathbf{H}_2\Big]\mathbf{r} + ... \tag{7}$$

In the following, it will be demonstrated that these expressions can be used together with the geometry of perspective projection to obtain a ranging equation. The analysis will also lead to the derivation of an equation for computing the range error.

The disparity vector $\mathbf{r}$ from equations (6) and (7) can next be eliminated in favor of other known quantities and the scene depth as follows. Assuming that the lens center is located at the origin of the vehicle body coordinate system and aligned with it, and that the camera and the vehicle are permitted to have only translational motions, the relationship between an image point x_p, y_p and the position of the corresponding object with respect to the inertial frame x, y, z are given by the perspective projection equations

$$x_p = f(x - x_0)/(z - z_0), y_p = f(y - y_0)/(z - z_0) \tag{8}$$

Here, f is the imaging device focal length, and x_0, y_0, z_0 coordinates of the vehicle location with respect to the inertial frame. It is assumed that the camera focal length and the components of the vehicle position

vector x_0, y_0, z_0 are known.

Next consider a translation of the camera/vehicle by a small distance $\Delta x_0, \Delta y_0, \Delta z_0$ in a positive sense. Note that $\Delta x_0, \Delta y_0, \Delta z_0$ may also be interpreted as the displacement of the second imaging device relative to the first as in a stereo arrangement. It is assumed that the location of the object point x, y, z remains unchanged during this motion. In this case, the object located at the point x, y, z in the scene, and observed at the pixel location x_p, y_p in the previous image plane would now appear at the point $x_p + \Delta x_p,\ y_p + \Delta y_p$ on the image plane. Using this fact, the disparity vector can be obtained as

$$\mathbf{r} = \delta \begin{bmatrix} (x_p \Delta z_0 - f \Delta x_0) \\ (y_p \Delta z_0 - f \Delta y_0) \end{bmatrix}, \quad \delta = \frac{1}{(z - z_0 - \Delta z_0)} \tag{9}$$

Note that the disparity vector is linear in the inverse of the scene depth. For notational convenience, the inverse of the scene depth at a pixel location is denoted by the symbol δ. The quantities within the parenthesis in the disparity vector can be computed if the vehicle-camera displacement, pixel location and the camera focal length are known. Substituting for $\mathbf{r}$ from (9) in the Taylor series approximation (6), (7) yields two polynomials

$$E_1 - E_2 = a_1\ \delta + a_2\ \delta^2 + a_3\ \delta^3 + a_4\ \delta^4 + ... \tag{10}$$

$$0 = b_1\ \delta + b_2\ \delta^2 + b_3\ \delta^3 + b_4\ \delta^4 + ... \tag{11}$$

The polynomial coefficient a_1 depends on the vehicle motion parameters and the first spatial partial derivatives of the images. The coefficient a_2 depends on the vehicle motion parameters and the second spatial partial derivatives of the two images and so on. The coefficients of the second polynomial, on the other hand, depends upon the differences in various order spatial partial derivatives in the two images. The

second equation may be thought of as a truncation error equation for the first polynomial. For example, if all but the first term is dropped in right hand side of equation (10), then the underlying assumption is that the image irradiance varies linearly in the spatial direction. In this case, the coefficient b_1 in the polynomial (11) is proportional to the difference between the spatial partial derivatives in the two images. If the two partial derivatives were exactly equal, then the error in range calculation is also zero. On the other hand, if they are not equal, the first term in polynomial (11) will not be zero. The magnitude of this term is then proportional to the error in using the first-order Taylor series approximation for satisfying the correspondence hypothesis.

The solution to the polynomial (10) yields the inverse of the scene depth δ at a particular pixel location. These equations have not been previously derived in the literature. In all that follows, the polynomial (10) will be referred to as the *Optical Ranging Polynomial* and the polynomial (11) will be termed as the *Optical Ranging Error Polynomial.* The optical ranging polynomial and the ranging error polynomial can be formulated at every pixel location in an image. Various numerical techniques can then be used to obtain δ at every pixel location in the image. This can done in closed-form for up to fourth degree approximation. If it is desired to use ranging polynomial of fifth degree or more, one of the several well known polynomial root finders can be used to obtain the solution.

Once the inverse of the scene depth δ at a particular pixel is computed using the optical ranging polynomial, the inertial coordinates of the corresponding object can be found as

$$x = \frac{x_p}{f}(\frac{1}{\delta} + \Delta z_0) + x_0, \quad y = \frac{y_p}{f}(\frac{1}{\delta} + \Delta z_0) + y_0, \quad z = \frac{1}{\delta} + z_0 + \Delta z_0 \tag{12}$$

It is important to observe that various kinds of anomalies can arise while using the ranging polynomial. For example, the assumption that various order partial derivatives exist everywhere in the image

is sometimes violated. Additionally, in regions of near uniform irradiance, or in regions where the spatial irradiance gradients are discontinuous, the polynomials (10)-(11) may not have a solution. To a certain degree, it is possible to eliminate such regions by using an appropriate threshold.

3 The Computational Algorithm

The first step in the implementation of the optical ranging polynomial is the computation of the polynomial coefficients $a_1, a_2, ...a_n$ and $b_1, b_2, ...b_n$. These coefficients depend on the various order spatial partial derivatives of the two images and the camera-vehicle motion parameters. In this work, the camera-vehicle parameters are assumed to be known from on-board inertial navigation system and geometric measurements. The remaining task is the estimation of image irradiance partial derivatives.

Several numerical techniques are available in the literature for the computation of partial derivatives[6]. These range from simple techniques such as central difference schemes to very sophisticated techniques that adapt to reject noise and unwanted frequency components in the input signal. It is well known in the signal processing literature that derivative estimation is a noise amplifying process. Given an irradiance distribution $E(x_p, y_p)$, the objective of the partial derivative estimators are to provide sufficiently noise free estimates of $\partial E/\partial x_p$, $\partial E/\partial y_p, \partial^2 E/\partial {x_p}^2$, $\partial^2 E/\partial {y_p}^2$, $\partial^2 E/\partial x_p \partial y_p$, ... Most of the approaches in the signal processing literature formulate the partial derivative estimation problem in the frequency domain. This makes them unattractive in conjunction with conventional TV cameras because the image is formed using a sequential scanning process.

In the following, a partial derivative estimator will be formulated directly in the spatial domain. Unlike the frequency domain estimators discussed in the image processing literature, the present formulation employs causal estimators[6] to improve speed. To a certain extent, this process compromises accuracy.

However, numerical experiments have shown that the error magnitude can be reduced by an appropriate selection of the estimator parameters. In order to simplify the development, it is assumed that the image irradiance distribution $E(x_p, y_p)$ can be factored into a product of two functions of one variable each. This allows the evaluation of two dimensional integrals as products of one dimensional integrals. In the following, estimated quantities will be denoted by a " ^ ". Thus,

$$E = e_1(x_p)\, e_2(y_p), \qquad \hat{E} = \hat{e}_1(x_p)\, \hat{e}_2(y_p) \tag{13}$$

The partial derivatives of the estimated picture $\hat{E}$ can be written in terms of total derivatives of its factors $\hat{e}_1$, $\hat{e}_2$ as:

$$\frac{\partial \hat{E}}{\partial x_p} = \hat{e}_2 \frac{d\hat{e}_1}{dx_p}, \quad \frac{\partial \hat{E}}{\partial y_p} = \hat{e}_1 \frac{d\hat{e}_2}{dy_p}, \quad \frac{\partial^2 \hat{E}}{\partial {x_p}^2} = \hat{e}_2 \frac{d^2\hat{e}_1}{d{x_p}^2}, \quad \frac{\partial^2 \hat{E}}{\partial {y_p}^2} = \hat{e}_1 \frac{d^2\hat{e}_2}{d{y_p}^2}, \quad \frac{\partial^2 \hat{E}}{\partial x_p \partial y_p} = \frac{d\hat{e}_1}{dx_p}\frac{d\hat{e}_2}{dy_p}, \ \ldots. \tag{14}$$

The estimation problem can next be formulated as two, coupled, one-dimensional problems. Additionally, it is possible to formulate the estimation problem either as a serial process or as a parallel process. In the former case, the processing is carried out first along the x_p direction and then along the y_p. In the latter case, the processing occurs simultaneously along both x_p and y_p directions. A serial implementation will be illustrated here since it is consistent with the image forming process. Let $\mathbf{p}$ be the n dimensional estimator state vector. The estimator dimension n is selected based on the order of partial derivatives to be estimated and the desired smoothness requirement. For example, if it is desired to estimate the first and second order partial derivatives with the requirement that the second order partial derivatives be smooth, n has be at least 3. Next, define a linear dynamic process evolving along the x_p direction with the measured picture irradiance E as the input.

$$\frac{d}{dx_p}\mathbf{p} = \mathbf{A}\ \mathbf{p} + \mathbf{B}\ E \tag{15}$$

The matrices **A** and **B** can be chosen to obtain the desired transmission gain and bandwidth for the x_p spatial frequencies. **A** is an $n \times n$ dimensional matrix, while **B** is an $n \times 1$ vector. Note that E is a scalar function of x_p, y_p. The output equation for this linear dynamic process can be defined to yield

$$\mathbf{r} = \mathbf{C}\ \mathbf{p} + \mathbf{D}\ E, \mathbf{r} = e_2[\hat{e}_1\ \frac{d\hat{e}_1}{dx_p}\ \frac{d^2\hat{e}_1}{dx_p{}^2}.....]^T \tag{16}$$

The matrices **C**, **D** should be chosen depending on the linear dynamic system (15) dimension and on the desired orders of the partial derivatives.

In order to take care of the y_p direction, construct a linear dynamic process in this direction with the first element of the vector **r**, viz., $\hat{e}_1 e_2$ as the input, i. e.,

$$\frac{d}{dy_p}\mathbf{q} = \mathbf{M}\ \mathbf{q} + \mathbf{N}\ \hat{e}_1 e_2 \tag{17}$$

q is an m vector, **M** is an $m \times m$ matrix while **N** is an $m \times 1$ vector. As in the x_p direction, the dimension of this linear dynamic process is chosen based on the desired partial derivatives and smoothness requirements. Once again, the matrices **M** and **N** can be chosen to obtain the desired gain and bandwidth for the y_p spatial frequency components. The output equation of this dynamic process can be chosen as

$$\mathbf{s} = \mathbf{K}\ \mathbf{q} + \mathbf{L}\hat{e}_1 e_2,\ \mathbf{s} = \hat{e}_1[\hat{e}_2\ \frac{d\hat{e}_2}{dy_p}\ \frac{d^2\hat{e}_2}{dy_p{}^2}.....]^T \tag{18}$$

The output matrices **K**, **L** can be chosen in the same manner as the output matrices **C**, **D** in equation (16). With the availabilty of the vectors **r**, **s**, the estimated picture and its various partial derivatives can be computed. The various elements of these vectors will be denoted by lower case letters in the following. It can be verified that

$$\hat{E} = s_1,\ \frac{\partial \hat{E}}{\partial x_p} = \frac{\hat{E}_1 r_2}{r_1},\ \frac{\partial \hat{E}}{\partial y_p} = s_2,\ \frac{\partial^2 \hat{E}}{\partial x_p{}^2} = \frac{\hat{E}_1 r_3}{r_1},\ \frac{\partial^2 \hat{E}}{\partial y_p{}^2} = s_3,\ \frac{\partial^2 \hat{E}}{\partial x_p \partial y_p} = \frac{r_2\ s_2}{r_1} \tag{19}$$

In equation (19), it is important to ensure that r_1 does not become zero at any point in the image. This can be accomplished by adding a constant bias to the input image and subtracting this bias at the output. Note that such an operation does not alter the partial derivative estimates.

It can be seen from the foregoing development that the image irradiance partial derivatives can be estimated as the image is being formed through the scanning process. As a result, by the time the image is complete, various coefficients of the ranging polynomial are available. Moreover, if a low-order ranging polynomial is used in the computations, the range calculations can also be completed as the image is being formed.

Various steps involved in these calculations are illustrated in the block diagram given in Figure 2. This figure assumes that an image pair is available at the beginning of the computations. The linear filters provide the estimated image together with a consistent set of partial derivatives. Next, the filtered second image is subtracted from the first to obtain irradiance changes at each pixel. The scene depth is not computed in regions of near-zero irradiance change, since the ranging equation is not valid in these regions. Instead, these points are assigned a pre-defined maximum scene depth. The spatial gradients and the irradiance changes are then combined with imaging device coordinates in the given inertial frame $x_0, y_0, z_0, \Delta x_0, \Delta y_0, \Delta z_0$ to obtain the x, y, z coordinates corresponding to every pixel location.

4 RESULTS AND DISCUSSIONS

A laboratory image pair is used to demonstrate the feasibility and performance of the ranging algorithm discussed in the previous section. This laboratory image pair is shown in Figures 3. The scene consisted of a dark wall in the background with a table in the foreground. A soda can together with two

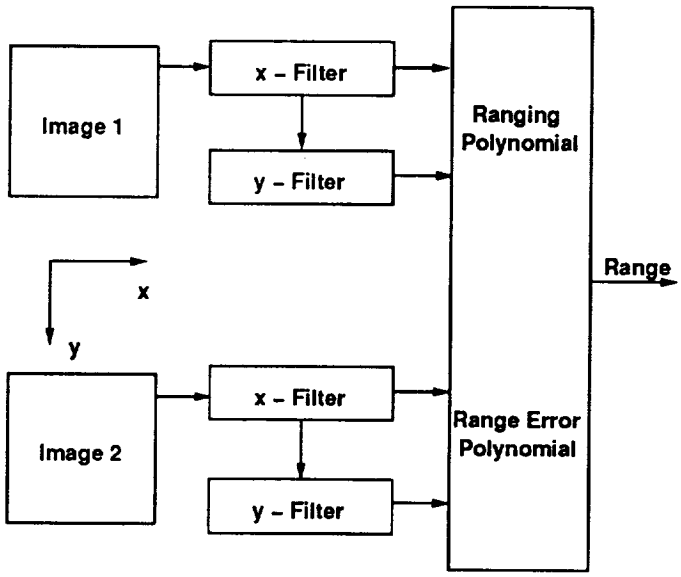

Figure 2: Vision-Based Ranging Scheme

pencils were then arranged on this table. A wire is strung across the two pencils to explore the feasibility of detecting obstacles with small dimensions. These images were obtained using a CCD (Charge Coupled Device) camera with a field-of-view of about 45 degrees and a focal length of about 6 mm. The images consisted of 512 $\times$ 512 pixel matrix with the scene irradiance being discretized in 256 levels of gray. The stereo base line, or the lateral displacement Δx_0 was 0.1 inches. The ranging algorithm was implemented on a SUN workstation in *C*.

Although ranging algorithms of various order have been implemented, the results using a first degree ranging polynomial, together with a first-order partial derivative estimator will be presented here. The partial derivative estimators employed for this example are of the form

$$\dot{p} = -0.5\ p + 0.5\ E, \quad \begin{bmatrix} e_2\hat{e}_1 \\ e_2\frac{d\hat{e}_1}{dx_p} \end{bmatrix} = \begin{bmatrix} 1 \\ -0.5 \end{bmatrix} p + \begin{bmatrix} 0 \\ 0.5 \end{bmatrix} E \tag{20}$$

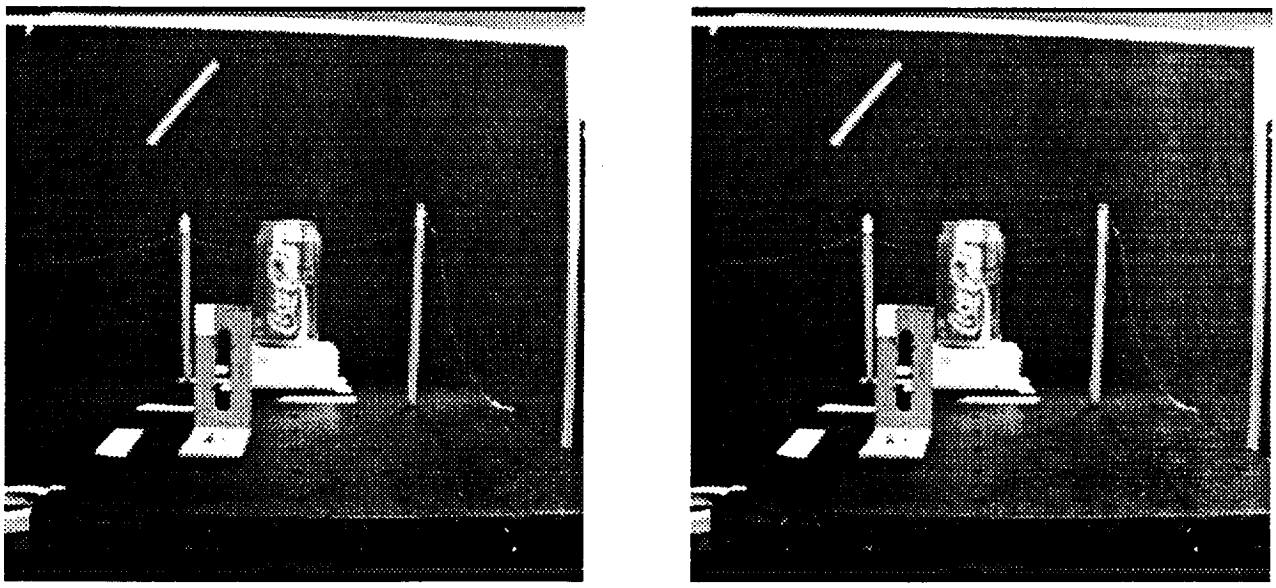

Figure 3: Left and Right Laboratory Images

$$\dot{q} = -0.5\ p + 0.5\ \hat{e}_1 e_2, \quad \begin{bmatrix} \hat{e}_1 \hat{e}_2 \\ \hat{\epsilon}_1 \frac{d\hat{e}_2}{dy_p} \end{bmatrix} = \begin{bmatrix} 1 \\ -0.5 \end{bmatrix} q + \begin{bmatrix} 0 \\ 0.5 \end{bmatrix} \hat{e}_1 e_2 \tag{21}$$

Various partial derivative estimates were computed using the expressions in (19). These values were then substituted in the first degree ranging polynomial to obtain the range estimates. Table 1 shows a comparison between computed and actual ranges to various objects in this scene. This table also gives the number of points at which the ranges were computed and the standard deviation.

It should be noted that the distribution of computed ranges corresponding to a particular object is not symmetric about the mean values given in Table 1. As a result, the standard deviation shown in the parenthesis does not truly reflect the error in estimates. A 3-D representation of the range data is shown in Figure 4. From this figure, it can be observed that the range estimates are more consistent in regions of higher contrast than in regions of low contrast.

Table 1: Comparison Between Actual Range (inches) and the Estimated Range (inches)

Object	Actual Range	Estimated Range (Std. Dev.)	No. of Points
Left Pencil	30.0	26.99 (7.48)	975
Right Pencil	26.0	23.24 (6.33)	2510
Tape-on-wall	60.0	55.94 (8.84)	850
Soda can	28.5	27.01 (7.59)	1738
Bracket	19.0	19.71 (7.23)	1070

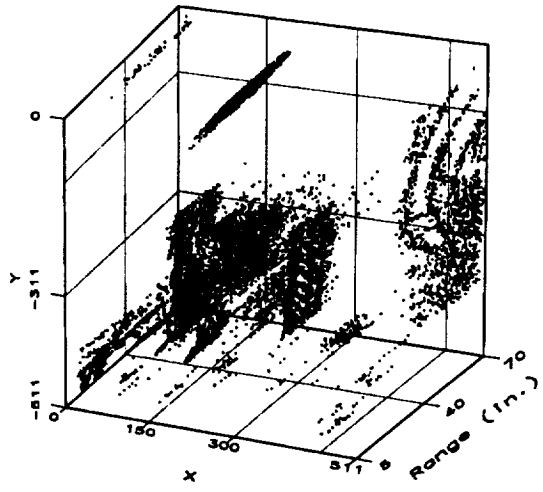

Figure 4: 3-D Representation of Computed Ranges

It is important to stress here that the range estimates are strongly influenced by the filter bandwidth. Higher bandwidth leads to partial derivative estimates that have a higher degree of fidelity. On the other hand, it also leads to a higher noise content at the output, often leading to inaccurate range estimates. Thus, as in any other signal processing application, selection of estimator parameters is largely an art if the noise characteristics are unknown.

5 CONCLUSIONS

This paper described the development and implementation of a fast technique for image-based passive ranging. This research was motivated by the need to automate the helicopter nap-of-the-earth flight regime. An optical ranging polynomial relating the scene depth with camera-vehicle parameters and various orders of image irradiance partial derivatives was derived. Another polynomial that predicts the truncation error involved in range computations was also developed. In order to enable rapid calculation of these polynomial coefficients, a partial derivative estimation method using causal linear filters was developed. Performance of the ranging algorithm was then illustrated using a laboratory image pair.

Current research focuses on improving the accuracy of this ranging algorithm and on the inclusion of additional camera-vehicle motion parameters.

ACKNOWLEDGEMENTS

The research support for the first author under NASA Cooperative Agreement NCC2-575 from Ames Research Center is gratefully acknowledged.

References

[1] Cheng, V. H. L., and Sridhar, B., "Considerations for Automated Nap-of-The-earth Rotorcraft Flight", *Proceedings of the 1988 American Control Conference*, Atlanta, GA, June 15-17, 1988.

[2] Cheng, V. H. L., "Concept Development of Automatic Guidance for Rotorcraft Obstacle Avoidance", *IEEE Transactions on Robotics and Automation*, Vol. 6, No. 2, April 1990, pp. 252-257.

[3] Baker, K., "MRSR- Managing the Landing Hazards", *Mars Rover Sample Return Scale Workshop* Final Report, Pasadena, CA, June 8-9, 1988.

[4] de Vries, J. P., and Norton, H. N., "A Mars Sample Return Mission Using a Rover for Sample Aquisition", *The Case for Mars II*, C. P. McKay (Ed.), *American Astronautical Society*, 1985.

[5] Hall, E. L., "Vision Sensing Techniques in Aeronautics and Astronautics", in *Machine Intelligence and Autonomy for Aerospace Systems*, E. Heer and H. Lum (eds.) , Vol 115 *Progress in Astronautics and Aeronautics*, American Institute of Aeronautics and Astronautics, 1989.

[6] Horn, B. K. P., *Robot Vision*, McGraw Hill, New York, 1986.

[7] Sridhar, B., and Phatak, A. V., "Simulation and Analysis of Image-Based Navigation System for Rotorcraft Low-Altitude Flight", *AHS National Specialist's Meeting on Automation Applications of Rotorcraft*, Atlanta, GA., April 4-6, 1988.

[8] Menon, P. K. A., and Sridhar, B.,"Passive Navigation Using Image Irradiance Tracking", *AIAA Guidance, Navigation, and Control Conference* , August 14-16, 1989, Boston, MA.

[9] Negahdaripour, S., and Horn, B. K. P., "Direct Passive Navigation", *IEEE Transactions on Pattern Analysis and Machine Intelligence*, Vol. PAMI-9, Jan. 1987, pp. 168-176.

[10] Skifstad, K. and Jain, R.,"Range Estimation from Intensity Gradient Analysis", *Machine Vision and Applications*, Vol. 2, 1989, pp. 81-102.

[11] Menon, P. K. A., and Sridhar, B.,"Image-Based Range Determination", *AIAA Guidance, Navigation, and Control Conference* , August 20-22, 1990, Portland, OR.

[12] Aggarwal, J. K., and Nandhakumar, N.,"On the Computation of Motion from Sequences of Images - A Review", *Proceedings of the IEEE*, Vol. 76, No. 8, August 1988, pp. 917-935.

[13] Duda, R. O., and Hart, P. E., *Pattern Classification and Scene Analysis*, John Wiley, New York, 1973.

[14] Horn, B. K. P., and Schunck, B. G., "Determining Optical Flow", *Artificial Intelligence*, Vol. 17, 1981, pp. 185-203.

Passive Obstacle Location for Rotorcraft Guidance

P. K. A. Menon*, G. B. Chatterji †and B. Sridhar‡
NASA Ames Research Center
Moffett Field, CA 94035

Abstract

Nap-of-the-earth flight mode is extremely demanding on the rotorcraft pilots. This fact has motivated the research in automating various components of low altitude rotorcraft flight operations. Concurrent with the development of guidance laws, efforts are underway to develop systems for locating the terrain and the obstacles using inputs from passive electro-optical sensors such as TV cameras and infra-red imagers. A passive obstacle location algorithm that uses image sequences from cameras undergoing translational and rotational motion is developed. The algorithm is in a general form and can operate in multi-camera imaging environments. Performance results using an image sequence from an airborne camera are given.

Introduction

Nap-of-the-earth (NOE) flight mode is one in which a rotorcraft flies close to the terrain, with an altitude clearance of less than about 50 feet, while avoiding various obstacles on the way under all weather conditions. The NOE flight regime is extremely taxing on the rotorcraft pilots who have to carry out many other duties in addition to flying the aircraft. This factor has motivated the research in automating the NOE flight regime[1-3].

The task of locating various obstacles within the field-of-view has emerged as the central problem in the development of pilot aids for nap-of-the-earth flight. Use of active sensors such as Radar or laser rangers are not desirable due to their significant power requirements and the difficulty in conducting covert missions with such devices on-board. This issue has driven the research in developing passive obstacle location schemes using conventional TV and infra-red imaging devices.

Several approaches to the image-based obstacle location problem have emerged in recent years[4-9]. Specifically, Reference 4 has discussed the development of a recursive obstacle location scheme for low altitude helicopter flight. In that approach, various features of interest in an image sequence such as regions of high contrast are used to determine the location of various objects within the field-of-view. Techniques such as these are termed as *feature-based* to distinguish them from techniques that do not explicitly use any object features for determining their location. Image-based obstacle location algorithms that do not explicitly employ features are termed *field-based* approaches. Various aspects of a field-based algorithm was discussed in References 7 - 9.

In the present work, the field-based obstacle location scheme discussed in References 7 - 9 is extended to permit the inclusion of rotational and translational motion of the imaging devices and the rotorcraft. While such an extension is non-trivial, this aspect needs to be addressed before an operational system can be synthesized.

Vision-Based Obstacle Location

Passive obstacle location methods using electro-optical sensors have their basis in the fact that the images obtained from sensors mounted on a moving vehicle will exhibit irradiance changes at each pixel. Relative location of various objects, vehicle motion parameters, relative location of the imaging devices, the scene surface reflectance, the location of illumination sources all influence this irradiance change. If the surface reflectance and the illumination are assumed to remain constant during the imaging process, then the observed image irradiance changes at each pixel are entirely due to the relative location of various objects within the field-of-view and the vehicle motion parameters. Additionally, if all the objects within the field of view are assumed fixed with respect to an inertial frame, then the irradiance change at each pixel location can be directly related to the location of these objects. In this case, if the vehicle motion parameters and the imaging device constants are known, it is possible to determine the location of various points within the field of view.

Image-based obstacle location algorithms operate on the basis of the *correspondence hypothesis*. The central idea here is to establish the correspondence be-

*Member AIAA, School of Aerospace Engineering, Georgia Institute of technology, Atlanta. Mailing Address : FSN Branch, M.S. 210-9, NASA Ames Research Center
†Member AIAA, Member of the Professional Staff, Sterling Software, Inc., 1121 San Antonio Road, Palo Alto, CA 94303
‡Research Scientist, Member AIAA, FSN Branch, M.S. 210-9.

tween various objects in a pair of images and to measure the displacement of these objects on the image plane. The measured displacement or the *disparity* can then be employed together with the perspective projection geometry for computing the location of various objects within the field-of-view.

In order further to crystallize these ideas, consider the various coordinate systems illustrated in Figure 1. The first of these is the image plane coordinate system

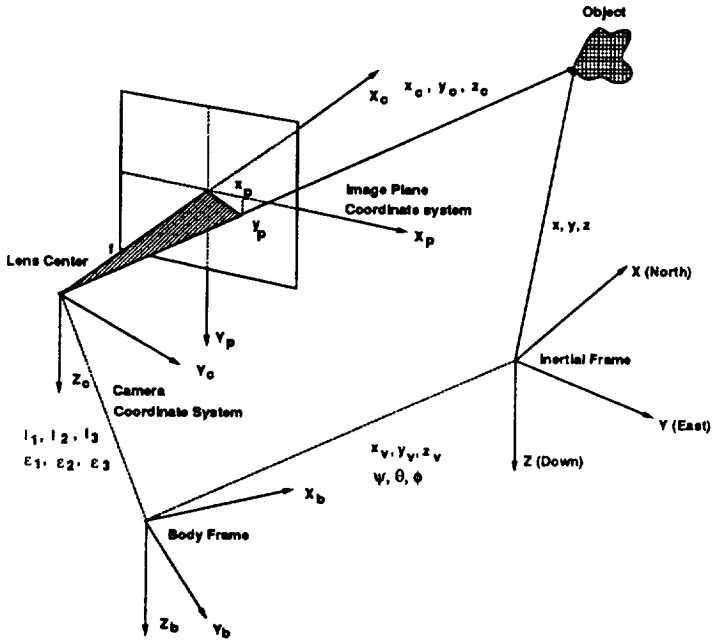

Figure 1: Coordinate System

with the major axis of the image plane being designated as the X_p axis and the minor axis being labelled the Y_p axis. The origin of this image plane coordinate system is located at the center of the aperture. In this coordinate system, an image may be defined as an irradiance distribution $E(x_p, y_p)$, with E being the irradiance specified on a gray scale at a point x_p, y_p on the image plane. Next consider the camera coordinate system X_c, Y_c, Z_c with the X_c axis passing through the origin of the image-plane coordinate system, and the axes Y_c, Z_c being parallel to the image plane coordinate system. The origin of the camera coordinate system is at the lens center, located one focal length f behind the image plane X_p, Y_p. Such an arrangement of the camera coordinate system is routinely employed in image processing work to avoid having to deal with inverted images.

The origin of the camera coordinate system is assumed to be located at a point l_1, l_2, l_3 with respect to the body axis, and oriented by three angles ϵ_1, ϵ_2, ϵ_3 about the Z_c, Y_c and X_c axes respectively. The vehicle body axis system is defined using the standard flight dynamics convention, viz., the X_b axis pointing along the nose of the rotorcraft, Y_b axis along the starboard direction, and the Z_b axis completing the right handed triad. The body axis system may be related to an inertial frame X, Y, Z through yaw, pitch, roll Euler angles ψ, θ, ϕ and the three translational components x_v, y_v, z_v. The definition of the inertial frame follows the standard flight dynamics convention with the X-axis pointing towards north, the Y-axis pointing towards east and the Z-axis pointed in the direction of local gravity vector.

A point x_p, y_p corresponding to the object in the image plane is related to its location with respect to the inertial frame x, y, z through various translations and rotations of the vehicle body frame and the camera frame, together with the perspective projection.

Let $E_1(x_p, y_p)$ and $E_2(x_p, y_p)$ be two different views of a sample scene. Assuming that these two images contain all the objects of interest and that to a large degree, the perceived irradiance of the scene has remained invariant during the imaging process, the correspondence hypothesis can be expressed as

$$E_1(x_p, y_p) = E_2(x_p + \Delta x_p, y_p + \Delta y_p) \qquad (1)$$

$$E_2(x_p, y_p) = E_1(x_p - \Delta x_p, y_p - \Delta y_p) \qquad (2)$$

Here, $\Delta x_p, \Delta y_p$ are the disparities between the corresponding points in the two images defined at every point on the image plane.

It is important to stress that the correspondence hypothesis expressed in (1) and (2) should be interpreted in a limited sense because it does not account for various occlusions that can arise during the imaging process. These occlusions arise due to the the viewing angle and the camera aperture dimensions. Note that equations such as (1) and (2) can be written for any number of images, provided that the objects of interest appear in all the images. Various methods for satisfying the correspondence hypothesis have been discussed in the literature[4-10]. In the present research, the correspondence hypothesis will be approximated by first expanding the expressions (1) and (2) in a Taylor series and then truncating them based on the acceptable computational complexity. Such an expansion treats disparities $\Delta x_p, \Delta y_p$ as perturbations about the specified pixel locations. Clearly, the error in such an approximation depends on the number of terms included in the Taylor series.

In all that follows, a bold face lower case letter will denote a vector, while a bold face upper case letter will denote a matrix. A superscript T will be used to denote the vector-matrix transpose operation. Define the disparity vector $\mathbf{d}$, the irradiance gradient vector $\mathbf{g}$, and the irradiance Hessian matrix $\mathbf{H}$ as

$$\mathbf{d} = \begin{bmatrix} \Delta x_p \\ \Delta y_p \end{bmatrix}, \quad \mathbf{g} = \begin{bmatrix} \partial E/\partial x_p \\ \partial E/\partial y_p \end{bmatrix},$$

$$\mathbf{H} = \begin{bmatrix} \partial^2 E/\partial {x_p}^2 & \partial^2 E/\partial x_p \partial y_p \\ \partial^2 E/\partial y_p \partial x_p & \partial^2 E/\partial {y_p}^2 \end{bmatrix} \quad (3)$$

Equations (1) and (2) can now be expanded using a two-dimensional Taylor series to yield

$$E_1 - E_2 = \mathbf{g}_2\mathbf{d} + \frac{1}{2}\mathbf{d}^T\mathbf{H}_2\mathbf{d} + ... \quad (4)$$

Similarly,

$$E_2 - E_1 = -\mathbf{g}_1\mathbf{d} + \frac{1}{2}\mathbf{d}^T\mathbf{H}_1\mathbf{d} - ..... \quad (5)$$

Expressions (4) and (5) relate the irradiance spatial partial derivatives to the irradiance change and the image disparities at every pixel. It is awkward to express the terms beyond second-order in (4) and (5) using the vector-matrix notation because they contain Tensors.

In the special case where the disparities $\Delta x_p, \Delta y_p$ arise from the vehicle motion resulting in apparent image velocities, the equations (4) and (5) with the first term on the right hand side is the *optical flow constraint equation*[10]. In this case, the apparent image velocity components are called the optical flow velocities. This characterization is avoided here because the disparities Δx_p, Δy_p may arise from other sources also, stereo camera arrangement being an example. By adopting the point-of-view proposed in the foregoing, equations (4) and (5) may be used for temporal image sequences from a single camera motion sequence as well as simultaneous images obtained from several cameras.

Adding and subtracting the expressions (4) and (5) results in

$$E_1 - E_2 = \frac{1}{2}\Big[\mathbf{g}_1 + \mathbf{g}_2\Big]\mathbf{d} + \frac{1}{4}\mathbf{d}^T\Big[\mathbf{H}_2 - \mathbf{H}_1\Big]\mathbf{d} + ... \quad (6)$$

$$0 = \Big[\mathbf{g}_2 - \mathbf{g}_1\Big]\mathbf{d} + \frac{1}{2}\mathbf{d}^T\Big[\mathbf{H}_1 + \mathbf{H}_2\Big]\mathbf{d} + ... \quad (7)$$

Next, as in Reference 8, equation (6) will be used for obstacle location, while the expression (7) will be used for computing the truncation error in the Taylor series approximation. The components of the disparity vector $\Delta x_p, \Delta y_p$ can now be related to the vehicle motion parameters and the location of various objects in the field-of-view.

Let x_c, y_c, z_c be the location of a point on an object with respect to the camera coordinate system. Since origin of the image plane is located at the point $[f\ 0\ 0]^T$ with respect to the camera frame, this object point would appear at a point x_p, y_p on the image plane. If the camera focal length is f, then perspective projection rules require that

$$\frac{x_p}{f} = \frac{y_c}{x_c} \quad (8)$$

$$\frac{y_p}{f} = \frac{z_c}{x_c} \quad (9)$$

Now, if x_b, y_b, z_b are the position vector components of the point x_c, y_c, z_c in the body axis system,

$$\begin{bmatrix} x_c \\ y_c \\ z_c \end{bmatrix} = \mathbf{T}_1 \begin{bmatrix} x_b - l_1 \\ y_b - l_2 \\ z_b - l_3 \end{bmatrix} \quad (10)$$

where

$$\mathbf{T}_1 = \begin{bmatrix} c\epsilon_2 c\epsilon_1 & c\epsilon_2 s\epsilon_1 & -s\epsilon_2 \\ s\epsilon_3 s\epsilon_2 c\epsilon_1 - c\epsilon_3 s\epsilon_1 & s\epsilon_3 s\epsilon_2 s\epsilon_1 + c\epsilon_3 c\epsilon_1 & s\epsilon_3 c\epsilon_2 \\ c\epsilon_3 s\epsilon_2 c\epsilon_1 + s\epsilon_3 s\epsilon_1 & c\epsilon_3 s\epsilon_2 s\epsilon_1 - s\epsilon_3 c\epsilon_1 & c\epsilon_3 c\epsilon_2 \end{bmatrix} \quad (11)$$

The variables c and s in the 3×3 matrix in (11) are the sine and cosine functions. In a more concise notation,

$$\mathbf{x}_c = \mathbf{T}_1(\mathbf{x}_b - \mathbf{l}) \quad (12)$$

Next, if the location of the same object with respect to an inertial frame is x, y, z, and the vehicle is located at a point x_v, y_v, z_v with respect to this inertial frame, the position components of the object point in the body frame are given by

$$\begin{bmatrix} x_b \\ y_b \\ z_b \end{bmatrix} = \mathbf{T}_2 \begin{bmatrix} x - x_v \\ y - y_v \\ z - z_v \end{bmatrix} \quad (13)$$

where

$$\mathbf{T}_2 = \begin{bmatrix} c\theta c\psi & c\theta s\psi & -s\theta \\ s\phi s\theta c\psi - c\phi s\psi & s\phi s\theta s\psi + c\phi c\psi & s\phi c\theta \\ c\phi s\theta c\psi + s\phi s\psi & c\phi s\theta s\psi - s\phi c\psi & c\phi c\theta \end{bmatrix} \quad (14)$$

Here, ψ, θ, ϕ are the yaw, pitch, and roll attitudes of the rotorcraft. Equation (13) can be written in a compact form as

$$\mathbf{x}_b = \mathbf{T}_2(\mathbf{x} - \mathbf{x}_v) \quad (15)$$

Since the objective is to eliminate the disparity vector $\mathbf{d}$ in favor of the object position vector components, equations (6) and (7) examine the changes in x_p, y_p in response to the changes in the vehicle location by Δx_v, Δy_v, Δz_v. For the sake of clarity, this can be carried out in two steps. First consider the changes in x_p, y_p in response to changes in x_c, y_c, z_c. This can be accomplished by evaluating the expressions (8) and (9) with the camera referenced object location being defined as $x_c + \Delta x_c$, $y_c + \Delta y_c$, $z_c + \Delta z_c$. Using elementary algebraic operations it can be shown that:

$$\Delta x_p = f\frac{\Delta y_c}{x_c + \Delta x_c} - x_p\frac{\Delta x_c}{x_c + \Delta x_c} \quad (16)$$

$$\Delta y_p = f\frac{\Delta z_c}{x_c + \Delta x_c} - y_p\frac{\Delta x_c}{x_c + \Delta x_c} \quad (17)$$

These changes are assumed to occur solely due to the motion of the rotorcraft. Next examine the changes in x_c, y_c, z_c due to the changes in vehicle position components x_v, y_v, z_v. Using the coordinate transformations discussed (12) and (15) one has that:

$$\Delta \mathbf{x}_c = \mathbf{T}_1 \Delta \mathbf{x}_b \tag{18}$$

$$\Delta \mathbf{x}_b = \Delta \mathbf{T}_2(\mathbf{x} - \mathbf{x}_v) - \mathbf{T}_2 \Delta \mathbf{x}_v - \Delta \mathbf{T}_2 \Delta \mathbf{x}_v \tag{19}$$

The matrix $\Delta \mathbf{T}_2$ is the change in the transformation matrix relating the body frame and the inertial frame caused by the changes in the vehicle attitude. Note that the equation (18) assumes that the *camera is fixed relative to the vehicle.* Equation (19) assumes that the *obstacles are fixed with respect to the inertial frame.* Next substituting (19) in (18) results in:

$$\Delta \mathbf{x}_c = \mathbf{T}_1[\Delta \mathbf{T}_2(\mathbf{x} - \mathbf{x}_v) - (\mathbf{T}_2 + \Delta \mathbf{T}_2)\Delta \mathbf{x}_v] \tag{20}$$

Using (12) and (15),

$$\mathbf{x} - \mathbf{x}_v = \mathbf{T_2}^T[\mathbf{T_1}^T \mathbf{x}_c + \mathbf{l}] \tag{21}$$

Substituting equation (21) in (20) yields:

$$\Delta \mathbf{x}_c = \mathbf{T}_1[\Delta \mathbf{T}_2 \mathbf{T_2}^T(\mathbf{T_1}^T \mathbf{x}_c + \mathbf{l}) - (\mathbf{T}_2 + \Delta \mathbf{T}_2)\Delta \mathbf{x}_v] \tag{22}$$

Finally, dividing expression (22) by x_c on both sides:

$$\begin{bmatrix} \Delta x_c/x_c \\ \Delta y_c/x_c \\ \Delta z_c/x_c \end{bmatrix} = \mathbf{T}_1 \Delta \mathbf{T}_2 \mathbf{T_2}^T \mathbf{T_1}^T \begin{bmatrix} 1 \\ x_p/f \\ y_p/f \end{bmatrix}$$
$$+\mathbf{T}_1 \Delta \mathbf{T}_2 \mathbf{T_2}^T \begin{bmatrix} l_1/x_c \\ l_2/x_c \\ l_3/x_c \end{bmatrix} - \mathbf{T}_1(\mathbf{T}_2 + \Delta \mathbf{T}_2) \begin{bmatrix} \Delta x_v/x_c \\ \Delta y_v/x_c \\ \Delta z_v/x_c \end{bmatrix} \tag{23}$$

For the sake of brevity, the equation (23) can be expressed in the form

$$\begin{bmatrix} \Delta x_c/x_c \\ \Delta y_c/x_c \\ \Delta z_c/x_c \end{bmatrix} = \begin{bmatrix} k_0 + k_3/x_c \\ k_1 + k_4/x_c \\ k_2 + k_5/x_c \end{bmatrix} \tag{24}$$

with parameters $k_0, k_1, k_2, k_3, k_4, k_5$ being computed using the operations indicated in equation (23). The rows of equation (24) can now be substituted in the expressions (16) and (17) to yield

$$\Delta x_p = \frac{fk_1 - x_p k_0 + (fk_4 - x_p k_3)/x_c}{1 + k_0 + k_3/x_c} \tag{25}$$

$$\Delta y_p = \frac{fk_2 - y_p k_0 + (fk_5 - y_p k_3)/x_c}{1 + k_0 + k_3/x_c} \tag{26}$$

Note that the Δx_p, Δy_p are bilinear with respect to the inverse of the object position component x_c measured with respect to the camera coordinate system. Next, the expressions (25) and (26) may be substituted in the Taylor series approximation of the correspondence equation (6) to yield an equation that relates the vehicle-camera motion parameters with the image irradiance partial derivatives. In order to simplify the development, only a linear approximation will be discussed in this paper. Approach to include second-order terms is direct. From (6), the first-order Taylor series approximation of the correspondence hypothesis is:

$$E_1 - E_2 = \frac{1}{2}\left[\frac{\partial E_1}{\partial x_p} + \frac{\partial E_2}{\partial x_p}\right]\Delta x_p + \frac{1}{2}\left[\frac{\partial E_1}{\partial y_p} + \frac{\partial E_2}{\partial y_p}\right]\Delta y_p \tag{27}$$

Substituting for the disparity components Δx_p, Δy_p in expression (27) from (25), (26) yields:

$$x_c = \frac{k_3 c_1 - a_1(fk_4 - x_p k_3) - b_1(fk_5 - y_p k_3)}{a_1(fk_1 - x_p k_0) + b_1(fk_2 - y_p k_0) - c_1(1 + k_0)} \tag{28}$$

where

$$a_1 = \frac{1}{2}\left[\frac{\partial E_1}{\partial x_p} + \frac{\partial E_2}{\partial x_p}\right] \tag{29}$$

$$b_1 = \frac{1}{2}\left[\frac{\partial E_1}{\partial y_p} + \frac{\partial E_2}{\partial y_p}\right] \tag{30}$$

$$c_1 = E_2 - E_1 \tag{31}$$

Various quantities on the right hand side of equation (28) can be obtained from on-board instruments and the given image sequences. Hence, equation (28) can be solved to obtain x_c. Once x_c is computed at every pixel location, the two remaining components of the object position vector at every pixel can be determined using the relations:

$$y_c = x_c x_p / f, \quad z_c = x_c y_p / f \tag{32}$$

The position of the object with respect to the inertial frame is then given by:

$$\mathbf{x} = \mathbf{x}_v + \mathbf{T_2}^T(\mathbf{T_1}^T \mathbf{x}_c + \mathbf{l}) \tag{33}$$

The instantaneous vehicle position vector $\mathbf{x}_v$, the instantaneous transformation matrix from the vehicle body frame to the inertial frame $\mathbf{T}_2$, its change $\Delta \mathbf{T}_2$, the constant transformation matrix from the vehicle body frame to the camera frame $\mathbf{T}_1$, the camera focal length f and its orientation angles are known from various on-board instruments.

The image sequence related quantities in the expression (28) are the image spatial partial derivatives $\partial E_1/\partial x_p$, $\partial E_1/\partial y_p$, $\partial E_2/\partial x_p$, $\partial E_2/\partial y_p$ and the irradiance difference $E_2 - E_1$ at every pixel. A method for estimating these quantities will be presented in the next section.

Partial Derivative Estimation

Several numerical techniques are available in the literature for the computation of the partial derivatives[10]. These range from simple central difference schemes to very sophisticated algorithms that reject noise and unwanted frequency components in the input signal. It is well known in the signal processing literature that derivative estimation is a noise amplifying process. Given an irradiance distribution $E(x_p, y_p)$, the objective of the partial derivative estimators are to provide sufficiently noise free estimates of $\partial E/\partial x_p$, $\partial E/\partial y_p$, $\partial^2 E/\partial {x_p}^2$, $\partial^2 E/\partial {y_p}^2$, $\partial^2 E/\partial x_p \partial y_p$, ... together with a consistent image irradiance distribution. Additionally, it is desirable to carryout this estimation process as fast as possible to enable real-time or near real-time implementation of the object location algorithm.

Frequency domain estimation methods are popular in the image processing literature[10]. While these approaches enable a direct formulation of the non-causal estimation problem, they are unattractive for use with electro-optical sensors that form images using a sequential scanning process. In the following, a partial derivative estimator will be formulated directly in the spatial domain. Unlike the frequency domain estimators, the present formulation will employ causal estimators to permit sequential computations. Although this approximation compromises accuracy to a certain extent, numerical experiments have shown that the error magnitude can be controlled by an appropriate selection of the estimator parameters.

Following the frequency domain image processing methods[10], the image irradiance distribution $E(x_p, y_p)$ will be assumed to be factored into a product of two functions of one variable each, denoted by the symbols $e_1(x_p)$ and $e_2(y_p)$. This factorization allows the evaluation of double integrals as products of two, single integrals. Note that such a factorization is routinely employed to produce solutions of linear partial differential equations[11]. In the following, estimated quantities will be denoted by a $\hat{}$. Thus,

$$E = e_1(x_p)\, e_2(y_p), \qquad \hat{E} = \hat{e}_1(x_p)\, \hat{e}_2(y_p) \tag{34}$$

$\hat{E}$ is the estimated image irradiance distribution. The partial derivatives of $\hat{E}$ can be written in terms of the total derivatives of its factors $\hat{e}_1$, $\hat{e}_2$ as:

$$\frac{\partial \hat{E}}{\partial x_p} = \hat{e}_2 \frac{d\hat{e}_1}{dx_p}, \quad \frac{\partial \hat{E}}{\partial y_p} = \hat{e}_1 \frac{d\hat{e}_2}{dy_p},$$

$$\frac{\partial^2 \hat{E}}{\partial {x_p}^2} = \hat{e}_2 \frac{d^2\hat{e}_1}{d{x_p}^2}, \quad \frac{\partial^2 \hat{E}}{\partial {y_p}^2} = \hat{e}_1 \frac{d^2\hat{e}_2}{d{y_p}^2},$$

$$\frac{\partial^2 \hat{E}}{\partial x_p \partial y_p} = \frac{d\hat{e}_1}{dx_p}\frac{d\hat{e}_2}{dy_p}, \ \ldots. \tag{35}$$

With this factorization, the estimation problem can be cast as two, coupled, one-dimensional estimation problems. Although the estimation problem can be formulated either as a serial process or as a parallel process[9], a serial implementation will be discussed in this paper.

Define $\mathbf{p}$ as the n dimensional estimator state vector. The estimator dimension n may be selected based on the order of partial derivatives to be estimated and the desired smoothness requirement. For instance, if it is desired to estimate the first-order and the second-order partial derivatives with the requirement that the second-order partial derivatives be smooth, n has to be at least 3. Next consider a linear dynamic process evolving along the x_p direction with the measured image irradiance E as the input.

$$\frac{d}{dx_p}\mathbf{p} = \mathbf{A}\,\mathbf{p} + \mathbf{B}\,E \tag{36}$$

This dynamic process is assumed to evolve along the image scan lines. The matrices $\mathbf{A}$ and $\mathbf{B}$ can be chosen to obtain the desired transmission gain and bandwidth for the x_p spatial frequencies. The output equation for this linear dynamic process can be defined as:

$$\mathbf{r} = \mathbf{C}\,\mathbf{p} + \mathbf{D}\,E, \quad \mathbf{r} = e_2[\hat{e}_1 \ \frac{d\hat{e}_1}{dx_p} \ \frac{d^2\hat{e}_1}{d{x_p}^2} \ldots\ldots]^T \tag{37}$$

The matrices $\mathbf{C}$, $\mathbf{D}$ should be chosen based on the linear dynamic system (36) dimension and on the desired orders of the partial derivatives.

Similarly, define a linear dynamic process evolving along the y_p direction, with the first element of the vector $\mathbf{r}$ as the input, i. e.,

$$\frac{d}{dy_p}\mathbf{q} = \mathbf{M}\,\mathbf{q} + \mathbf{N}\,e_2\hat{e}_1 \tag{38}$$

The matrices $\mathbf{M}$ and $\mathbf{N}$ can be chosen to obtain the desired gain and bandwidth for the y_p spatial frequency components. The output equation of this dynamic process can be chosen as

$$\mathbf{s} = \mathbf{K}\,\mathbf{q} + \mathbf{L}\hat{e}_1 e_2, \quad \mathbf{s} = \hat{e}_1[\hat{e}_2 \ \frac{d\hat{e}_2}{dy_p} \ \frac{d^2\hat{e}_2}{d{y_p}^2} \ldots\ldots]^T \tag{39}$$

with the matrices $\mathbf{K}$, $\mathbf{L}$ being chosen in the same manner as the output matrices $\mathbf{C}$, $\mathbf{D}$ in equation (37). The vectors $\mathbf{r}$ and $\mathbf{s}$ can now be used to compute the estimated image irradiance and its various partial derivatives. Elements of these vectors will be denoted by lower case letters in the following. It can be verified that

$$\hat{E} = s_1, \quad \frac{\partial \hat{E}}{\partial x_p} = \frac{s_1 r_2}{r_1}, \quad \frac{\partial \hat{E}}{\partial y_p} = s_2,$$

$$\frac{\partial^2 \hat{E}}{\partial {x_p}^2} = \frac{s_1 r_3}{r_1}, \quad \frac{\partial^2 \hat{E}}{\partial {y_p}^2} = s_3,$$

$$\frac{\partial^2 \hat{E}}{\partial x_p \partial y_p} = \frac{r_2\, s_2}{r_1} \tag{40}$$

In equation (40), it is important to ensure that the first element of the **r** vector r_1 does not become zero at any point on the image. This can be assured by adding a constant bias to the input image E and subtracting this bias at the output. Note that such an operation does not alter the partial derivative estimates.

Since the partial derivative estimation process was formulated keeping the image forming process in view, these quantities are available as the image is being formed. As a result, by the time the image scanning process is complete, various parameters required in equation (28) can be computed. Thus, after the availability of the first frame, the object location computations can be completed at the camera frame rate.

A block diagram of the object location algorithm is given in Figure 2. This block diagram assumes that

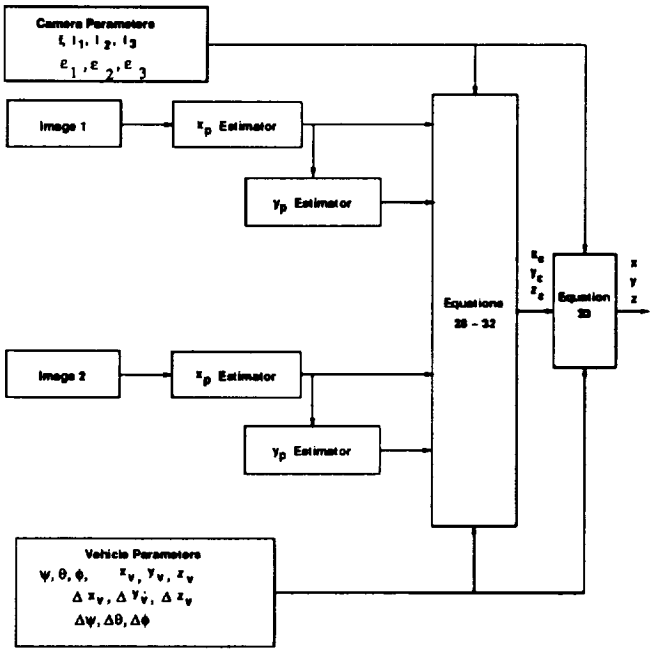

Figure 2: The Object Location Algorithm

an image pair is available at the beginning of the computations. The estimators along the x_p and y_p directions provide the noise attenuated partial derivatives together with consistent image irradiance estimates. The coefficients of equation (28) are then computed by combining this information with the vehicle-camera motion data. The position vector component x_c corresponding to every point on the image plane is then computed by applying the expression (28) at every pixel. The vehicle and the camera rotational and translational data required for this calculation is assumed to be available from on-board instruments. The other components of the position vector y_c, z_c are then determined using the expression (32) at every pixel.

The quantities x_c, y_c, z_c are computed only at regions where the inter-frame irradiance changes and the spatial partial derivatives are sufficiently large. The remaining points are assigned a pre-defined maximum scene depth. Once the position vectors in the camera frame become available, the expression (33) can be used to transform the position components into the inertial frame.

Results and Discussions

The performance of the obstacle location algorithm was tested using two different image sequences. The first of these was a laboratory scene used in References 8 and 9. The second test image sequence was obtained from a camera mounted on the nose of a helicopter. Results obtained using the second image sequence will be discussed in this paper. Two images from the airborne camera are shown in Figures 3 and 4. These

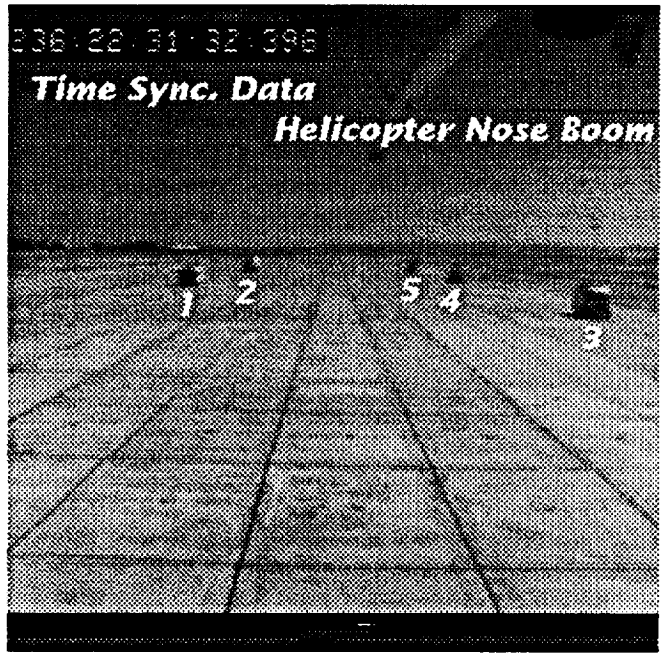

Figure 3: The First Sample Image

images consist of a 512 × 512 pixel arrays, with 8 bit gray-scale digitization. The camera was operating at a rate of 30 frames/second. During the imaging process, the rotorcraft was flying at an altitude of about 12 feet above the runway at a speed of 32.6 feet/second. The images in Figure 3 and 4 are temporally separated by 0.17 seconds. During this time, the rotorcraft underwent a translational motion of $[5.41, -0.44, 0.02]^T$ feet and experienced an attitude motion of 0.059 degrees about the pitch axis, -0.08 degrees about the yaw axis, and 0.12 degrees about the roll axis.

Besides other things, the Figures 3 and 4 show a runway, and five vehicles parked on the two sides. The

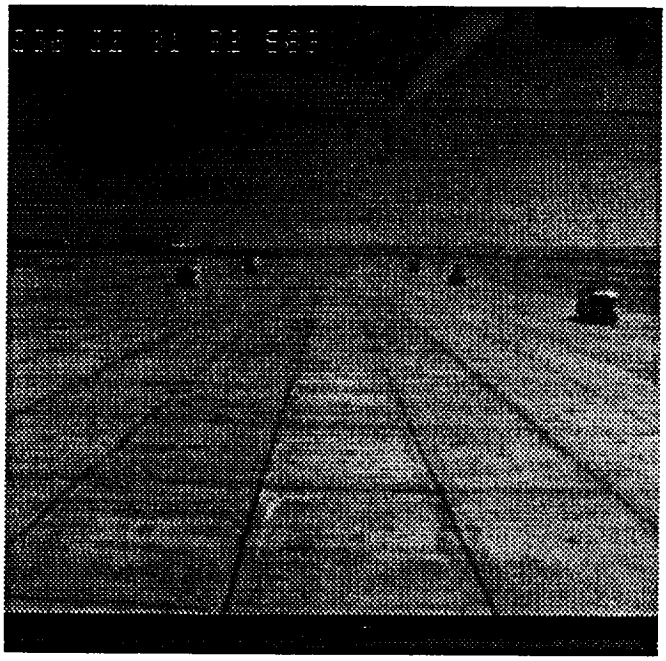

Figure 4: The Second Sample Image

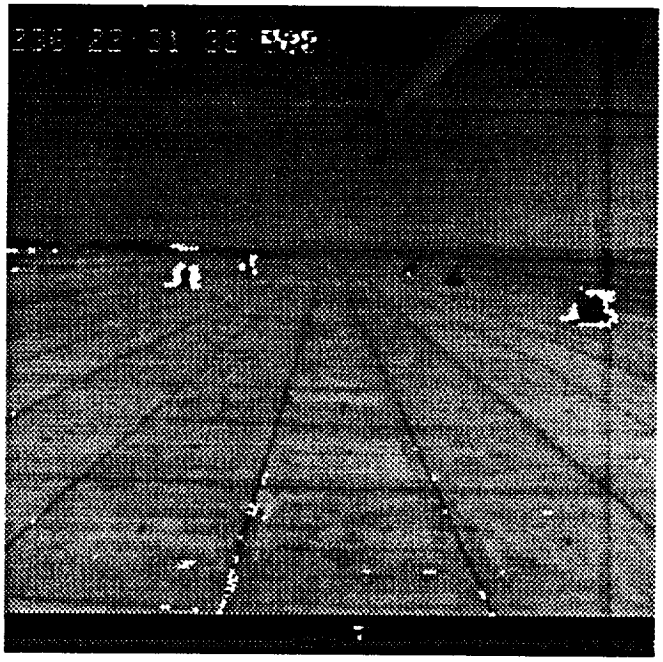

Figure 5: Points at which Object Location data is Computed

instrumented nose boom of the helicopter is clearly visible at the top right hand part of the image. Time sync. parameters identifying this frame are displayed in a sub-picture on the top left-hand-side of the image.

In order to compute the spatial partial derivatives together with a consistent irradiance distribution, these images were processed though irradiance estimators of the form:

$$\frac{dp}{dx_p} = -5.0\, p + 5.0\, E,$$

$$\begin{bmatrix} r_1 \\ r_2 \end{bmatrix} = \begin{bmatrix} 1 \\ -5.0 \end{bmatrix} p + \begin{bmatrix} 0 \\ 5.0 \end{bmatrix} E \qquad (41)$$

$$\frac{dq}{dy_p} = -5.0\, p + 5.0\, \hat{e}_1 e_2,$$

$$\begin{bmatrix} s_1 \\ s_2 \end{bmatrix} = \begin{bmatrix} 1 \\ -5.0 \end{bmatrix} q + \begin{bmatrix} 0 \\ 5.0 \end{bmatrix} \hat{e}_1 e_2 \qquad (42)$$

Output of these estimators were used in equation (40) to form the various partial derivatives. These values were then used together with the vehicle motion data obtained from the on-board inertial navigation system to compute the distance to various obstacles.

The object location data was computed at 480 points on the image plane. In Figure 5, the points at which the location data was computed are shown as white dots. This represents about 0.2 % of the possible 262,144 points. The object location data can be reliably recovered only at those points where a significant image intensity change is detected between frames.

Object	Actual Range	Estimated Range	Number of Points
Vehicle 1	356.4	335.6	113
Vehicle 2	607.0	395.9	24
Vehicle 3	232.8	202.1	160

Table 1. Comparison between Actual Range (feet) and Estimated Range (feet) for Some of the Objects in the Scene

Table 1 summarizes the comparison between computed and actual locations of some of the objects in this scene. This table also gives the number of points at which the computations were carried out for each object. Eventhough the image was not of high quality, note that the algorithm determines the location of two vehicles with acceptable accuracy. There is a large error in the location of the vehicle number 2. At this stage it appears that this inaccuracy may be caused by the low resolution of the image. Additional tests are currently being carried out to determine the image resolution requirement for obtaining a desired position determination accuracy.

Conclusions

A passive image-based obstacle location algorithm for use in the guidance of rotorcraft during nap-of-the-earth flight was described. The algorithm uses the vehicle-camera translation and rotational motion data together with the image sequences to compute the location of various objects within the field of view.

The method uses a Taylor series approximation of the correspondence hypothesis together with the perspective projection geometry. The present research generalizes previous work on an object location algorithm to include both the translational and rotational motion of the imaging devices and the vehicle. The resulting algorithm is more general and can operate in multi-camera imaging environments. The performance results using an image sequence from an airborne camera are given.

Acknowledgements

The research support for the first author under NASA Cooperative Agreement NCC2-575 from Ames Research Center is gratefully acknowledged.

References

[1] Cheng, V. H. L., and Sridhar, B., "Considerations for Automated Nap-of-The-earth Rotorcraft Flight", *Journal of the American Helicopter Society*, Vol. 36, No. 2, April 1991, pp. 61-69.

[2] Cheng, V. H. L., "Concept Development of Automatic Guidance for Rotorcraft Obstacle Avoidance", *IEEE Transactions on Robotics and Automation*, Vol. 6, No. 2, April 1990, pp. 252-257.

[3] Menon, P. K. A., Chatterji, G. B., and Sridhar, B., "Vision-Based Optimal Obstacle-Avoidance Guidance for Rotorcraft", *AIAA Guidance, Navigation, and Control Conference*, August 12 - 14, 1991, New Orleans, LA.

[4] Sridhar, B., Suorsa, R., and Hussien, B., "Passive Range Estimation for Rotorcraft Low Altitude Flight", to appear in *Machine Vision and Applications*, 1991.

[5] Negahdaripour, S., and Horn, B. K. P., "Direct Passive Navigation", *IEEE Transactions on Pattern Analysis and Machine Intelligence*, Vol. PAMI-9, Jan. 1987, pp. 168-176.

[6] Skifstad, K. and Jain, R.,"Range Estimation from Intensity Gradient Analysis", *Machine Vision and Applications*, Vol. 2, 1989, pp. 81-102.

[7] Menon, P. K. A., and Sridhar, B.,"Passive Navigation Using Image Irradiance Tracking", *AIAA Guidance, Navigation, and Control Conference* , August 14-16, 1989, Boston, MA.

[8] Menon, P. K. A., and Sridhar, B.,"Image-Based Range Determination," *AIAA Guidance, Navigation, and Control Conference* , August 14-16, 1990, Portland, OR. Also to appear in the *Journal of Guidance, Control, and Dynamics*, 1991.

[9] Menon, P. K. A., Chatterji, G. B., and Sridhar, B., "A Fast Algorithm for Image-Based Ranging," *SPIE International Symposium on Optical Engineering and Photonics in Aerospace Sensing*, April 1-5, 1991, Orlando, FL.

[10] Horn, B. K. P., *Robot Vision*, McGraw Hill, New York, 1986.

[11] Pipes, L. A., *Applied mathematics for Engineers and Physicists*, McGraw Hill, New York, 1958.

5. Derivative-Free Vision-Based Ranging

In all the computational schemes discussed in this report, the parameters enabling ranging were the spatial partial derivatives of the image. It is well known in the signal processing discipline that derivative estimation is a noise amplifying process. Consequently, if a derivative free method can be synthesized, then it would be less sensitive to picture noise.

This idea forms the basis for the ranging scheme discussed in the following paper. In this scheme, instead of satisfying the correpondence hypothesis using partial derivative estimates as in previous chapters, the integral error between a predicted value of image irradiance and those from the actual measurements are minimized. The solution is required to satisfy a differential constraint derived by approximating the correspondence hypothesis using Padé expansion.

Minimization of the integral irradiance error subject to the differential constraint results in a calculus of variations problem. The necessary conditions for a minimum yield a set of linear two-point boundary-value problems, which can be solved using the backward sweep method. In this process, the sum and the difference between two images are used to form a Riccati equation and a linear differential equation. These equations are integrated from the right edge of the image to the left edge to compute the *feedback gains* for the range estimator. Multiplying these feedback gains with the difference between the actual and the predicted image irradiances then produce the range estimates.

A paper outlining this work has been communicated for presentation at the *1992 AIAA Guidance, Navigation, and Control Conference*, and is included in the following.

Vision-Based Stereo Ranging as an Optimal Control Problem

P. K. A. Menon*, B. Sridhar†and G. B. Chatterji ‡
NASA Ames Research Center
Moffett Field, CA 94035

Abstract

The recent interest in the use of machine vision for flight vehicle guidance is motivated by the need to automate the nap-of-the-earth flight regime of helicopters. Vision-based stereo ranging problem is cast as an optimal control problem in this paper. A quadratic performance index consisting of the integral of the error between observed image irradiances and those predicted by a Pade' approximation of the correpondence hypothesis is then used to define an optimization problem. The necessary conditions for optimality yield a set of linear two-point boundary-value problems. These two-point boundary-value problems are solved in feedback form using a version of the backward sweep method. Application of the ranging algorithm is illustrated using a laboratory image pair.

Introduction

Passive ranging has emerged as a central issue in nap-of-the-earth helicopter flight guidance[1-3] and autonomous planetary rover mission[4-6] as evidenced by the recent appearence of several papers in this area. Research on both the sensors and guidance algorithms are currently underway. The status of research activity on the nap-of-the-earth guidance problem is summarized in Reference 3. The research reported in this paper is a component of the helicopter guidance problem.

Image-based passive ranging is an active research area in the robotics discipline[7]. Application of this technology for flight vehicle guidance is a more recent development. Driven by the need to determine range to various obstacles within the field-of-view, Reference 8 outlines the development of an image-based recursive range determination scheme for nap-of-the-earth helicopter flight guidance. In that approach, various features such as edges or regions of high contrast in an image sequence were used to determine the range to various objects within the field-of-view. Techniques such as this are termed as *feature-based* ranging to distinguish them from techniques that do not explicitly use any features for range determination. *Field-based* ranging algorithms, on the other hand do not explicitly employ any features for range computations. Various aspects of the development of a field-based ranging algorithm was described in References 9 - 12. The algorithm developed in these papers relied on the image irradiance partial derivatives to compute the range. The analysis considered both motion and stereo image sequences.

Present paper reports on the development of a field based stereo ranging scheme that does not require spatial partial derivative estimates. This research develops a differential constraint based on the approximation of the correspondence hypothesis using Pade' expansion in a registered stereo pair. Under certain conditions, this expansion can be shown to be identical to the Taylor series expansion employed in References 9 - 12. Using perspective projection relationships, the image disparity is next eliminated in favor of the stereo baseline, camera focal length and range. The state variable in the resulting differential constraint is the sum of the image irradiances and the control variable is the range to various points within the field-of-view. Integral of a quadratic form in the error between the measured irradiances and those pre-

*Member AIAA, School of Aerospace Engineering, Georgia Institute of technology, Atlanta. Mailing Address : FSN Branch, M.S. 210-9, NASA Ames Research Center
†Research Scientist, Member AIAA, FSN Branch, MS 210-9
‡Member AIAA, Member of the Professional Staff, Sterling Software, Inc.

dicted by the Pade' approximation of the correspondence hypothesis is then defined as the performance index. Necessary conditions for minimizing the performance index subject to the differential constraint are obtained by the application of optimal control theory[13]. This process produces a set of linear two-point boundary-value problems which can be solved for range in state feedback form using a version of the backward sweep algorithm[13].

The ensuing sections will discuss the development of this algorithm in further detail. The performance of the optimal stereo algorithm will be demonstrated using a laboratory image pair.

Stereo Ranging

Images obtained from a pair of spatially separated cameras will exhibit irradiance differences at each pixel. These differences depend on the relative location of various objects, relative location of the cameras, the scene surface reflectance and the location of illumination. If the scene surface reflectance is relatively invariant between the two images, the reason for observed image irradiance changes at each pixel may be attributed to the relative location of various objects within the field-of-view. This fact forms the basis for correspondence hypothesis.

According to the correspondence hypothesis, the relative displacement of the corresponding objects in an image pair or the *disparity* can be employed together with the perspective projection geometry to compute the range to these objects. Following the existing literature, the frontal image plane representation will be used for image description. The ensuing analysis will deal with monochromatic stereo pairs obtained using identical cameras.

Consider a registered stereo pair together with the coordinate systems as shown in Figure 1. In Figure 1, the major axes of the two image planes are designated as the X_p axis and the minor axes are labelled the Y_p axis. The origin of this image plane coordinate system is located at the center of the aperture. The range z to various objects within the field-of-view will be measured with respect to a coordinate system fixed to the origin of the first camera lens, located one focal length f behind the image plane with the X and Y axis being parallel to X_p and Y_p axes. The second camera is offset

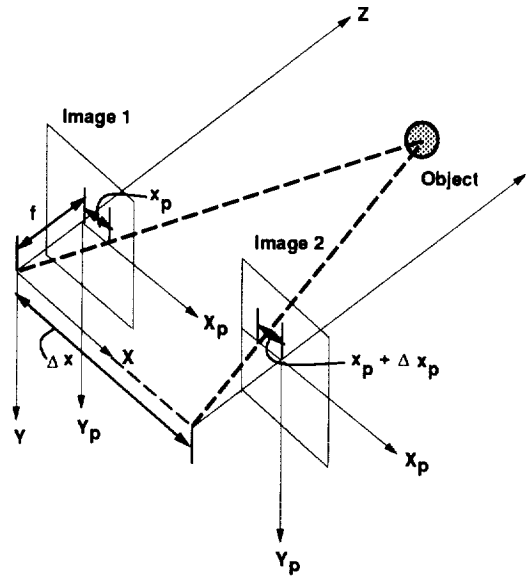

Figure 1: The coordinate system.

from the orgin of this sytem by a distance Δx along the X axis. The distance Δx is termed as the stereo baseline.

In the image plane coordinate system, an image may be defined as an irradiance distribution $E(x_p, y_p)$ in the X_p, Y_p plane, with E being the irradiance specified on a gray scale at a point (x_p, y_p) on the image plane. It is assumed here that except at finite number of points, the image irradiance distribution is continuous along the horizontal direction x_p. This is a reasonable assumption because imaging sensors perform spatial integration. Since the analysis assumes registered stereo pairs, any number of discontinuities are permitted along the y_p direction. For the purposes of the present analysis, nonlinear effects contributed by gray scale quantization will be ignored.

Let $E_1(x_p, y_p)$ and $E_2(x_p, y_p)$ be a given stereo pair obtained from cameras with identical parameters. Assume that the two images contain all the objects of interest and that to a large degree, the irradiance of the scene is independent of the camera position. Further assume that the two images are perfectly *registered*[7]. In this case, the correspondence hypothesis may be expressed as

$$E_1(x_p) = E_2(x_p + \Delta x_p), \quad y_p = constant \qquad (1)$$

This equation states that an object at the point (x_p, y_p) in the first image will appear at the point $(x_p + \Delta x_p, y_p)$ in the second image. Here, Δx_p is

the disparity between the corresponding objects in the two images. Since different points in the image plane may correspond to different objects within the field-of-view, the disparity Δx_p may vary as a function of x_p. The depth information is encoded in these disparities. Note that the disparities in the y_p direction are zero because the stereo pair is assumed to be registered. Further, note that the limited camera field-of-view and the various occlusions that can arise in real scenes may result in the correspondence hypothesis not being valid at every point on the image pair.

Pade' Approximation

The correpondence hypothesis may be satisfied in various ways. Indeed, the method employed for satisfying the correspondance hypothesis is the main feature that distinguishes one stereo ranging algorithm from another. The feature-based family of methods[8] attempt to decrease the complexity involved in satisfying the correspondence hypothesis by first extracting the features of interest in an image such as edges or regions of high contrast and then establishing the correspondence between them. This step reduces the correspondence task by a significant amount. Pixel by pixel correlation methods have also been proposed for satisfying the correspondence hypothesis[14].

In the present paper, an alternate approach for satisfying the correspondence hypothesis will be advanced. Using Laplace transforms[15] together with the shift theorem, the correspondence equation (1) over small patches can be written as:

$$E_1(s) = e^{s\Delta x_p} E_2(s) \tag{2}$$

Here s is the Laplacian operator. According to equations (1), and (2), the image irradiance distribution in the second image is simply the image irradiance in the first image shifted by the unknown disparity at a pixel. Expression (2) can next be expanded using Pade' approximation[16]. The expression (2) is first rewritten as

$$e^{-\frac{s\Delta x_p}{2}} E_1(s) = e^{s\frac{\Delta x_p}{2}} E_2(s) \tag{3}$$

Expanding both sides,

$$E_1(s) - \frac{1}{2} s E_1(s)\Delta x_p + \ldots\ldots = E_2(s) + \frac{1}{2} s E_2(s)\Delta x_p + \ldots\ldots \tag{4}$$

Retaining the two leading terms on both sides and inverse transforming yields the differential equation

$$2(E_1 - E_2)\frac{1}{\Delta x_p} = \frac{d}{dx_p}(E_1 + E_2) \tag{5}$$

A similar expression was derived in Reference 10 using forward and backward expansion of the Taylor series. In order to assure continuous dependence of the left hand side of the expression (5) on Δx_p, it will be assumed that $E_1 - E_2 \neq 0$ over any finite interval of x_p. It is sometimes useful to retain higher-order terms in the Pade' expansion. However, the resulting differential equation for correspondence hypothesis will be nonlinear in $1/\Delta x_p$, making the solution process more complex.

Next, the geometry of image forming process will be used to eliminate the unknown disparity Δx_p from expression (5) in favor of camera parameters and range. From the perspective projection geometry, an object located at a position $(x,\ z)$ will appear at a point

$$\frac{x_p}{f} = \frac{x}{z} \tag{6}$$

in the first image. Since the second image in the registered stereo pair is located at $(x + \Delta x)$, the same object will appear at a point

$$\frac{x_p + \Delta x_p}{f} = \frac{x + \Delta x}{z} \tag{7}$$

in the second image. Δx_p is the disparity at a point on the image plane corresponding to an object. An expression relating the disparity, stereo baseline and the range to an object can be obtained by subtracting expression (6) from expression (7), Viz.

$$\Delta x_p = f\frac{\Delta x}{z} \tag{8}$$

Note that the stereo baseline Δx and the camera focal length f are known. Expression (8) relates the observed disparity Δx_p at a pixel location to the range to an object z. Using expression (8) in the approximation for the correspondence hypothesis (5) yields

$$\frac{d}{dx_p}(E_1 + E_2) = \frac{2(E_1 - E_2)}{f\Delta x} z \tag{9}$$

Next, define two new variables

$$G = E_1 + E_2,\ A = \frac{2(E_1 - E_2)}{f\Delta x} \qquad (10)$$

So that the expression (9) becomes

$$\dot{G} = Az \qquad (11)$$

From this point on, a dot over variables will be used to denote differentiation with respect to the independent variable x_p. Expression (11) relates the sum and differences of the observed image irradiances with the range to various objects within the field-of-view. If the image irradiances, focal length and the stereo baseline are given, then the coefficient $A(x_p)$ can be computed at every point on the image plane. In this case, expression (11) is a varying coefficient first-order linear differential equation with z as the input and G as the state.

In the next section, the differential constraint expressed by equation (11) will be used together with the measured image irradiance to determine the range as a function of x_p.

Ranging as a Two-Point Boundary-Value Problem

The data available in a registered stereo pair are the image irradiances $E_1(x_p, y_p)$ and $E_2(x_p, y_p)$ along every y_p within the camera frame. According to the differential constraint approximating the correspondence hypothesis given (11), at every y_p coordinate, the derivative of the sum of the irradiances when divided by the varying coefficient $A(x_p)$ will yield the range z as a function of the image plane coordinate x_p. References 9 - 12 approched the ranging problem in precisely this manner. Specifically, in Reference 12, the image irradiance derivatives were first computed using linear estimators. An approximation to the correspondence hypothesis such as equation (11) was then used to compute range. In the following, an alternative to this two step procedure will be developed.

Since the differential constraint (11) is only an approximation and because of the fact that the observed irradiances are corrupted by noise, one may require that this differential constraint be satisfied in a minimum integral square error fashion. To this end, consider the problem

$$\min_z \left[\frac{\gamma}{2}[G - \hat{G}]^2|_{x_p=x_p(r)} + \int_{x_p(l)}^{x_p(r)} \left\{\frac{\alpha}{2}[G - \hat{G}]^2 + \frac{\beta}{2}z^2\right\}dx\right] \qquad (12)$$

subject to the differential constraint

$$\dot{G} = A\ z \qquad (13)$$

$\hat{G}$ is the sum of the *measured irradiances*, and the coefficient $A(x_p)$ is computed from the measured irradiances and camera parameters using the expression (10). The upper and lower integration limits $x_p(l)$, $x_p(r)$ correspond to the left and right image boundaries. Although by no means essential, in order to simplify the ensuing development, it will be assumed that the sum of the measured irradiances $\hat{G}$ and G computed from the differential constraint (13) are equal at the left boundary of the image. This implies that the left boundary condition $G(x_p(l)) = \hat{G}(x_p(l))$ is specified, while the right boundary condition is free.

The first term weighted by the parameter γ in (12) helps to ensure that the measured sum of irradiances $\hat{G}$ and the predicted sum of irradiances G are close at the right edge of the image. The weighting factors α and β in the performance index (12) can be used to establish the trade-off between irradiance error and the range. Bryson's rule[13] can be used to select the weighting factors as :

$$\alpha \cong \frac{1}{[x_p(r) - x_p(l)]G_M} \qquad (14)$$

$$\beta \cong \frac{1}{[x_p(r) - x_p(l)]z_M} \qquad (15)$$

$$\gamma \cong \frac{1}{G_M|_{x_p=x_p(r)}} \qquad (16)$$

where G_M is the maximum acceptable value of $(G - \hat{G})^2$ and z_M is the maximum acceptable value of z^2.

Attention is drawn to the fact that the second term in integrand of (12) is essential to ensure the existence of a non-trivial solution. This term has the effect of limiting the magnitude of the range with respect to irradiance changes. The weighting factors α, β are permitted to be functions of x_p. It is assumed here that the computation proceeds from the left boundary of the image to the right boundary.

The expressions (12) and (13) define an optimal control problem, with G as the state variable and z as the control variable. Necessary conditions for a minimum can be obtained by formally

applying Pontriagin's minimum principle[13]. The first step here is the formulation of the variational Hamiltonian[13] as :

$$H = \frac{\alpha}{2}[G - \hat{G}]^2 + \frac{\beta}{2}z^2 + \lambda A\, z \qquad (17)$$

λ is the unknown costate. The necessary conditions for optimum are[13] :

$$\dot{\lambda} = -\alpha[G - \hat{G}] \qquad (18)$$

$$z = -\frac{\lambda A}{\beta} \qquad (19)$$

Since the sum of the irradiances G is required to satisfiy the measured value $\hat{G}$ exactly at the left boundary of the image plane, the costate λ at this boundary is unspecified. At the right boundary, the term minimizing the square of the deviations on the right boundary dictates the value of the costate, i. e.

$$\lambda(x_p(r)) = \gamma[G - \hat{G}]|_{x_p = x_p(r)} \qquad (20)$$

Substituting for z in (13) using expression (19) yields the two-point boundary-value problem at each specified value of y_p as :

$$\dot{G} = -\frac{A^2}{\beta}\lambda,\ G(x_p(l))\ Specified \qquad (21)$$

$$\dot{\lambda} = -\alpha[G - \hat{G}],$$
$$\lambda(x_p(l))\ unknown,\ \lambda(x_p(r)) = \gamma[G - \hat{G}]|_{x_p = x_p(r)} \qquad (22)$$

The linear two-point boundary value problem (21), (22) can be solved in feedback form for G and λ by using a version of the backward sweep[13], as will be demonstrated in the following. Substituting these values in expression (19) then yields range at each point on the image plane.

Since the state is specified at one of the boundaries and because the system has a forcing input $\hat{G}$, postulate a solution for costate λ as :

$$\lambda = SG + K \qquad (23)$$

The first term takes care of the instantaneous dependence of the costate on the state G, while the second term accounts for the external input $\hat{G}$.

In order that expression (23) satisfies the boundary condition (20), it is necessary that

$$S(x_p(r)) = \gamma,\ K(x_p(r)) = -\gamma\hat{G} \qquad (24)$$

Differentiating the expression (23) and substituting for $\dot{G}$ and $\dot{\lambda}$ from (21) and (22) yields

$$-\alpha(G - \hat{G}) = \dot{S}G - S\frac{A^2}{\beta}[SG + K] + \dot{K} \qquad (25)$$

Separating terms

$$S\frac{A^2}{\beta}K + \alpha\hat{G} - \dot{K} = G(\dot{S} - S^2\frac{A^2}{\beta} + \alpha) \qquad (26)$$

Since expression (26) must hold for arbitrary values of G, one has that

$$\dot{S} = S^2\frac{A^2}{\beta} - \alpha \qquad (27)$$

$$\dot{K} = S\frac{A^2}{\beta}K + \alpha\hat{G} \qquad (28)$$

with the boundary condition being given by (24).

Expression (27) is a Riccati differential equation, while (28) is a linear differential equation. Once the value of S and K are known as a function of x_p, the range can be computed as

$$z = -\frac{[SG + K]A}{\beta} \qquad (29)$$

The equation (29) is a linear feedback law for range z in terms of the state G and the weighting factors. In a following subsection, implementation of the range computation algorithm will be given in further detail.

Note that two-point boundary-value problems such as the one discussed above can be derived for every pair of lines in the registered stereo pair. Additionally, if the weights α, β, γ are assigned certain statistical significance, the optimization problem discussed in the foregoing can be posed as the *smoothing problem* in estimation theory[13].

Second-Order Necessary Conditions

It is known[13] that the sufficient conditions for an optimum requires the second variation to be strictly positive. This requirement can be met by satisfying the Legendre-Clebsch and Jacobi necessary conditions in strengthened form. Each of

these necessary conditions will be briefly examined for the stereo ranging scheme in the following.

(1) Legendre-Clebsch necessary condition :

This necessary condition examines the sign of the second partial derivative of the variational Hamiltonian with respect to the control variable z. Thus, a necessary condition for optimality is :

$$\frac{\partial^2 H}{\partial z^2} > 0 \tag{30}$$

This condition can be found to be satisfied if

$$\beta > 0 \tag{31}$$

Since the parameter β is a user specified quantity, the Legendre-Clebsch necessary condition does not impose any restrictions on the computational scheme.

(2)Jacobi's necessary condition :

The stereo ranging process described in the foregoing is a linear optimal control problem. Hence, Jacobi's necessary condition will be satisfied with a margin if the differential equations (27) and (28) produce finite values and if the variable S is positive[13]. Thus, if the range estimates emerging from the present computations are finite, Jacobi's necessary condition will be met with a margin.

In summary, if the parameter β is chosen to be positive and if the resulting the range estimates remain finite, the results would be optimal with respect to the specified performance index.

The Computational Algorithm

Since the ranging scheme will be tested using discretized images, the algorithm implementation will be discussed in terms of such images. Consider an image consisting of $m \times n$ pixel array. Let the horizontal field-of-view be ψ radians and the vertical field-of-view be θ radians, with f as the camera focal length. As the stereo image pair is registered, the analysis can be carried out separately for m pair of lines. Along any picture line, the distance between the centers of any two pixels is given by :

$$\delta = \frac{2f \tan \psi/2}{n} \tag{32}$$

Various differential equations involved in the stereo algorithm can now be discretized using this distance.

The first step in the computational algorithm is the formation of quantities

$$A_i = \frac{2(E_1 - E_2)}{f\Delta x}|_i \tag{33}$$

and

$$\hat{G}_i = (E_1 + E_2)|_i \tag{34}$$

for $i = 1, 2, 3.....n$, at every pixel along each of the m lines of the registered stereo pair. These quantities are stored for subsequent use. The camera focal length f and the stereo baseline Δx are constants of this process. If the coefficient $A(x_p)$ is zero anywhere on the image plane, it can be replaced by a very small value in order to ensure complete controllability of the process defined by (13).

Next, the difference equations

$$S_{j+1} = S_j + {S_j}^2 \frac{{A_j}^2 \delta}{\beta} - \alpha\delta \tag{35}$$

$$K_{j+1} = K_j + S_j \frac{{A_j}^2 \delta}{\beta} K_j + \alpha \hat{G}_j \delta \tag{36}$$

for $j = n, n-1, n-2, ...1$, are propagated from the right edge of the image to the left edge using the specified conditions on the right edge $S_n = \gamma$, $K_n = -\gamma \hat{G}_n$. The results are then stored in two arrays.

As the third step, propagate the differential constraint

$$G_{k+1} = G_k - \frac{{A_k}^2 \delta}{\beta}[S_k G_k + K_k] \tag{37}$$

for $k = 1, 2, ..n$, using the condition $G_1 = \hat{G}_1$ from the left boundary of the image to the right edge of the image. Store the G_k history in an array.

The final step is the computation of the range using the stored histories S, K, G using the expression

$$z_k = -\frac{[S_k G_k + K_k]A_k}{\beta} \tag{33}$$

.

This procedure is repeated for every m horizontal line in the two images. A flow chart illustrating various steps in the range computations is shown in Figure 2. In the next section, the use of this stereo ranging scheme will be illustrated using a laboratory image pair.

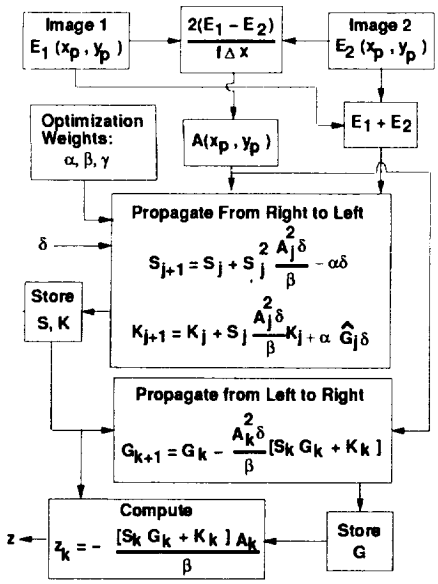

Figure 2: The stereo ranging scheme.

Results and Discussions

The ranging algorithm was tested using a laboratory stereo pair shown in Figures 3 and 4.

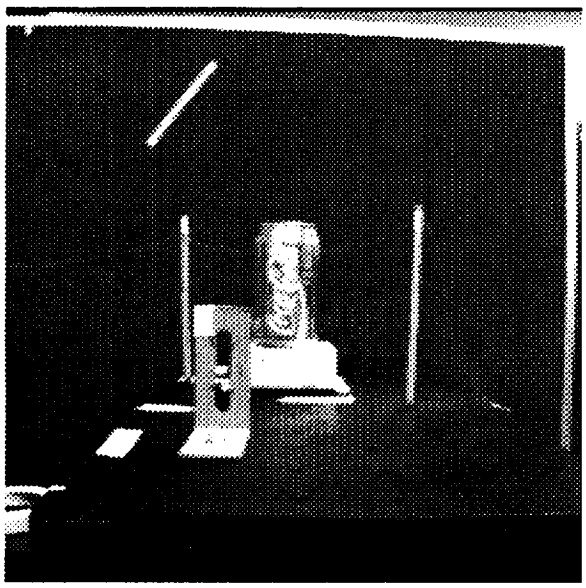

Figure 3: The laboratory stereo pair: left image.

The scene consisted of a dark wall in the background with a table in the foreground. A soda can together with two pencils were then arranged on this table. A wire is strung across the two pencils to explore the feasibility of detecting obstacles with small dimensions. A plan view of the various objects within the field-of-view is given in Figure

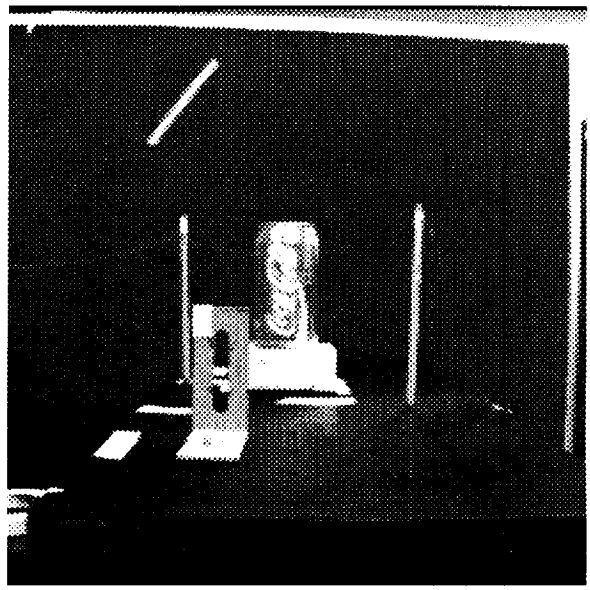

Figure 4: The laboratory stereo pair: right image.

5. The stereo images were produced using a CCD (Charge Coupled Device) camera with a field-of-view of about 45 degrees and a focal length of about 6 mm. The stereo baseline was 0.1 inches. The gray scale consisted of 256 levels corresponding to 8 bit digitization of the CCD image. The CCD output was digitized and processed on a SUN workstation.

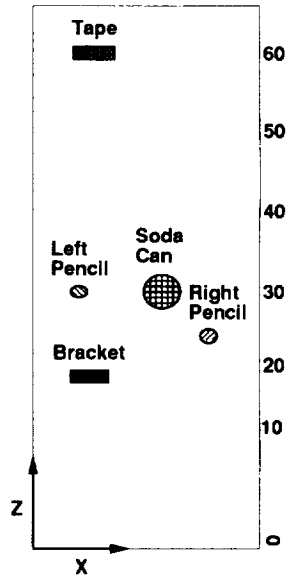

Figure 5: A plan view of the various objects in the field-of-view.

Sum and difference between the two images in the stereo pair are next formed. These are shown in Figures 6 and 7. Range calculations are car-

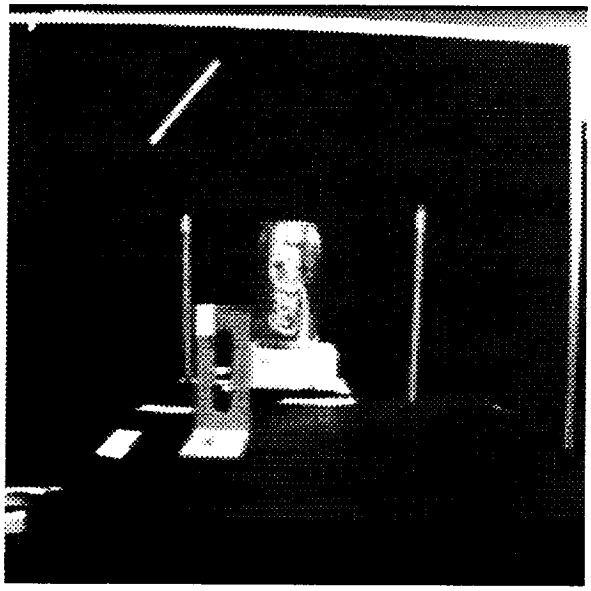

Figure 6: The laboratory stereo pair: the sum of the irradiances.

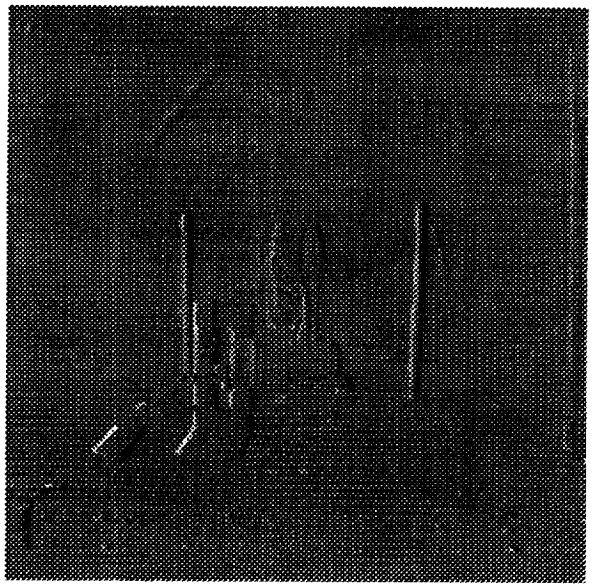

Figure 7: The laboratory stereo pair: the difference between the irradiances.

ried out using the data available in these images. The weighting factors used in generating the results given in this paper are $\alpha = 1.0$, $\beta = 0.001$, $\gamma = 1 \times 10^6$. The solution to the Riccati equation (35) and the equation (36) generated using these weighting factors are illustrated in figures 8 and 9.

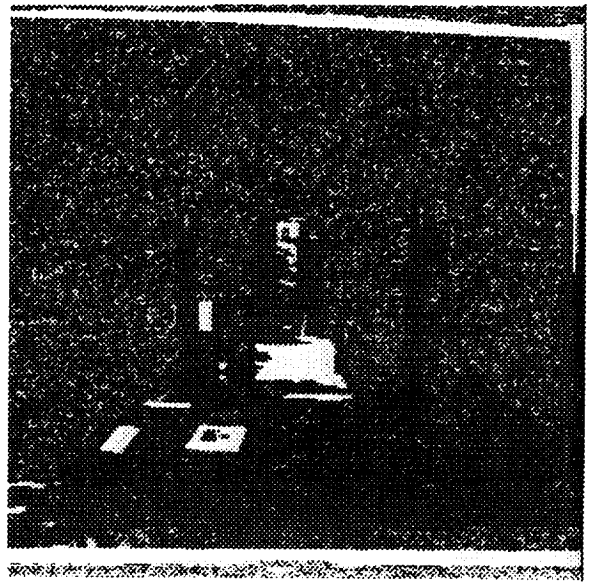

Figure 8: Solution of the Riccati equation, S.

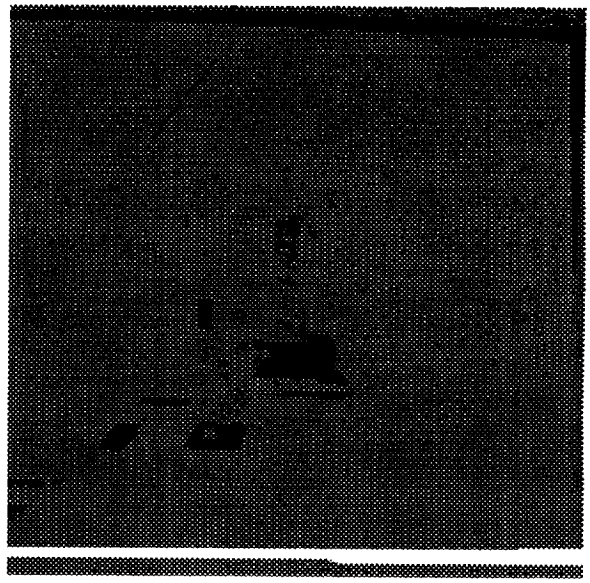

Figure 9: Solution of the equation (36), K.

These images are scaled so that black corresponds to zero and white corresponds to the maximum value. Note that the value of S is always greater than zero. The results of the range calculation are summarized in Table 1. Range estimates are accurate to within 10% in most cases. To illustrate the

Table 1: Comparison Between Actual Range (inches) and the Estimated Range (inches)

Object	Actual Range	Estimated Range	No. of Points
Left Pencil	30.0	24.13	911
Right Pencil	26.0	23.37	1889
Tape-on-wall	60.0	57.82	639
Soda can	28.5	21.43	2139
Bracket	19.0	18.55	982

nature of range output corresponding to the soda can, a histogram showing the number of points at one inch intervals is given in Figure 10. The asymmetric nature of the range estimate distribution can be seen from this picture. The range com-

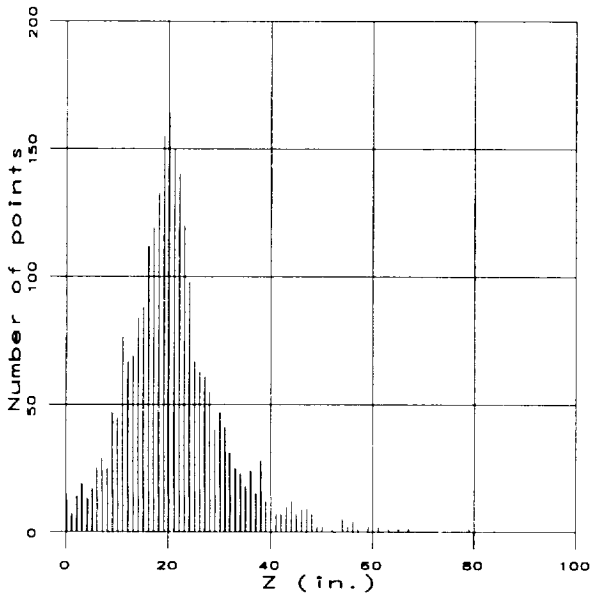

Figure 10: Range histogram for the soda can.

puted at points of small irradiance differences are suceptable to noise. As a result, the ranges corresponding to such points are dropped from further consideration. From Table 1 it may be observed that the computed ranges compare favorably with the actual ranges. The number of range points correponding to various objects show the dense nature of computed range points. Typically, range is computed at about 10 % of the points on the image plane. To further illustrate the performance of the ranging algorithm, the computed ranges are displayed in a 3-D format in Figure 11. Relative

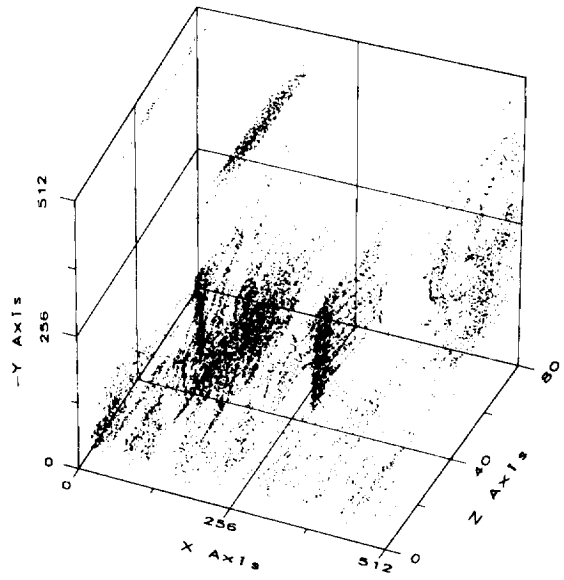

Figure 11: Computed ranges from the laboratory image pair.

placement of various range points can be visualized from this figure. In Figure 12, the sum of the irradiances produced by the differential constraint (13) while computing the ranges is illustrated. Figures

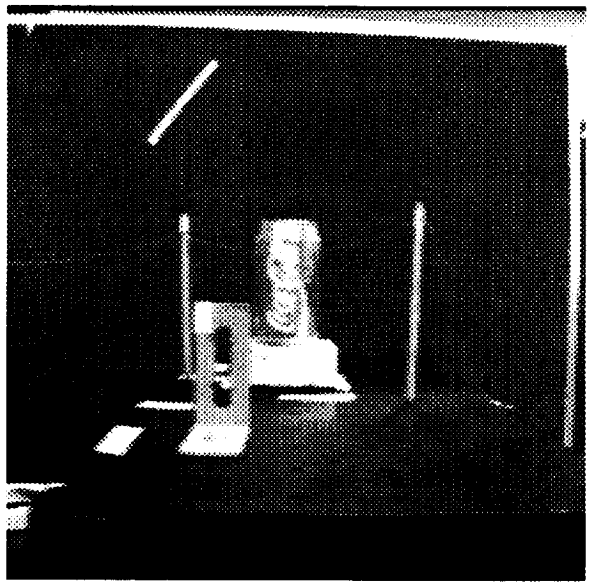

Figure 12: Sum of the irradiances predicted by the ranging algorithm.

12 and 6 can be compared to evaluate the effect of the weighting parameters α, β, γ. Image in Figure 12 is a smoothed version of image 6. The weighting parameters α, β, γ should be chosen to retain adequate fidelity between Figures 6 and 12.

The accuracy of the present range calcula-

tion can be improved by employing a finer gray scale quantization. Further improvement can be achieved by increasing the pixel density in the image plane. Additionally, one may implement a ranging algorithm based on higher-order Pade' approximation of the correspondence equation. Note that in the foregoing, the constraint that the computed range should be greater than zero was not explicitly included. Modification of the present formulation to include this requirement will be a future research item.

Conclusions

Vision-based stereo ranging was cast an optimal control problem in this paper. The correspondence hypothesis was approximated using Pade' approximation and was used as a differential constraint in an optimization problem with a quadratic performance index. The state variable in this formulation was the sum of the image irradiances and the control variable was the range to various objects within the field-of-view.

Since this differential constraint is only an approximation and due to the fact that the observed irradiances are corrupted by noise, it was satisfied in a minimum error sense by defining a performance index. The performance index consisted of a weighted linear combination of the square of the irradiance error between the actual irradiance and that predicted by the correspondence hypothesis, and the range from the image plane.

The necessary conditions for optimality yield linear two-point boundary value problems which were solved using a version of backward sweep method. Second-order necessary conditions ensuring the optimality of the range estimates were explored. A discrete implementation of the algorithm was then discussed. Finally, the ranging algorithm performance was demonstrated using a laboratory image pair.

The contributions of the present research are the following

- A new approximation for correpondence hypothesis in stereo ranging was developed using Pade' expansion.
- The image-based ranging problem was formulated as an optimal control problem, obviating the need for computing partial derivatives as in previous research.
- It was shown that the optimality of the range estimates can be assured under certain mild restrictions.
- The performance of the stereo ranging algorithm was demonstrated using a laboratory stereo pair.

Acknowledgements

The research support for the first author under NASA Cooperative Agreement NCC2-575 from Ames Research Center is gratefully acknowledged.

The image pairs used in this work were generated by Mr. R. Suorsa of NASA Ames Research Center.

The authors would like thank the FSN Branch Chief Dr. Dallas Denery for his interest and support of this work.

References

[1] Cheng, V. H. L., and Sridhar, B., "Considerations for Automated Nap-of-The-earth Rotorcraft Flight", *Proceedings of the 1988 American Control Conference*, Atlanta, GA, June 15-17, 1988.

[2] Cheng, V. H. L., "Concept Development of Automatic Guidance for Rotorcraft Obstacle Avoidance", *IEEE Transactions on Robotics and Automation*, Vol. 6, No. 2, April 1990, pp. 252-257.

[3] Sridhar, B., Cheng, V. H. L., and Swenson, H. N., "Status of Automatic Guidance Systems for Rotorcraft in Low Altitude Flight", *AGARD Symposium on Air Vehicle Mission Control and Management*, October 22-25, 1991, Amsterdam, The Netherlands.

[4] Baker, K., "MRSR- Managing the Landing Hazards", *Mars Rover Sample Return Scale Workshop* Final Report, Pasadena, CA, June 8-9, 1988.

[5] de Vries, J. P., and Norton, H. N., "A Mars Sample Return Mission Using a Rover for Sample Aquisition", *The Case for Mars II*, C. P. McKay (Ed.), *American Astronautical Society*, 1985.

[6] Hall, E. L., "Vision Sensing Techniques in Aeronautics and Astronautics", in *Machine Intelligence and Autonomy for Aerospace Systems*, E. Heer and H. Lum (eds.) , Vol 115 *Progress in Astronautics and Aeronautics*, American Institute of Aeronautics and Astronautics, 1989.

[7] Horn, B. K. P., *Robot Vision*, McGraw Hill, New York, 1986.

[8] Sridhar, B., Cheng, V. H. L., and Phatak, A. V., "Kalman Filter Based Range Estimation for Autonomous Navigation Using Imaging Sensors", *IFAC Symposium on Automatic Control in Aerospace*, July 17 - 21, 1989, Tsukuba, Japan.

[9] Menon, P. K. A., and Sridhar, B.,"Passive Navigation Using Image Irradiance Tracking", *AIAA Guidance, Navigation, and Control Conference* , August 14-16, 1989, Boston, MA.

[10] Menon, P. K. A., and Sridhar, B.,"Image-Based Range Determination", *AIAA Guidance, Navigation, and Control Conference* , August 14-16, 1990, Portland, OR. Also to appear in the *Journal of Guidance, Control, and Dynamics*, 1991

[11] Menon, P. K. A., Chatterji, G. B., and Sridhar, B., "A Fast Algorithm for Image-Based Ranging", *SPIE International Symposium on Optical Engineering and Photonics in Aerospace Sensing*, April 1-5, 1991, Orlando, FL

[12] Menon, P. K. A., Chatterji, G. B., and Sridhar, B., "Passive Obstacle Location for Rotorcraft Guidance", *AIAA Guidance, Navigation, and Control Conference* , August 12-14, 1991, New Orleans, LA.

[13] Bryson, A. E. and Ho, Y. C., *Applied Optimal Control*, Hemisphere, New York, 1975

[14] Barniv, Y.,"Application of Velocity Filtering to Optical Flow Calculations", NASA TM 102802, August 1990.

[15] Pipes, L. A., *Applied mathematics for Engineers and Physicists*, McGraw Hill, New York, 1958.

[16] Hale, F. J., *Introduction to Control System Analysis and Design*, Prentice Hall, Englewood Cliffs, NJ., 1988.

6. Guidance Law for Vision-Based Aircraft Maneuvers

The range data produced by vision-based ranging algorithms are in discrete form. Typically, the data is available only at about 10 % of the points. A need exists for deriving guidance laws that use the sparse range data to generate a clear trajectory joining the initial and final conditions. An exploratory look in this direction is discussed in the following paper.

In this work, an optimal control problem that maximizes the sum of the distances to various range points within the field of view subject to differential constraints arising from the helicopter point-mass equations of motion are considered. The performance index additionally includes the square of the vehicle acceleration and the flight time, both of which serve to ensure that the resulting trajectories are implementable. Feedback linearization of the helicopter dynamics is used to make the present optimal control problem amenable to analysis. Necessary conditions for optimality yield a linear two-point boundary-value problem which can be solved in feedback form. Inverse transformation of the result then produces the desired guidance law. The present analysis resulted in the synthesis of a nonlinear guidance law in state feedback form. A paper based on this research was presented at the *1991 AIAA Guidance, Navigation, and Control Conference*. This paper is given in the following.

Vision-Based Optimal Obstacle-Avoidance Guidance for Rotorcraft

P. K. A. Menon*, G. B. Chatterji †and B. Sridhar‡
NASA Ames Research Center
Moffett Field, CA 94035

Abstract

An optimal guidance scheme for vision-based obstacle avoidance is developed. The proposed approach is useful for automating low-altitude rotorcraft flight. It explicitly accounts for the discrete nature of range information available from vision-based sensors and uses a linear combination of flight time, square of the vehicle acceleration and the square of the distance to various sensed obstacles as the performance index. A sixth-order, three-degree-of-freedom nonlinear point-mass vehicle model is included in the analysis. Numerical results using a sample image sequence is given.

Introduction

Passive vision-based obstacle-detection sensors are currently being developed by NASA for use with automated nap-of-the-earth rotorcraft flight[1-6]. The objective is to automate the low-altitude rotorcraft flight regime using vision-based sensors such as low-light television and infrared imagers. The first aspect of this problem, viz., the problem of ranging using motion and stereo image sequences is currently being addressed by several researchers[2-6].

The focus of the present paper will be the development of a guidance law for synthesizing flyable trajectories using the vision-based sensor derived range data. Due to the discrete nature of the current imaging sensors and because of the fact that the range can be computed only at those regions where a contrast exists, the range information is typically available only at about 10 % of the points in an image. This necessitates the development of obstacle-avoidance guidance laws that use the discrete range data to synthesize implementable trajectories.

The robotics literature is replete with obstacle-avoidance algorithms, most of which have a heuristic basis; see Reference 7 for example. Algorithms that use various approximations for obstacles[8] and those that require extensive numerical calculations[9] have also been discussed in the literature. With the exception of the heuristic algorithm discussed in Reference 10, these guidance laws are primarily useful for two-dimensional maneuvers and assume the availability of the exact obstacle dimensions and location.

In the present research, optimal control theory[11] will be used in conjunction with feedback linearization to synthesize a guidance law for obstacle avoidance. The research will employ a nonlinear point-mass helicopter model. It will be assumed that the initial and final vehicle position and velocity are specified. Using a performance index consisting of a linear combination of the flight time, square of the rotorcraft acceleration magnitude and the sum of the distances to various obstacles, an optimal control law will be obtained in closed form. For this initial study, it will be assumed that the obstacles are fixed. Generalization to the case of moving obstacles is not difficult, although non-trivial. Further, the vehicle as well as the obstacles will be represented by points. Using a previously discussed methodology[12], it is possible to tailor the present formulation to include the geometric dimensions of the helicopter and the obstacles. This aspect of the obstacle avoidance guidance will be investigated in a future research. Finally, it may be noted in passing that the present methodology is useful for other vision-based guidance tasks such as spacecraft docking and autonomous vehicle guidance.

Vehicle Model

The three-degree-of-freedom point-mass model for a rotorcraft is given by the following six first-order nonlinear differential equations :

$$V' = \frac{T\sin\theta - D}{m} - g\sin\gamma \tag{1}$$

$$\chi' = \frac{T\cos\theta\sin\phi}{mV\cos\gamma} \tag{2}$$

$$\gamma' = \frac{T\cos\theta\cos\phi}{mV} - \frac{g\cos\gamma}{V} \tag{3}$$

$$x' = V\cos\gamma\cos\chi \tag{4}$$

*Member AIAA, School of Aerospace Engineering, Georgia Institute of technology, Atlanta. Mailing Address : FSN Branch, M.S. 210-9, NASA Ames Research Center

†Member AIAA, Member of the Professional Staff, Sterling Software, Inc. 1121 San Antonio Road, Palo Alto, CA 94303

‡Research Scientist, Member AIAA, FSN Branch, M.S. 210-9

$$y' = V\cos\gamma\sin\chi \tag{5}$$

$$z' = V\sin\gamma \tag{6}$$

Here, x is the down range, y the cross range, z altitude, V airspeed, γ the flight-path angle, χ heading angle, T main-rotor thrust, m the vehicle mass and g is the acceleration due to gravity. A prime over a variable indicates differentiation with respect to time. The variable D is the vehicle drag, determined using the atmospheric density ρ, airspeed V, the reference area s and the drag coefficient C_D as:

$$D = \frac{1}{2}\rho V^2 s C_D \tag{7}$$

The drag coefficient for the UH-60 helicopter from Reference 13 will be employed in this work. The coordinate system used in deriving the vehicle model is illustrated in Figure 1. The control variables in these equations

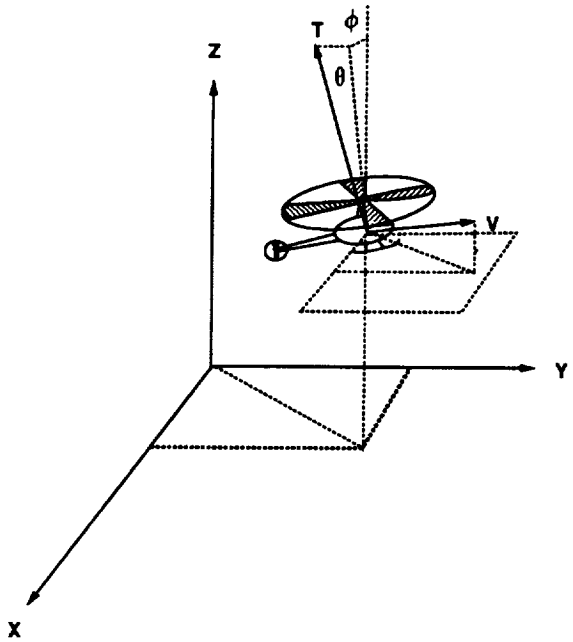

Figure 1: The coordinate system

are the rotor thrust orientation angle θ measured with respect a plane normal to the velocity vector, the bank angle ϕ measured with respect to the local vertical, and the main rotor thrust magnitude T.

If one attempts to derive an obstacle-avoidance guidance law using the nonlinear vehicle model described in the foregoing, the solution can only be obtained using numerical methods. The objective here, however, is to obtain a feedback law. To meet this objective, the nonlinear system will be first transformed to a linear time-invariant form using a coordinate transformation. This transformation implicitly assumes the availability of the vehicle velocity vector components from on-board measurements. The guidance problem is then solved in the transformed coordinates. Inverse transformation of the result then produces the nonlinear feedback guidance law.

Differentiating the down-range, cross-range, altitude equations once with respect to time, the rotorcraft equations of motion can be expressed in the following form.

$$x'' = a_x, \quad y'' = a_y, \quad z'' = a_z \tag{8}$$

The right hand sides of these equations are given by

$$a_x = V'\cos\gamma\cos\chi - \chi' V\cos\gamma\sin\chi - \gamma' V\sin\gamma\cos\chi \tag{9}$$

$$a_y = V'\cos\gamma\sin\chi + \chi' V\cos\gamma\cos\chi - \gamma' V\sin\gamma\sin\chi \tag{10}$$

$$a_z = V'\sin\gamma + \gamma' V\cos\gamma \tag{11}$$

The variables V', γ', χ' may be eliminated from equations (9) - (11) using expressions (1) - (3).

The vehicle acceleration components a_x, a_y, a_z will be treated as the new control variables in the guidance problem and will be termed the *pseudo-control variables* in the ensuing. Note that the system dynamics is linear in terms of the pseudo-control variables. If these variables were known, together with the vehicle velocity vector components x', y', z', the actual control variables can be computed as:

$$\phi = \tan^{-1}\left[\frac{a_y\cos\chi - a_x\sin\chi}{\Gamma}\right] \tag{12}$$

$$\theta = \tan^{-1}\left[\frac{\cos\phi(N_1 + N_2) + N_3}{\Gamma}\right] \tag{13}$$

$$T = \frac{m\Gamma}{\cos\theta\cos\phi} \tag{14}$$

where,

$$V = \sqrt{x'^2 + y'^2 + z'^2} \tag{15}$$

$$\gamma = \sin^{-1}(z'/V), \quad \chi = \tan^{-1}(y'/x') \tag{16}$$

$$N_1 = a_x\cos\gamma\cos\chi + a_y\cos\gamma\sin\chi \tag{17}$$

$$N_2 = (a_z + g)\sin\gamma, \quad N_3 = D\cos\phi/m \tag{18}$$

$$\Gamma = (g + a_z)\cos\gamma - a_x\sin\gamma\cos\chi - a_y\sin\gamma\sin\chi \tag{19}$$

The vehicle model is now in the form of a linear time-invariant system. If the obstacle avoidance problem is formulated in transformed coordinates, it can be solved in closed form.

Guidance Law Development

Given the current vehicle position and the desired final vehicle position, the objective is to produce a trajectory that maximizes the sum of the square of the distances from the vehicle to the various obstacles located at the points x_i, y_i, z_i, $i = 1, 2, ...n$. Further, to enhance the trajectory masking, the vehicle is required to stay as close as possible to a specified altitude z_r while using the least square of vehicle acceleration magnitude. It is sometimes desirable to execute the mission in minimum flight time. Thus, a composite performance index of the following form may be specified.

$$\min_{a_x,a_y,a_z} \int_0^{t_f} \left\{ \zeta + \frac{(1-\zeta)}{2} \left[\alpha({a_x}^2 + {a_y}^2 + {a_z}^2) \right.\right.$$

$$+\mu(z - z_r)^2 - \beta \sum_{i=1}^{n} [(x - x_i)^2$$

$$\left.\left. +(y - y_i)^2 + (z - z_i)^2] \right] \right\} dt \qquad (20)$$

The initial vehicle position components x_0, y_0, z_0, the velocity components x'_0, y'_0, z'_0 , the obstacle position components x_i, y_i, z_i, $i = 1, 2, ...n$, the final vehicle position components x_f, y_f, z_f, and the velocity components x'_f, y'_f, z'_f are assumed to be specified. The positive parameters ζ, α, μ, β in the performance index establish the relative weighting of flight time, vehicle acceleration, altitude deviation from the reference altitude and the distance to various obstacles. For reasons that will be made clear in the ensuing, the parameters ζ, β and μ are required to satisfy the constraints

$$0 < \zeta < 1, \quad n\beta > \mu \qquad (21)$$

The variational Hamiltonian[11] for this problem is defined as

$$H = \zeta + \frac{(1-\zeta)}{2} \left\{ \alpha({a_x}^2 + {a_y}^2 + {a_z}^2) \right.$$

$$+\mu(z - z_r)^2 - \beta \sum_{i=1}^{n} [(x - x_i)^2$$

$$\left. +(y - y_i)^2 + (z - z_i)^2] \right\} + \lambda_{x'} a_x$$

$$+\lambda_{y'} a_y + \lambda_{z'} a_z + \lambda_x x' + \lambda_y y' + \lambda_z z' \qquad (22)$$

The necessary conditions for optimality are

$$\lambda'_{x'} = -\lambda_x, \ \lambda'_{y'} = -\lambda_y, \ \lambda'_{z'} = -\lambda_z \qquad (23)$$

$$\lambda'_x = (1-\zeta)\beta \sum_{i=1}^{n} (x - x_i) \qquad (24)$$

$$\lambda'_y = (1-\zeta)\beta \sum_{i=1}^{n} (y - y_i) \qquad (25)$$

$$\lambda'_z = (1-\zeta) \left[\beta \sum_{i=1}^{n} (z - z_i) - \mu(z - z_r) \right] \qquad (26)$$

$$a_x = \frac{-\lambda_{x'}}{\alpha(1-\zeta)}, \ a_y = \frac{-\lambda_{y'}}{\alpha(1-\zeta)}, \ a_z = \frac{-\lambda_{z'}}{\alpha(1-\zeta)} \qquad (27)$$

The strict upper bound on the parameter ζ in equation (21) is required to ensure that the control variables remain finite.

Since all the states are specified at the initial and final time, no boundary conditions can be specified on the costates. The state-costate system for this problem is linear. Consequently, the closed-form solution can be obtained by proceeding as follows. Differentiate the $\lambda'_{x'}$, $\lambda'_{y'}$, $\lambda'_{z'}$ equations (23) with respect to time and substitute for λ'_x, λ'_y, λ'_z from the expressions (24) - (26). This yields :

$$\lambda''_{x'} = -(1-\zeta)\beta \sum_{i=1}^{n} (x - x_i) \qquad (28)$$

$$\lambda''_{y'} = -(1-\zeta)\beta \sum_{i=1}^{n} (y - y_i) \qquad (29)$$

$$\lambda''_{z'} = -(1-\zeta) \left[\beta \sum_{i=1}^{n} (z - z_i) - \mu(z - z_r) \right] \qquad (30)$$

Next, substitute for a_x, a_y, a_z in terms of the costates $\lambda_{x'}$, $\lambda_{y'}, \lambda_{z'}$ in the x'', y'', z'' equations to yield:

$$x'' = \frac{-\lambda_{x'}}{\alpha(1-\zeta)}, \ y'' = \frac{-\lambda_{y'}}{\alpha(1-\zeta)}, \ z'' = \frac{-\lambda_{z'}}{\alpha(1-\zeta)} \qquad (31)$$

Differentiating the equations (31) twice with respect to time and substituting for $\lambda''''_{x'}$, $\lambda''''_{y'}$, $\lambda''''_{z'}$ from (28) - (30) results in three fourth-order linear differential equations of the form

$$x'''' = \frac{\beta}{\alpha} [nx - \sum_{i=1}^{n} x_i] \qquad (32)$$

$$y'''' = \frac{\beta}{\alpha} [ny - \sum_{i=1}^{n} y_i] \qquad (33)$$

$$z'''' = \frac{n\beta - \mu}{\alpha} z - \frac{\beta}{\alpha} \sum_{i=1}^{n} z_i + \frac{\mu}{\alpha} z_r \qquad (34)$$

Denoting $\sigma_1 = \sqrt[4]{\frac{n\beta}{\alpha}}$, the eigenvalues of the equations (32) and (33) are

$$\sigma_1, -\sigma_1, j\sigma_1, -j\sigma_1 \tag{35}$$

Note that $j = \sqrt{-1}$. Similarly, denoting $\sigma_2 = \sqrt[4]{\frac{n\beta-\mu}{\alpha}}$, the eigenvalues for the equation (34) are given by :

$$\sigma_2, -\sigma_2, j\sigma_2, -j\sigma_2 \tag{36}$$

The constraint on the product $n\beta$ as in equation (21) is essential for the obtaining the real eigenvalues in (36).

Now, from the theory of linear differential equations[14], the general solutions to the necessary conditions (32) - (34) can be obtained as:

$$x(t) = A_x e^{\sigma_1 t} + B_x e^{-\sigma_1 t} + C_x \sin\sigma_1 t + D_x \cos\sigma_1 t + s_x \tag{37}$$

$$y(t) = A_y e^{\sigma_1 t} + B_y e^{-\sigma_1 t} + C_y \sin\sigma_1 t + D_y \cos\sigma_1 t + s_y \tag{38}$$

$$z(t) = A_z e^{\sigma_2 t} + B_z e^{-\sigma_2 t} + C_z \sin\sigma_2 t + D_z \cos\sigma_2 t + s_z \tag{39}$$

where

$$s_x = \frac{1}{n}\sum_{i=1}^{n} x_i, \; s_y = \frac{1}{n}\sum_{i=1}^{n} y_i \tag{40}$$

$$s_z = \frac{1}{n\beta-\mu}\left[\beta\sum_{i=1}^{n} z_i - \mu z_r\right] \tag{41}$$

$A_x, A_y, A_z, B_x, B_y, B_z, C_x, C_y, C_z, D_x, D_y, D_z$ are the constants determined using the specified boundary conditions. It may be verified that the costates in this problem are given by:

$$\lambda_{x'} = \alpha(\zeta-1)\sigma_1{}^2\left[A_x e^{\sigma_1 t} + B_x e^{-\sigma_1 t} - C_x \sin\sigma_1 t - D_x \cos\sigma_1 t\right] \tag{42}$$

$$\lambda_{y'} = \alpha(\zeta-1)\sigma_1{}^2\left[A_y e^{\sigma_1 t} + B_y e^{-\sigma_1 t} - C_y \sin\sigma_1 t - D_y \cos\sigma_1 t\right] \tag{43}$$

$$\lambda_{z'} = \alpha(\zeta-1)\sigma_2{}^2\left[A_z e^{\sigma_2 t} + B_z e^{-\sigma_2 t} - C_z \sin\sigma_2 t - D_z \cos\sigma_2 t\right] \tag{44}$$

$$\lambda_x = \alpha(1-\zeta)\sigma_1{}^3\left[A_x e^{\sigma_1 t} - B_x e^{-\sigma_1 t} - C_x \cos\sigma_1 t + D_x \sin\sigma_1 t\right] \tag{45}$$

$$\lambda_y = \alpha(1-\zeta)\sigma_1{}^3\left[A_y e^{\sigma_1 t} - B_y e^{-\sigma_1 t} - C_y \cos\sigma_1 t + D_y \sin\sigma_1 t\right] \tag{46}$$

$$\lambda_z = \alpha(1-\zeta)\sigma_2{}^3\left[A_z e^{\sigma_2 t} - B_z e^{-\sigma_2 t} - C_z \cos\sigma_2 t + D_z \sin\sigma_2 t\right] \tag{47}$$

Next, applying the given boundary conditions along the x, y, z axes leads to the matrix equations

$$\begin{bmatrix} x_0 - s_x \\ x'_0 \\ x_f - s_x \\ x'_f \end{bmatrix} = \mathbf{P}\begin{bmatrix} A_x \\ B_x \\ C_x \\ D_x \end{bmatrix} \tag{48}$$

$$\begin{bmatrix} y_0 - s_y \\ y'_0 \\ y_f - s_y \\ y'_f \end{bmatrix} = \mathbf{P}\begin{bmatrix} A_y \\ B_y \\ C_y \\ D_y \end{bmatrix} \tag{49}$$

$$\begin{bmatrix} z_0 - s_z \\ z'_0 \\ z_f - s_z \\ z'_f \end{bmatrix} = \mathbf{Q}\begin{bmatrix} A_z \\ B_z \\ C_z \\ D_z \end{bmatrix} \tag{50}$$

where

$$\mathbf{P} = \begin{bmatrix} 1 & 1 & 0 & 1 \\ \sigma_1 & -\sigma_1 & \sigma_1 & 0 \\ e^{\sigma_1 t_f} & e^{-\sigma_1 t_f} & S_1 & C_1 \\ \sigma_1 e^{\sigma_1 t_f} & -\sigma_1 e^{-\sigma_1 t_f} & \sigma_1 C_1 & -\sigma_1 S_1 \end{bmatrix} \tag{51}$$

$$\mathbf{Q} = \begin{bmatrix} 1 & 1 & 0 & 1 \\ \sigma_2 & -\sigma_2 & \sigma_2 & 0 \\ e^{\sigma_2 t_f} & e^{-\sigma_2 t_f} & S_2 & C_2 \\ \sigma_2 e^{\sigma_2 t_f} & -\sigma_2 e^{-\sigma_2 t_f} & \sigma_2 C_2 & -\sigma_2 S_2 \end{bmatrix} \tag{52}$$

$$S_1 = \sin\sigma_1 t_f, \; C_1 = \cos\sigma_1 t_f \tag{53}$$

$$S_2 = \sin\sigma_2 t_f, \; C_2 = \cos\sigma_2 t_f \tag{54}$$

The matrix equations (48) - (50) can be solved to yield the 12 arbitrary constants in the problem if the final time t_f were known.

The final time can be determined by invoking a constant of motion in this problem. Since the variational Hamiltonian is autonomous, and since the time

weight parameter ζ is constrained to be greater than zero, the final time may be found using the transversality condition:

$$H(t) = H(t_f) = 0 \tag{55}$$

Satisfaction of this condition would involve a one-dimensional search wherein one would assume a final time and determine the value of the variational Hamiltonian by first finding the arbitrary constants and then substituting for the states, costates and the control variables. If this results in the satisfaction of equation (55), then the optimal final time has been found. Otherwise, update the assumed final time and repeat these calculations. One-dimensional search techniques such as the method of bisections can be used to rapidly determine this quantity.

Note that at this stage, the solution is in open-loop form. Since the position of the obstacles and the vehicle states may not be known exactly, a closed-loop solution is desirable for on-board implementation. To this end, assume that the current time is the initial time, $t = 0$. The current vehicle states then become the initial conditions and the final time t_f becomes the time-to-go, denoted by the variable t_{go}. The current commanded vehicle accelerations are then given by the expressions

$$a_x = {\sigma_1}^2\Big[x - s_x - 2D_x\Big] \tag{56}$$

$$a_y = {\sigma_1}^2\Big[y - s_y - 2D_y\Big] \tag{57}$$

$$a_z = {\sigma_2}^2\Big[z - s_z - 2D_z\Big] \tag{58}$$

The unknowns in the expression (56) - (58) are the arbitrary constants D_x, D_y, D_z. These may be found using the matrix equations (48) - (50). The resulting closed-loop guidance law will be of the form

$$a_x = k_1(x - s_x) + k_2(x_f - s_x) + k_3x' + k_4x'_f \tag{59}$$

$$a_y = k_1(y - s_y) + k_2(y_f - s_y) + k_3y' + k_4y'_f \tag{60}$$

$$a_z = k_5(z - s_z) + k_6(z_f - s_z) + k_7z' + k_8z'_f \tag{61}$$

where

$$k_1 = \frac{{\sigma_1}^2 \sin\sigma_1 t_{go} \sinh\sigma_1 t_{go}}{\cos\sigma_1 t_{go}\cosh\sigma_1 t_{go} - 1} \tag{62}$$

$$k_2 = \frac{{\sigma_1}^2(\cos\sigma_1 t_{go} - \cosh\sigma_1 t_{go})}{\cos\sigma_1 t_{go}\cosh\sigma_1 t_{go} - 1} \tag{63}$$

$$k_3 = \frac{\sigma_1[\sin\sigma_1 t_{go}\cosh\sigma_1 t_{go} - \cos\sigma_1 t_{go}\sinh\sigma_1 t_{go}]}{\cos\sigma_1 t_{go}\cosh\sigma_1 t_{go} - 1} \tag{64}$$

$$k_4 = \frac{\sigma_1(\sinh\sigma_1 t_{go} - \sin\sigma_1 t_{go})}{\cos\sigma_1 t_{go}\cosh\sigma_1 t_{go} - 1} \tag{65}$$

$$k_5 = \frac{{\sigma_2}^2 \sin\sigma_2 t_{go} \sinh\sigma_2 t_{go}}{\cos\sigma_2 t_{go}\cosh\sigma_2 t_{go} - 1} \tag{66}$$

$$k_6 = \frac{{\sigma_2}^2(\cos\sigma_2 t_{go} - \cosh\sigma_2 t_{go})}{\cos\sigma_2 t_{go}\cosh\sigma_2 t_{go} - 1} \tag{67}$$

$$k_7 = \frac{\sigma_2[\sin\sigma_2 t_{go}\cosh\sigma_2 t_{go} - \cos\sigma_2 t_{go}\sinh\sigma_2 t_{go}]}{\cos\sigma_2 t_{go}\cosh\sigma_2 t_{go} - 1} \tag{68}$$

$$k_8 = \frac{\sigma_2(\sinh\sigma_2 t_{go} - \sin\sigma_2 t_{go})}{\cos\sigma_2 t_{go}\cosh\sigma_2 t_{go} - 1} \tag{69}$$

The only unknown parameter in these equations is the time-to-go. This quantity can be computed using a one-dimensional numerical search just as in the computation of t_f discussed previously.

Once the variables a_x, a_y, a_z are calculated, the real control variables of the aircraft can be recovered using the transformations given in equations (12) -(14). Further details of the guidance law implementation will be described in the next section.

Note that the controls emerging from the present development satisfy the strengthened Legendre-Clebsch necessary condition. Verification of the Jacobi's necessary condition will be a future research item.

Algorithm Implementation and Evaluation

The obstacle-avoidance guidance law was implemented on a nonlinear point-mass simulation of the rotorcraft. The salient steps in implementing the guidance law are: at each guidance interval,

1. Select the acceleration weight α, the obstacle-avoidance weight β, the altitude-deviation constraint weight μ and the time weight ζ.

2. Compute the eigenvalue magnitude σ_1, σ_2, and s_x, s_y, s_z using the given formulae.

3. Using the current states and the final states, compute the time-to-go using the transversality condition $H(t_0) = 0$.

4. Compute the feedback gains $k_1 ... k_8$ and calculate the desired vehicle accelerations a_x, a_y, a_z in feedback form.

5. Using the commanded vehicle acceleration, compute the required rotorcraft main rotor thrust T, thrust orientation angle θ and the bank angle ϕ.

In order to evaluate the performance of the guidance law, trajectories were generated using a range map obtained using the algorithm discussed in Reference 2. Figure 2 shows the sample scene obtained from a camera fixed on the nose of a helicopter flying at an altitude

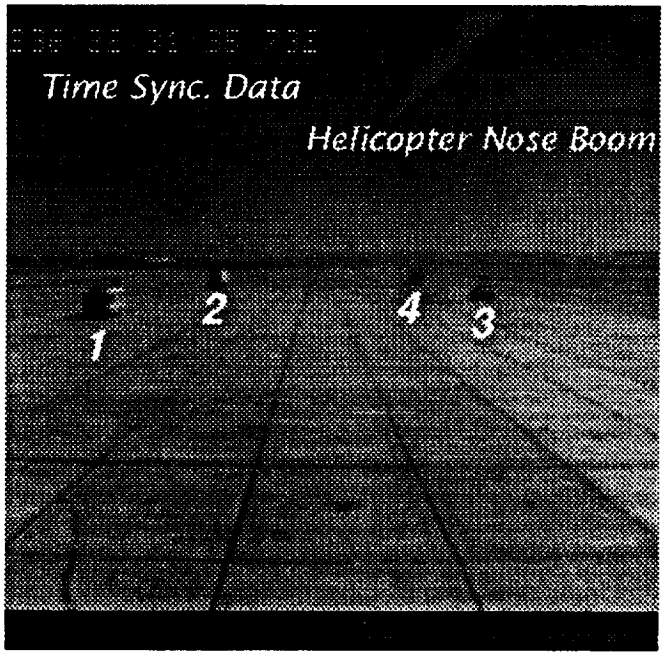

Figure 2: A Sample Image

of about 7 feet. Besides other things, the scene shows a runway, and four vehicles parked on the two sides. The instrumented nose boom of the helicopter is clearly visible at the top right hand part of the image. Parameters identifying this frame are displayed in a sub-picture on the top left hand side of the image.

This image consisted of a 512 × 512 pixel array, with 8 bit gray-scale digitization. The range data was obtained by processing several of these airborne camera images using the vision-algorithm discussed in Reference 2. This algorithm produced range data at the points denoted by small white squares in Figure 3. The range data was available at 293 points on the image plane. This represents about 0.1 % of the possible 262,144 points. The range data is recovered only at those points where a significant image intensity change is detected between frames. However, note that the algorithm determines the range to the four vehicles parked on the sides of the runway.

For the purposes of illustration, the mission to be flown was assumed to be that of a helicopter transitioning from forward flight to a landing mode with zero vertical velocity and small horizontal velocity. The target touch-down is chosen to be at a point between the

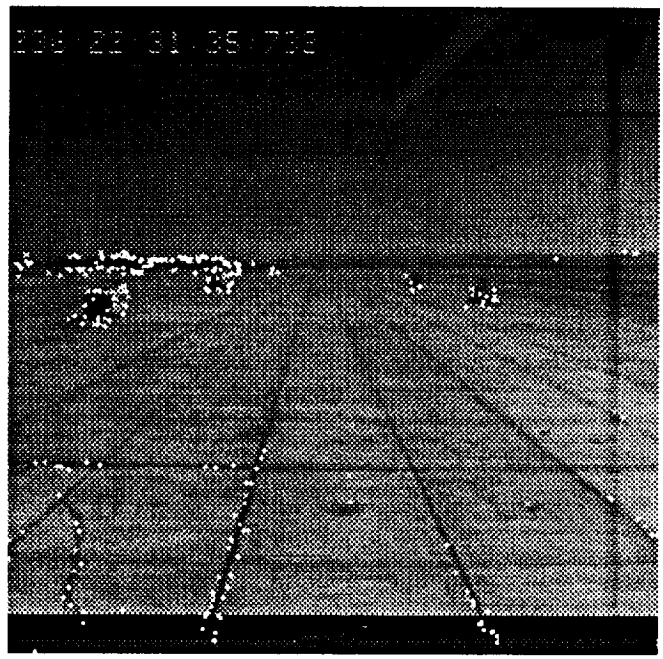

Figure 3: Available Range Data

stationary vehicles 1 and 2. The boundary conditions corresponding to this trajectory were as follows. The initial velocity vector was $[0.0, -38.0, 0.0]^T$ feet/s, and the vehicle position vector was $[532.0, 590.0, 7.0]^T$ feet. The specified final velocity and position vectors were $[1.0, 0.0, 0.0]^T$ feet/s , and of $[740.0, 0.0, 0.0]^T$ feet respectively. The weighting factors in the performance index were chosen as $\zeta = 0.96, \alpha = 0.5, \mu = 0.0, \beta = 10^{-06}$. The flight time for this trajectory turns out to be 20 seconds.

The evolution of the rotorcraft altitude as a function of down range is shown in Figure 4. Although the present analysis considers only point obstacles, these obstacles have been *denoted by small circles* for the sake of clarity. The horizontal projection of the trajectory is shown in Figure 5. In order to illustrate the obstacle avoidance charecteristics of the trajectory, the distance to the nearest obstacle at each time instant along the vehicle trajectory is plotted in Figure 6. In the present example, the minimum distance was about 8.25 feet. Note that it may be possible to further increase this clearance by increasing the obstacle avoidance weight parameter β. The rotorcraft airspeed along the trajectory is shown in Figure 7. The vehicle initially accelerates through the turn before decelerating to satisfy the specified terminal velocity. The temporal evolution of the rotorcraft heading angle is illustrated in Figure 8. The guidance law commands a large heading angle correction towards the end to meet the specified final boundary condition on the airspeed. Throughout the maneuver, the vehicle load factor was within 1.02, and the maximum magnitude of the rotor thrust orientation angle θ was less than about 12 degrees. The bank angle

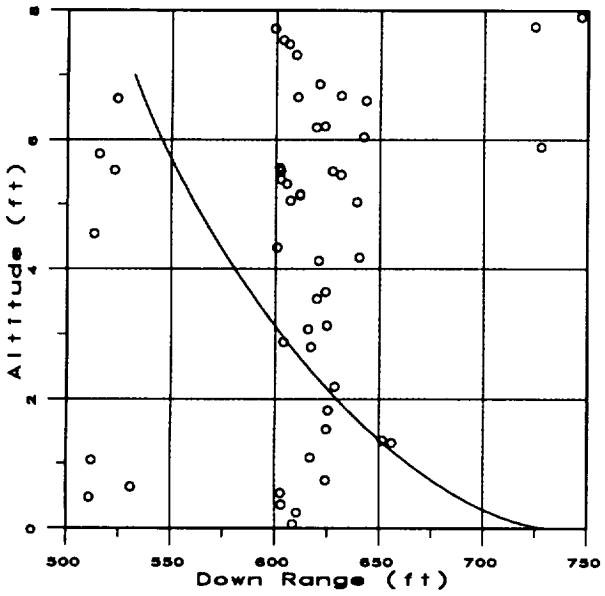

Figure 4: Down Range Vs Rotorcraft Altitude

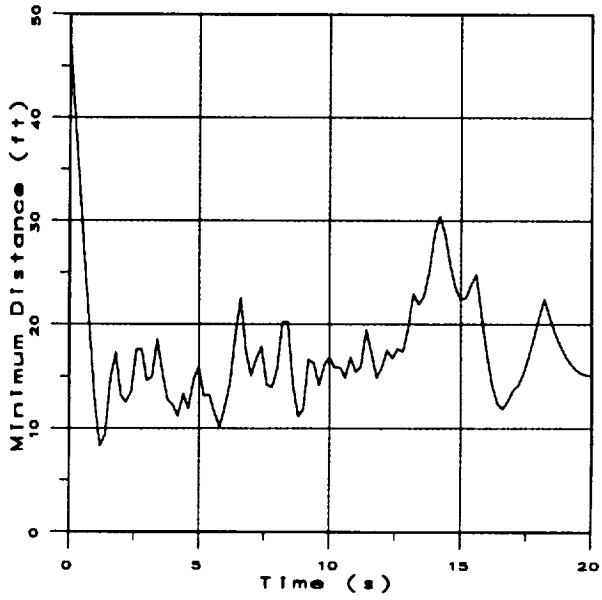

Figure 6: Distance to the closest Obstacle along the Rotorcraft Trajectory

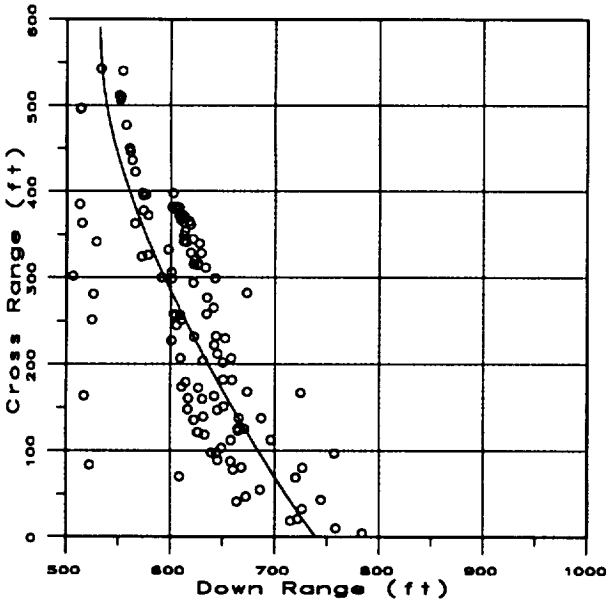

Figure 5: Horizontal Projection of the Rotorcraft Optimal Trajectory

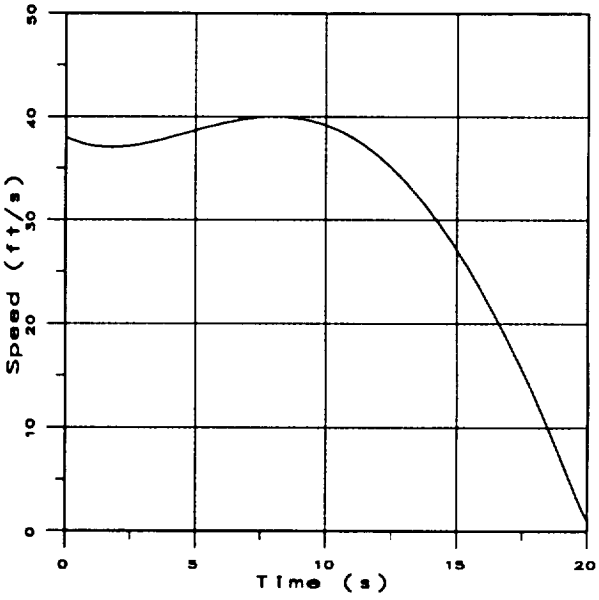

Figure 7: Optimal Trajectory: Rotorcraft Airspeed Vs Time

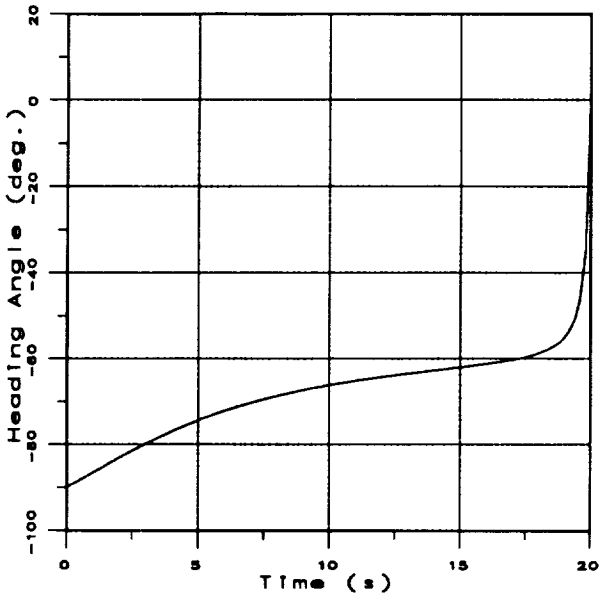

Figure 8: Temporal evolution of the Heading Angle along the Optimal Trajectory

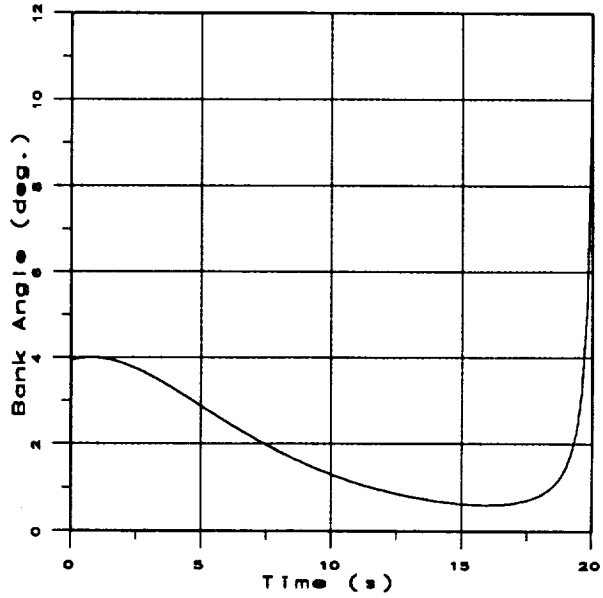

Figure 9: Optimal Trajectory: Rotorcraft Bank Angle Vs Time

ϕ was well within 15 degrees as may be observed from Figure 9. To get a feel for the nature of trajectories produced by the guidance law, the rotorcraft trajectory is next superimposed on the sample image using a perspective projection in Figure 10. The point marked with an inverted 'T' denotes the current position of the helicopter. The vertical lines are used to indicate the helicopter altitude above the runway surface along the trajectory. The obstacle-avoidance characteristics are apparent from this figure.

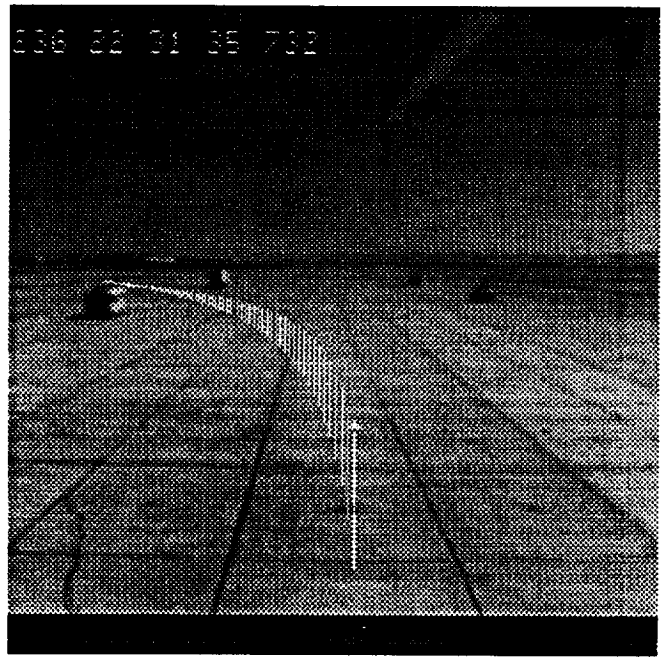

Figure 10: Perspective Projection of the Optimal Trajectory on the Image Plane

Conclusions

Development of an obstacle-avoidance guidance law that uses vision-based range data was presented. This analysis used a sixth-order nonlinear point-mass model of the helicopter together with a linear combination of flight time, square of the rotorcraft acceleration magnitude and the square of the distance to various obstacles as the performance index. The obstacles were represented as points.

The rotorcraft model was first transformed into linear, time-invariant form using a coordinate transformation. The guidance problem was then solved using the transformed model. The resulting guidance law is in linear feedback form. Inverse transformation of the guidance law yields the vehicle guidance commands. The performance of the guidance law was illustrated using a realistic vision-derived range data.

The present guidance law is useful for other vision-based guidance tasks such as spacecraft docking and autonomous vehicle guidance.

Acknowledgement

The research support for the first author under NASA Ames Research Center Cooperative agreement No. NCC2-575 is gratefully acknowledged.

The authors would like to thank FSN Branch Chief Dr. Dallas Denery for his interest and for various suggestions to improve this work. Thanks are due to Dr. V. H. L. Cheng for reviewing this paper.

References

[1] Cheng, V. H. L., and Sridhar, B., "Considerations for Automated Nap-of-The-earth Rotorcraft Flight", *Journal of the American Helicopter Society*, Vol. 36, No. 2, pp. 61-69, April 1991.

[2] Sridhar, B., Suorsa, R., and Hussien, B., "Passive Range Estimation for Rotorcraft Low Altitude Flight", To appear in *Machine Vision and Applications*, 1991.

[3] Negahdaripour, S., and Horn, B. K. P., "Direct Passive Navigation", *IEEE Transactions on Pattern Analysis and Machine Intelligence*, Vol. PAMI-9, Jan. 1987, pp. 168-176.

[4] Skifstad, K. and Jain, R., "Range Estimation from Intensity Gradient Analysis", *Machine Vision and Applications*, Vol. 2, 1989, pp. 81-102.

[5] Menon, P. K. A., and Sridhar, B., "Image-Based range Determination," *AIAA Guidance, Navigation, and Control Conference* , August , 1990, Portland, OR.

[6] Barniv, Y., "Application of Velocity Filtering to Optical Flow Calculations", NASA TM 102802, August 1990.

[7] Zhu, D., and Latombe, J-C., "New Heuristic Algorithms for Efficient Hierarchical Path Planning", *IEEE Transactions on Robotics and Automation*, Vol. 7, No. 1, February 1991, pp. 9-20.

[8] Katib, O., "Real-Time Obstacle Avoidance for Manipulators and Mobile Robots", *Proceedings of the 1985 IEEE International Conference on Robotics and Automation*, Mar. 25-28, 1985, St. Louis, MO, pp. 500-505.

[9] Gilbert, E. G., and Johnson, D. W., "Distance Functions and their Application to Robot Path Planning in the Presence of Obstacles", *IEEE Journal of Robotics and Automation*, Vol. RA-1, No. 1, pp. 21-30, March 1985.

[10] Cheng, V. H. L., "Concept Development of Automatic Guidance for Rotorcraft Obstacle Avoidance", *IEEE Transactions on Robotics and Automation*, Vol. 6, No. 2, April 1990, pp. 252-257.

[11] Bryson, A. E. and Ho, Y. C., *Applied Optimal Control*, Hemisphere, New York, 1975.

[12] Menon, P. K. A., and Duke, E.L., "Time-Optimal Aircraft Pursuit-Evasion with a Weapon Envelope Constraint," to appear in the *Journal of Guidance, Control and Dynamics*, 1991.

[13] Hilbert, K. B., "A Mathematical Model of the UH-60 Helicopter", NASA TM 85890, April 1984.

[14] Ince, E. L., *Ordinary Differential Equations*, Dover, New York, 1956.

7. Conclusions

This report outlined the research carried out on the development of field-based ranging algorithms for rotorcraft nap-of-the-earth flight. Based on various publications that have resulted from this work, the contributions may be summarized as follows :

- A field-based method for ranging using motion image sequences was developed by combining the Horn-Schunk image constraint equation with expressions for incremental perspective projection and an irradiance tracking filter. This scheme was tested using a simulated image sequence and included the translational camera motion. The spatial-temporal sampling requirements to obtain a specified ranging accuracy were examined.

- The field-based ranging algorithm was next generalized to include both motion and stereo image sequences by replacing the Horn-Schunk image constraint equation with a multi-dimensional Taylor series approximation for the correspondence hypothesis. This step produces a set of ranging equations, together with expressions that predict the error involved in the Taylor series approximation. Several orders of the ranging algorithm was tested using laboratory image sequences. The lowest-order approximation was found to be adequate in most image sequences collected in the laboratory.

- The ranging algorithms require estimates of the spatial partial derivatives of the image irradiances. A method for estimating partial derivatives by product factorization of the images was developed. This method converts the partial derivative estimation problem into a set of linear lumped-parameter estimation problems. This method was tested on several laboratory images and found to produce excellent partial derivative estimates. The factorization approach for partial derivative estimation was next used in conjunction with the ranging equation to yield a fast stereo ranging algorithm.

- By defining various coordinate systems and the incremental transformations, the image-based ranging algorithm was extended to include rotational and translational motion of the rotorcraft and the cameras. Both ranging equation as well as the range error equation were developed. It was shown that ranging can be accomplished if the incremental translation and incremental rotation angle of the camera are known.

- The need for the computation of the partial derivative before ranging prompted research on methods that do not require partial derivative estimates. Specifically, the stereo ranging problem was examined. First, it was shown that a Padé approximation can be used to approximate the correspondence hypothesis. Depending on the nature of the image sequence, it might be useful to employ different orders of Padé approximation. For the stereo problem, the first-order approximation produces a varying coefficient first-order linear ordinary differential equation. This ordinary differential equation turns out to be identical to that synthesized by combining the backward and forward Taylor series approximation of the correspondence equation. Instead of satisfying this differential equation by first computing derivatives, an optimization problem was posed whereby the irradiance predicated by the Padé approximation is compared with that from the actual irradiance. Ranges that minimize the integral of the irradiance error along each image line is then found using the necessary conditions for optimality.

- Finally, research on using the discrete vision-based range data for optimal vehicle guidance was initiated. The problem of optimally navigating a rotorcraft through a field of point obstacles was

considered. This research used a point-mass vehicle model and a quadratic criterion. Necessary conditions for optimality are then used to obtain a nonlinear feedback guidance law.

A few papers were presented at various national conferences based on the present research. These are listed below in the order in which they appeared.

[1] Menon, P. K. A., and Sridhar, B., "Passive Navigation Using Image Irradiance Tracking," *AIAA Guidance, Navigation, and Control Conference* , August 14-16, 1989, Boston, MA. Parts of this work was also presented at NASA Vision Science and Technology Workshop, Nov. 30 - Dec. 2, 1988, NASA Ames Research Center, Moffett Field, CA; and AIAA Houston Chapter Invitational Conference on Guidance and Control, NASA Johnson Space Research Center, February 12, 1990.

[2] Menon, P. K. A., and Sridhar, B., "Image-Based Range Determination," *AIAA Guidance, Navigation, and Control Conference* , August 14-16, 1990, Portland, OR; Also being revised for the *Journal of Guidance, Control, and Dynamics.* Parts of this work was also presented at NASA Workshop on Vision-Based Rotorcraft Navigation, September 19, 1990.

[3] Menon, P. K. A., Chatterji, G. B., and Sridhar, B., "A Fast Algorithm for Image-Based Ranging," *SPIE International Symposium on Optical Engineering and Photonics in Aerospace Sensing*, April 1-5, 1991, Orlando, FL.

[4] Menon, P. K. A., Chatterji, G. B., and Sridhar, B., "Passive Obstacle Location for Rotorcraft Guidance," *AIAA Guidance, Navigation, and Control Conference* , August 12-14, 1991, New Orleans, LA.

[5] Menon, P. K. A., Chatterji, G. B., and Sridhar, B., "Electro-Optical Navigation for Aircraft," Submitted for consideration in the *IEEE Transactions on Aerospace and Electronic Systems.*

[6] Menon, P. K. A., Chatterji, G. B., and Sridhar, B., "Vision-Based Optimal Obstacle-Avoidance Guidance for Rotorcraft," *AIAA Guidance, Navigation, and Control Conference* , August 12-14, 1991, New Orleans, LA.

[7] Menon, P. K. A., Sridhar, B., and Chatterji, G. B., "Vision-Based Ranging as an Optimal Control Problem," Paper communicated to *AIAA Guidance, Navigation, and Control Conference* , August 10 - 12, 1992, Hilton Head, SC.

With this background, the following items are suggested as promising future research directions.

1. The ranging algorithms discussed in this report use a pair of images. It is sometimes desirable to carry out ranging using several images simultaneously. Indeed, such an approach may yield more accurate range estimates. The field-based ranging algorithms need to be reformulated to simultaneously handle mutiple images.

2. The present ranging algorithms uses just the scene irradiances and perspective projection geometry to construct range to various objects within the field-of-view. This process completely

ignores the relationship between surface brightness, direction of illumination and the surface orientation. Invoking appropriate reflectance models such as the *Lambertian surface model* in conjunction with the ranging equations developed under the present research may yield more consistent range estimates. Such an approach would directly produce 3-D surface descriptions.

Acknowledgement

The author would like to acknowledge the contributions of Dr. B. Sridhar and Mr. G. B. Chatterji towards this research.

This research was carried out under NASA Cooperative Agreement No. NCC2-575. Dr. V. H. L. Cheng served as the technical monitor. Thanks are due to Dr. Cheng for technical discussions and constructive critism.

Several interesting discussions with Dr. Y. Barniv helped in the formulation of the image-based ranging problem. Along the way, Mr. Chima Njaka of UC Santa Barbara and Mr. Shahril Ibrahim of USC provided computational assistance. The image sequences and the range display software used to test the ranging algorithm were supplied by Mr. R. Suorsa and Mr. P. Smith of the FSN Branch.

FSN Branch Chief Dr. Dallas Denery has been a source of inspiration throughout this research. The author would like to thank him for several discussions, critism, encouragement and support.

The author thanks Professor D. P. Giddens, Director of the School of Aerospace Engineering, for the permission to conduct this research at NASA Ames Research Center.

References

[1] Sridhar, B., Cheng, V. H. L., and Swenson, H. N., "Status of Automatic Guidance Systems for Rotorcraft in Low Altitude Flight," *AGARD Symposium on Air Vehicle Mission Control and Management*, October 22-25, 1991, Amsterdam, The Netherlands.

[2] Horn, B. K. P., *Robot Vision*, McGraw Hill, New York, 1986.

[3] Horn, B. K. P., and Schunk, B. G., "Determining Optical Flow," *Artificial Intelligence*, Vol. 17, 1981, pp. 185-206.

[4] Bertero, M., Poggio, T. A., and Torre, V., "Ill-Posed Problems in Early Vision," *Proceedings of the IEEE*, Vol. 76, No. 8, August 1988, pp. 869-889.

REPORT DOCUMENTATION PAGE

Form Approved
OMB No. 0704-0188

1. AGENCY USE ONLY *(Leave blank)*	2. REPORT DATE	3. REPORT TYPE AND DATES COVERED
	December 1991	Contractor Report

4. TITLE AND SUBTITLE

Image-Based Ranging and Guidance for Rotorcraft

5. FUNDING NUMBERS

NCC2-575

6. AUTHOR(S)

P. K. A. Menon

7. PERFORMING ORGANIZATION NAME(S) AND ADDRESS(ES)

Georgia Institute of Technology
School of Aerospace Engineering
Atlanta, GA 30332-0150

8. PERFORMING ORGANIZATION REPORT NUMBER

A-93061

9. SPONSORING/MONITORING AGENCY NAME(S) AND ADDRESS(ES)

Ames Research Center
Moffett Field, CA 94035-1000

10. SPONSORING/MONITORING AGENCY REPORT NUMBER

NASA CR-177608

11. SUPPLEMENTARY NOTES

Point of Contact: Victor H. L. Cheng, Ames Research Center, MS 210-9, Moffett Field, CA 94035-1000
(415) 604-5424

12a. DISTRIBUTION/AVAILABILITY STATEMENT

Unclassified-Unlimited
Subject Category – 04

12b. DISTRIBUTION CODE

13. ABSTRACT *(Maximum 200 words)*

This report documents the research carried out under NASA Cooperative Agreement No. NCC2-575 during the period Oct. 1988-Dec. 1991. Primary emphasis of this effort was on the development of vision-based navigation methods for rotorcraft nap-of-the-earth flight regime. A family of field-based ranging algorithms were developed during this research period. These ranging schemes are capable of handling both stereo and motion image sequences, and permits both translational and rotational camera motion. The algorithms require minimal computational effort and appear to be implementable in real time. A series of papers were presented on these ranging schemes, some of which are included in this report.

A small part of the research effort was expended on synthesizing a rotorcraft guidance law that directly uses the vision-based ranging data. This work is discussed in the last section.

14. SUBJECT TERMS

Field-based, Optimal ranging, Optimal guidance

15. NUMBER OF PAGES

79

16. PRICE CODE

A05

17. SECURITY CLASSIFICATION OF REPORT	18. SECURITY CLASSIFICATION OF THIS PAGE	19. SECURITY CLASSIFICATION OF ABSTRACT	20. LIMITATION OF ABSTRACT
Unclassified	Unclassified		